EFFECT OF CASING WALL ANGLE ON THE PERFORMANCE OF DIFFUSER

A major thesis submitted

In partial fulfillment for the requirements of the award of degree of

Master of Engineering

In

Thermal Engineering

By

NAGENDRA KUMAR SHARMA

ROLL NO. 2202

(Session 2005-07)

Under the Guidance of

Prof. B.B.ARORA Prof. B.D.PATHAK

Department of Mechanical Engineering

Delhi College of Engineering

University of Delhi

Session 2005-07

Candidate's Declaration

I hereby declare that the work which being present in the major thesis entitled "**Effect of Casing Wall Angle on the Performance of Diffuser**" in the partial fulfillment for the award of degree of **MASTER of ENGINEERING** with specialization in "**THERMAL ENGINEERING"** submitted to **Delhi College of Engineering, University of Delhi,** is an authentic record of my own work carried out under the supervisions of Prof B.D.PATHAK and Prof. B.B.ARORA , Department of Mechanical Engineering Delhi College of Engineering, University of Delhi. I have not submitted the matter in this dissertation for the award of any other Degree or Diploma or any other purpose whatever.

NAGENDRA KUMAR SHARMA

College Roll No. 05-THR-2005

University Roll No: 2202

Certificate

This is to certify that the above statement made by NAGENDRA KUMAR SHARMA is true to the best of our knowledge and belief.

(**B.B.ARORA**)
Asstt Professor
Department of Mechanical Engg.
Delhi College of Engineering, Delhi

(**B.D.PATHAK**)
Asstt. Professor
Department of Mechanical Engg
Delhi College of Engineering, Delhi

Acknowledgement

It is a great pleasure to have the opportunity to extent my heartiest felt gratitude to everybody who helped me throughout the course of this dissertation.

It is distinct pleasure to express my deep sense of gratitude and indebtedness to my learned supervisors Prof B.D.PATHAK and Prof. B.B.ARORA Department of Mechanical Engineering, Delhi College of Engineering, for their invaluable guidance, encouragement and patient review. Their continuous inspiration only has made me complete this dissertation. .

I would also like to take this opportunity to present my sincere regards to my teachers for their kind support and encouragement.

I am thankful to my friends and classmates for their unconditional support and motivation for this dissertation.

NAGENDRA KUMAR SHARMA

05-THR-2005

University Roll No. 2202

Abstract

A diffuser is a device for converting the kinetic energy of an incoming fluid into pressure. As the flow proceeds through the diffuser there is continuous retardation of the flow resulting in conversion of kinetic energy into pressure energy. Such a process is termed as diffusion. Diffuser forms an important part in flow machinery and structures. The present study involves the CFD analysis of effect of inlet swirl and casing wall angle on flow characteristics. The annular diffuser considered in the present case has both the hub and casings are diverging with equal angles and hub angle keeping constant as 5°. The geometries of all the diffusers are calculated for constant area ratio 3 and casing wall angles of 15°, 20°, and 25°. Swirl angle of 12°, 17°, 25° are introduced at the inlet. The characteristic quantities such as pressure coefficient distribution at hub and casing walls, velocity profiles at various sections and flow patterns have been presented for studying. Introduction of swirl is found to substantially increase the rate of rise of pressure coefficient at casing wall. Advanced turbulence models are required to study the effects of strong swirl at inlet. The difference in pressure coefficient between hub and casing wall increases with increase in swirl angle. For casing wall angle 15° there is no separation observed at the casing wall for no swirl condition. With further increase in angle there is a separation at the casing wall. A high amount of swirl is required to suppress the separation on the casing wall for casing wall angle of 25°.

CONTENTS

List of Figures

Validation Graph

List of Colour Maps of Pressure and Velocity

List of Pressure Coefficient graphs at Re = 3× 10^5

Comparative Graphs of Pressure Coefficient at Various Casing Wall Angle

Graphs of Velocity Distribution at Various Sections

Comparative Graphs of Velocity for Varying Swirl Angle

Comparative Graphs of Velocity for Varying Casing Wall Angle

Graphs of Swirl Velocity Distribution at Various Sections

NOMENCLATURE

A	Area
AR	Area ratio
B	blockage factor
C	Constants
C_P	Pressure recovery co-efficient
C_{PI}	Ideal pressure recovery co-efficient
D	Diameter
G	generation of turbulence kinetic energy
g	acceleration due to gravity
K	Total pressure loss co-efficient
k	Turbulent kinetic energy
P	Static pressure
P_t	Total pressure
Re	Reynolds number
S	Swirl Number of flow
S_m	Mass added
U	Velocity
w	Swirl velocity
x,y,z	Cartesian coordinate system
Y_M	fluctuating dilatation in compressible turbulence.

Symbols

$\bar{\bar{\tau}}$	Stress tensor
μ	Laminar viscosity
μ_t	Turbulent viscosity
2θ	Equivalent cone angle
Γ	Circulation
ε	Turbulent kinetic energy dissipation rate
η	Diffuser effectiveness
θ	Wall angle
ν	Kinematics viscosity
ξ	Total pressure loss co-efficient
ρ	Density
Σ	Turbulent Prandtl no.

Subscript

B	Blocked
ci	casing inlet
co	casing outlet
E	Effiective
eq	Equivalent flow
hi	hub inlet
ho	hub outlet
in	inlet
m	maximum
out	outlet
r	radial direction
t	tangential direction
x	longitudinal direction

INTRODUCTION CHAPTER 1

A diffuser is a device that increases the pressure of a fluid at the expense of its kinetic energy Japikse and Pampreen [1978]. The cross-section area of diffuser increases in the direction of flow, therefore fluid is decelerated as it flows through it causing a rise in static pressure along the stream. Such a process is known as diffusion. The flow process near the diffuser walls is subjected to greater retardation due to the formation and development of the boundary layer. A study of the parameters governing the development of the boundary layer and their relationship with diffuser performance is, therefore vital in optimizing the design of a diffuser Adkin, Jacobsen and chevealier [1983].

The flow in the diffuser is governed by the behavior of the boundary layers at the diffuser walls. The deceleration of the flow through the diffuser produces a pressure rise in the stream wise direction. The wall shear layers are therefore subjected to a positive or adverse pressure gradient. As is well known, adverse pressure gradients cause the boundary layer thicken and possibly separate from the diffuser walls, forming areas of back flow in diffusers. The net result of thickening of the wall boundary layers or the formation of region of backflow is the blockage of the flow area which reduces the effective area available to the flow. Reduction the effective flow area in turn results in a reduced pressure rise through the diffuser. The interaction of wall shear layers and / or separated zone with the core flow in diffusers is very complicated; therefore diffuser design and performance estimation is largely based on experimental data and empiricism.

Diffusers are extensively used in centrifugal compressors, axial flow compressors, ram jets, combustion chambers, inlet portions of jet engines etc. The energy transfer in these turbo machineries involves the exchange of significant levels of kinetic energy in order to accomplish the intended purpose. As a consequence, very large levels of residual kinetic energy frequently accompany the work input and work extraction processes, sometime as much as 50% of the total energy transferred. A small change in pressure recovery can increases the efficiency significantly. Therefore diffusers are absolutely essential for good turbo machinery performance.

The design requirements for a good diffuser are as following-

1. Convey the flow efficiently transferring a portion of the kinetic energy into a static pressure rise.
2. It must accept a variety of inlet conditions including extreme swirl, blockage and Mach number.
3. Deliver the fluid with reasonable velocity and angle profiles without separated regions.
4. Wall curvature must not have a deleterious effect upon passage performance.
5. Pressure recovery achieved over a short axial length.

While obtaining the best possible design, some limitations are imposed on a diffuser:

1. Limited length
2. Specified area ratio
3. Specified cross- sectional shape
4. Maximum static pressure recovery
5. Minimum stagnation pressure loss

It is not hard to appreciate that the performance of the diffuser directly and often strongly influences the overall efficiency of the turbo machine. Thus the detailed processes which occur in diffusing elements must be carefully understood and thoroughly optimized if good turbo machinery performance is to be obtained.

1.1 Axial Diffuser –

In axial diffusers, fluid flows along the axis of diffusers and there is continuous retardation of the flow. Axial diffuser is divided in to the following categories-

- Ø Conical diffuser
- Ø Channel diffuser
- Ø Annular diffuser

The basic geometric parameters for these types of diffusers are as follows:

1.1.1 For conical diffuser-

Non dimensional length, L/W_1

Aspect ratio, AS = b/W_1

Area ratio, AR = A_2/A_1

$$AR = 1 + 2\left(L/W_1\right)\tan\theta$$

1.1.2 For channel diffuser-

Non dimensional length, L/D_1

Area ratio, AR = A_2/A_1

$$AR = \left[1 + 2\left(L/D_1\right)\tan\theta\right]^2$$

1.1.3 For annular diffuser-

Non-dimensional length, $L/\Delta r$ or L/h

Area ratio, AR = A_2/A_1

$$AR = \left[1 + 2\left(L/h_1\right)\sin\theta\right] \qquad \text{(For equiangular case)}$$

1.2 ANNULAR DIFFUSER

For decades researchers have paid more attention to conical diffuser and channel diffuser than to annular diffusers. But, the annular diffusers have a very strong industrial significance and have received attention in recent years. These types of diffuser are very much used in aircraft applications. With the help of annular diffuser the maximum presser recovery is achieved within the shortest possible length. With annular diffuser, good performance is possible with large wall angles since an inner surface is present to guide the flow radially outward. The annular diffuser affords the possibility of introducing many different geometric combinations since there is now an inner surface that can be varied independently of the outer surface.

It is more difficult to define the essential geometric parameters for annular diffusers since the numbers of independent variables are large. The essential variables to define the geometry of annular diffuser are two wall angles, area ratio, non-dimensional length and inlet radius ratio. As the number of variables increases, geometry becomes more complex. By suitable combination of these variables we can find out number of geometry. The present study investigates the equiangular type of annular diffuser. In

these types of annular diffusers both hub and casing are diverging outward with same angle of divergence.

A survey of diffuser research has revealed that considerably more investigations have been carried out on two dimensional and conical diffusers. Much of the extent data covering annular diffusers was done in the experimental laboratory Stafford and James [1957]. But, the annular diffusers have a very strong industrial significance and have received attention in recent years. These types of diffuser are very much used in aircraft applications. With the help of annular diffuser the maximum presser recovery is achieved within the shortest possible length. With annular diffuser, good performance is possible with large wall angles since an inner surface is present to guide the flow radially outward. The annular diffuser affords the possibility of introducing many different geometric combinations since there is now an inner surface that can be varied independently of the outer surface. It is more difficult to define the essential geometric parameters for annular diffusers since the numbers of independent variables are large Goebel and Japikse [1981]. The essential variables to define the geometry of annular diffuser are two wall angles, area ratio, non-dimensional length and inlet radius ratio. As the number of variables increases, geometry becomes more complex. This has not been economically possible by experiments and hence led to the development of computational fluid dynamic methods to analyze the performance characteristics of annular diffuser Arora, Pathak and Singh [2005].

1.3 Diffuser performance parameter

1.3.1 Geometric parameters

Any duct geometry with an increasing area in the stream wise direction constitutes subsonic diffuser geometry. Therefore, the number of different diffusers geometries that can be conceived is infinite. However in practice, adequate design data are available for a limited number of geometries.

1. Rectangular cross section or planner diffusers
2. Conical diffusers
3. Straight walled annular diffusers

Other commonly used diffuser geometries include the radial and axiradial diffusers which are used at the exit of radial and axial turbo machines, respectively. These geometric parameters can be consolidated to a few non dimensional parameters that are found to be important in terms of diffuser performance. The first is the area ratio, AR, the area ratio of diffuser exit to inlet areas. The area ratio is measure of the theoretical diffusion or pressure recovery expected. The second important parameter is the dimensionless diffuser length define as: N/Wi or L/Wi for planar diffusers, N/ Ri or N/Ri for conical diffusers, and L/(Rit - Rih) , for annular diffusers. This dimensionless diffuser length in combination with the area ratio AR is measure of the overall pressure gradient expected across the diffuser. The third geometric parameter commonly used in displaying diffuser performance is the wall divergence angle--20 for planar and conical diffusers and 6 and 9h' for annular diffusers. The divergence angles, length, and area ratio are related as follows [10].

1.3.1.1 Aerodynamic blockage

Thin inlet boundary layers tends to be beneficial to high diffuser recovery and those longer diffusers necessary to achieve high levels of recovery as the inlet boundary thickness increases as stated by Hoadley D,et.al, 1969.

The blockage is the fraction or percentage of the inlet passage area which is occluded the boundary layer displacement thickness on all walls. The displacement thickness is taken as equal on all surfaces and then the following relationships ensue:

B = 2*/h for annular diffusers where h is annular height at inlet

$B = 2*/D_1$ for conical diffusers with uniform inlet boundary layers

1.3.1.2 Reynolds number:

Viscosity is an important parameter in any fluid dynamic process and normally appears in the form of a Reynolds number. Diffusers are characterizes by Reynolds number based on an inlet hydraulic diameter. Shaalan, et al [1975] studies reported in this field suggest that the Reynolds number is a comparatively weak parameter as long as the flow is fully turbulent regime.

1.3.1.3 Inlet Mach number:

The Mach number at the inlet to the diffuser was thought to be important at values as low as approximately 0.7 and performance to fall off past this point. No significance on Mach number develops at throat for Mach numbers of less than 1.0 is studied by Thayer E B, [1971].

1.3.1.4 Inlet Turbulence intensity

The turbulence intensity is most frequently defined as an RMS value:

$$Tu = \frac{\left[\frac{1}{3}\left(u'^2 + v'^2 + w'^2\right)\right]^{1/2}}{U}$$

This equation defines the parameter most frequently used to specify the over all level of inlet turbulence intensity is given by Shaalan, et al [1975].

1.3.1.5 Effect of Compressibility:

With compressible flow both area, A, and density, p, increases with passage down the diffuser so that the reduction in velocity V, will be greater than in the case of incompressible flow where only the cross sectional area increases. It therefore follows that the pressure recovery coefficient should also be greater.

$$v = \frac{m}{\rho . A}$$

The rate of increase in value of Cp is not rapid until Mach number of 0.6 have been exceeded and than the effect is most pronounced when area ratios are low. These low area ratios correspond to the diffuser inlet vision and flow separation would therefore occur here as a result of predicted increasing adverse pressure gradient caused by the higher subsonic inlet mach number.

1.3.2 Design Performance Parameters

Performance parameters are very helpful in designing and predicting the performance of diffusers. These parameters reveal that diffuser geometry will give the desire output or not. The following parameters are important to find out diffuser performance.

1.3.2.1 Static Pressure Recovery Coefficient

The pressure recovery coefficient of a diffuser is most frequently defined as the static pressure rise through the diffuser divided by the inlet dynamic head

$$C_p = \frac{p_2 - p_1}{\frac{1}{2}\rho v^2_{av1}}$$

where subscripts 1 and 2 refers to diffuser inlet and outlet conditions respectively. V_{avi} represents the average velocity at the inlet. An ideal pressure recovery can be defined if the flow is assumed to be isentropic. Then, by employing the conservation of mass, this relation can be converted to an area ratio for incompressible flow

$$C_p = 1 - \frac{1}{AR^2}$$

1.3.2.2 Diffuser Effectiveness

The diffuser effectiveness is simply the relation between the actual recovery and the ideal pressure recovery. $\eta = C_p / C_{pi}$

This is an excellent parameter for judging the probable level of performance when it is necessary to estimate the expected performance under unknown conditions, relative to available data.

1.3.2.3 Total Pressure Loss Coefficient

The total pressure loss coefficient reflects the efficiency of diffusion and drag of the system. The most common definition of loss coefficient is as the ratio of total pressure rise to the diffuser inlet dynamic head.

$$K = \frac{\bar{p}_{01} - \bar{p}_{02}}{\frac{1}{2}\rho v^2_{av1}} \qquad K = \frac{\left(\bar{u}_1^2 - \bar{u}_2^2\right)}{U_i^2} - C_p = \left(\alpha_1 - \alpha_2 / AR^2\right) - C_p$$

where p_{02} is the total pressure in the core region at the exit, the over bar indicate the mass averaged quantity, and α_1 and α_2 are the kinetic energy parameters at the inlet and exit of the diffuser.

For the case where the velocity profile at the inlet of diffuser is flat with a thin wall boundary layer, α_1=1 However, due to the thickening of boundary layer through the

diffuser, α_2 is generally greater than unity. Nonetheless, it is often assumed that kinetic energy coefficient is equal to unity, then

$$K = C_{pi} - C_p$$

1.3.2.4 Ideal Pressure Recovery

Another parameter of interest is the ideal pressure recovery, C1, which is the pressure recovery coefficient assuming an inviscid flow through diffuser, which represent the maximum pressure recovery attainable by the given diffuser. When the definition of pressure recovery, the Bernoulli equation, and the conservation of mass and conservation of angular momentum principles are all employed, the following relationship is obtained for Cpi.

1.3.3 SWIRLING FLOWS

1.3.3.1 Physics of Swirling and Rotating Flows

In swirling flows, conservation of angular momentum (rw or $r^2\Omega$ = constant) tends to create a free vortex flow, in which the circumferential velocity, w, increases sharply as the radius, r, decreases (with w finally decaying to zero near r = 0 as viscous forces begin to dominate). A tornado is one example of a free vortex. Figure depicts the radial distribution of w in a typical free vortex.

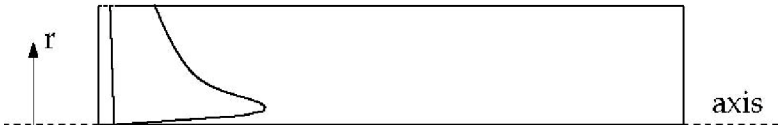

Typical Radial Distribution of w in a Free Vortex

It can be shown that for an ideal free vortex flow, the centrifugal forces created by the circumferential motion are in equilibrium with the radial pressure gradient:

$$\frac{\partial p}{\partial r} = \frac{\rho \omega^2}{r}$$

As the distribution of angular momentum in a non-ideal vortex evolves, the form of this radial pressure gradient also changes, driving radial and axial flows in response to the highly non-uniform pressures that result. Thus, as you compute the distribution of swirl in your FLUENT model, you will also notice changes in the static pressure distribution and corresponding changes in the axial and radial flow velocities. It is this high degree of

coupling between the swirl and the pressure fleld that makes the modeling of swirling flows complex.

In flows that are driven by wall rotation, the motion of the wall tends to impart a forced vortex motion to the fluid, wherein w/r or Ω is constant. An important characteristic of such flows is the tendency of fluid with high angular momentum (e.g., the flow near the wall) to be flung radially outward. This is often referred to as “radial pumping”, since the rotating wall is pumping the fluid radially outward.

1.3.3.2 Method of swirl generation

Methods of including rotation in a stream of fluid can be divided into three principle category:

- Tangential entry of the fluid stream, or a part of it, into the cylindrical duct.
- The use of guide vanes in axial tube flow.
- Rotation of mechanical devices which impart swirling motion to the fluid passing through them. This includes rotating vanes or grids and rotating tubes.

1.4 Motivations:

The purpose of this study is to investigate the level of knowledge and in certain important areas the lack thereof, concerning the performance of annular diffusers. For decades investigators have conducted individual studies without a careful consideration of how all the studies may be interwoven. A pattern of consistent behavior among the database elements for annular diffusers is established in this investigation. However, it may be of even greater significance that the investigation reveals areas where critical design knowledge is missing. It will be observed that conducting individual investigations of annular diffuser performance has blinded most investigators from seeing the larger picture and the critical interactions between the different variables which have been discussed in the literature. This study begins by looking at historical data, then proceeds to investigate the parametric dependence, resulting in the development of a preliminary design set of equations and then finally by careful examination of further investigations which are needed before the annular diffuser design problem will be well understood.

LITERARTUER SURVEY CHAPTER 2

Diffusers are ducts that convert flow kinetic energy to pressure by decelerating the flow. Flow decelerations is affected by varying the cross sectional area. Goebel J. H., Japikse D., [1981] stated that for mass conservation it follows that diffusers with incompressible fluids, and for subsonic flow as well, are duct with increasing area along the flow direction. A diffuser is a device that increases the pressure of a fluid at the expense of its kinetic energy stated Japikse and Pampreen [1978]. The flow process near the diffuser walls is subjected to greater retardation due to the formation and development of the boundary layer. A study of the parameters governing the development of the boundary layer and their relationship with diffuser performance is, therefore vital in optimizing the design of a diffuser - Adkin, Jacobsen and Chevealier [1983].

Much of the extant data covering annular diffusers comes from the period from the 1950s through the 1980s. In this period of time, a considerable amount of research was done in the experimental laboratory to uncover some of the unusual performance characteristics of annular diffusers. By the late 1980s, however, the experimental research had reduced substantially due to a lack of government funding in a number of countries where the work had previously been extensive. It is, therefore, useful to review the data which has been made available and to look for patterns within this data. It is also necessary to determine how this data may best be used in future design studies and where it needs to be further improved. Much of the original data was taken in order to support studies of axial compressor discharge diffusion as flow leaves a compressor and enters a combustion chamber. Other work was done for exhaust diffusers of hydroelectric turbines, small gas turbines, and turbochargers. While these topics are still important today and there are important unresolved questions, the level of activity has reduced. Now important research topics must be carefully selected for the more limited studies possible in future years. Figure la shows a plot of many different annular diffuser data sets which cover a wide range of swirl angles, blockage, turbulence intensity, and geometric parameters. Figure lb shows the classical diffuser performance map for an annular diffuser by Sovarn and Klomp [1967]. This map was the first investigation to introduce the topic of aerodynamic blockage. The map actually is a generalized composite of many different investigations

Sovran and Klomp [1967] and Howard et al. [1967] produced the first widely used annular diffuser maps for channel diffusers. Sovran and Klomp conducted a large number of performance measurements which spanned a broad selection of geometric types of diffusers. The map is only a broad representation of the bulk of configurations tested in the vicinity of their best performance areas. The poorer diffusers are not well defined by the map. These maps also show optimal diffuser geometrics under different conditions and two optimum lines are established. The line of Cp* shows the best area ratio for a given length/passage height ratio, and the line of Cp** shows the best length/ passage height ratio for a given area ratio. The same results were find out by Howard et al [1967]. The important difference between this and the Sovran and Klomp [1967] map was that the latter was made for very low inlet aerodynamic blockage whereas the former study was carried out for fully developed inlet profiles, implying high aerodynamic blockage Along the line of peak recovery there is fairly good agreement between the two maps but in the region of heavy transitory stall the maps disagree substantially.

In this early work of Hoadley and Hughes [1969], an ideal pressure recovery contour is plotted parallel to the actual pressure recovery. This suggests that much of the effect of geometry and swirl can be taken care of in the ideal pressure recovery and that a sensible way of developing a correlation for static pressure recovery performance will be to use diffuser effectiveness which is $\eta = Cp / Cpi$ or in other words the ratio of the actual pressure recovery coefficient divided by the ideal pressure recovery coefficient. A variety of past experiences suggests that there is some development of progressive stalling occurring which will not be reflected in the ideal pressure recovery, but must be dealt with in the actual pressure recovery.

The ideal pressure recovery coefficient is derived directly from basic principles. It is the pressure recovery that would be achieved if the flow was strictly one dimensional, inviscid, filled the entire passage and, therefore, by implication, has no blockage, no boundary layer buildup, and no deviation of flow either entering or leaving.

Takehira et al [1977] presented extensive data for a large set of both straight annular diffusers and curved wall diffusers, and determined that the use of strong curvature at the exit of diffuser was not debilitating but did produce a penalty compared to non-curved diffusers or diffusers with curvature at the inlet. Adkins et al [1983] tested an annular diffuser of constant outer radius and a conical center body with cones of different angles. In general the pressure recovery increases with decreasing cone angle

for various area ratios, but the 13.2° and sometimes the 45° cone angle produced lower pressure recoveries than an equivalent sudden expansion. This was attributed to a large and rapid separation at the base of the cone where the diffuser starts. Adding a radius to the base of the cone so that it smoothly blended into the upstream hub, was found to improve the performance.

An extensive study of diffusers which, although annular, begin with a circular cross section was reported by Ishikawa and Nakamura [1989]. The author found that the performance of the diffuser differed significantly depending on whether it is parallel or diverging for L/r1 greater than about 2. When both types have the same non dimensional length and area ratio, the parallel diffuser has the higher Cp. The lines of optimum performance are also drawn. The line of Cp shows the best area ratio for a given non dimensional length, and the line of Cp shows the best non dimensional length for a given area ratio. In the case of the latter line, there is no difference between the parallel and diverging diffuser.

Ishikawa and Nakamura [1989], also attempted to compare their results with those of Sovran and Klomp[1967], for a conventional annular diffuser for the same wall length and area ratio, their diffuser was superior, but since the inlet conditions were different in the two studies, this conclusion is only tentative. It was also found that the addition of a conical centre body improves the performance of simple conical diffusers with appreciable or large stall. The study carried out by Moller [1965], who designed an axial to radial band with the intention of eliminating diffusion in the inlet region; found that the peak pressure recovery for the entire band and radial diffuser sections was 0.88 and 0.82 for the low blockage and high blockage cases, respectively. Cockrell and Markland [1963], reported that a variation in the area ratio from 2.5 to 8.0 has a small effect on the loss coefficients of conical diffusers.

2.1 Effect of Geometric Parameters

In an annular diffuser, a number of different geometric variables can influence the variation of pressure recovery and inlet condition of flow. The basic equations of motion reveal the importance of both geometric and aerodynamic parameters on the ultimate performance of annular diffuser. The specification of a wide variety of geometric parameters is essential before the performance of diffuser is given. Arora B.B., Pathak B.D. [2005] studied effect of geometry on the performance of annular diffuser. Japikse Dr. David [2003] gave the correlations for annular diffuser

performance with geometry, swirl and blockage**.** Krystyna, Prync-Skotniczny [2006] analysed numerically the impact of conical diffuser geometry change on velocity distribution in its outlet cross-section.

2.1.1 Passage Divergence and Length

Area ratio and non-dimension length prescribes the overall diffusion and pressure-gradient respectively, which is the principle factor in boundary layer development. The study by Henry and Wood [1958] is useful to understand the subsonic annular diffuser. Two diffusers with area ratio 2.1 and divergence of 5° and 10° were tested at various Mach number. It found by this study that most of data clusters around a line of constant effectiveness. It is also observed that the inner wall is being starved of fluid. If a higher divergence had been used, then one might anticipate stall on the inner surface. An extensive study is carried out by Kmonicek and Hibs [1974] in which, the pressure loss coefficient is found out on the basis of the work of compression required to meet the static pressure rise, the results are very interesting but difficult to understand due to use of unconventional terminology.

Johnston [1959] and Johnston [1953] reported a study of four different annular diffusers. Three of the four agree tolerably well with the basics Sovran and Klomp [1967] map, one of them disagree substantially; the case a strong disagreement is probably in stall. Srinath [1968] studied four equiangular annular diffuser with 2θ = 7^o, 10^o, 15^o and 20^o respectively. Tests were reported with a variety of $L/\Delta r$ values. The line of best pressure recovery shown as CP* by Sovran and Klomp [1967] was again confirmed, and Srinath's map is quite similar to that of Howard et al. [1967]. Srinath [1968], also observed that the existence of a down stream pipe improved the pressure recovery of the diffuser itself.

2.1.2 Wall Contouring

Several annular diffuser studies have been published in which contoured walls were an essential part of the design problem. Thayer [1971], reported that curved wall diffusers had pressure recovery as high as 0.61 to 0.65 for an area ratio of 2.15. An extensive study by Stevens and Williams [1980], reported that for curved wall diffuser, good pressure recovery was found for a loss significantly below the level which would be expected from pressure recovery loss correlation , but pressure

recovery values were lower then those which would be expected from the Sovran and Klomp [1967], map. Upon careful examination, it was determined that the boundary layers in this diffuser are different from those which would be expected in most diffuser studies. Takehira et al [1977], presented extensive data for a large set of both straight annular diffusers and curved wall diffusers, and determined that the use of strong curvature at the exit of diffuser was not debilitating but did produce a penalty compared to no curved diffusers or diffusers with curvature at the inlet.

An additional study by Japikse [2000] shows that wall contouring is an important parameter regarding pressure recovery. Adkins et al [1983], tested an annular diffuser of constant outer radius and a conical centre body with cones of different angles.

2.2 Effects of Flow Parameters

2.2.1 Aerodynamic Blockage

The aerodynamic blockage on annular diffusers is much less well understood than it is in channel and conical diffusers. Coladipietro et al [1974] reported that for short diffusers, the variation of pressure recovery with blockage was similar to the channel and conical diffusers; that is the pressure recovery decreased with increasing blockage. However, for the long diffusers, higher performance was observed at the higher blockage levels.

Stevens and Williams [1980] determined that pressure recovery initially decreases with increased blockage but then for very long inlet lengths where the flow is able to achieve a fully developed form, the pressure recovery again rises. From a careful study of these data it is evident that not only the inlet boundary layer displacement thickness but also other higher order effects such as turbulence intensity and boundary layer mixing phenomena can greatly alter the measured result. In another study by Geobel and Japikse [1981] found that the pressure recovery reduces as aerodynamic blockage increases. In concluding this section several notes can be made. First, the influence of inlet conditions on annular diffuser performance is more complicated than for channel and conical diffuser. In this case, both the hub and casing surfaces can develop boundary layers with significantly different histories. The two differing boundary layers will experience different growth processes as they pass through the diffuser. Furthermore, blockage on one wall has the effect of modifying the effective flow area and hence the core flow velocity, thereby influencing the growth of the

boundary layer on the opposite wall. Hence complex interactions can develop within the diffuser.

2.2.2 Inlet Swirl

The method of swirl generation can itself influence the performance of an annular diffuser and, therefore, consideration must be given first to this question. Most investigators have chosen to generate swirled in a radial inflow plane in order to take advantage of the simple cascade design geometry. Others have preferred to use axial cascade which have the advantage that they more closely simulate specific turbo machinery flow condition and permit control of the spacing between the diffuser and the vanes in form that may be more typical of an actual turbo machine. On the other hand axial cascade invariably introduces tip and hub leakage since the cascades are of a variable geometry type, an effective sealing is impossible. In addition to inlet swirl, there may be changes in inlet turbulence intensity, velocity or total pressure gradients, vorticity or wake shading, and inlet aerodynamic blockage may change indirectly as a function of the swirl angle as it is varied. In order for firm conclusion to be drawn, the effect of swirl variation must be deciphered from the performance data.

Divehi and Kartavenko [1975] also reported by the same type of study that the best performance can be achieved between the ranges of 10º to 20º of inlet swirl angle. A study is presented by Japikse and Pamprreen [1979] of an exhaust diffuser and hood found that substantial recovery has been achieved even up to swirl angle in excess of 40º. Steenbergen W. J. Voskamp [1998] the rate of decay of swirl in turbulent pipe flow. He found that on increase of swirl number the rate of increase. Guo Bayou et al [2001]done the CFD simulation of precession in sudden pipe expansion flows with low inlet swirl. It seems that higher swirl level require fine grid. Numerical Investigation of Swirling Flow in Annular Diffusers With a Rotating Hub Installed at the Exit of Hydraulic Machines is done by Kochevsky A.N. [2000] Numerical investigation of swirl flow on conical diffuser was done by the Walter Gyllenram et al [2004] . Najafi A.F. [2005] have done. Numerical analysis of turbulent swirling decay pipe flow The flow characteristics through a rotating honeycomb and resulting downstream swirling decay flow through a fixed pipe have been investigated in this research. The modelling of the rotating honeycomb is observed to be of major importance for the prediction of the downstream flow. Several methods are used and tested. The flow field properties obtained by the honeycomb tubes which are the

annular cylinders in our axi-symmetric computations have a considerable effect on the downstream flow. Ogor Buntiæ et al, [2006]give the An Adaptive Turbulence Model for Swirling Flow .

Srinath [1968] considered an axial flow equiangular diffuser with swirl between 0° and 15°. Peak pressure recovery was found at approximately 10°and then decreased rapidly. Hoadley and Hughes [1969] tested an annular diffuser with a cylindrical inner body and reported that best recovery was achieved at approximately 10° of swirl.

2.2.3 Inlet Turbulence

With long approach pipes diffuser performance rises as approach length increases. This was first noted in the Cockrell and Markland [1963] and attributed this to changes in turbulence which enhances mixing transverse to flow directions, thus reducing the distortions. Indeed, the core turbulence intensity of developing pipe flow rises significantly from La /D is equal to 20 to 45 and than remains nearly constant. Two studies have been published which considered variation in inlet turbulence intensity or structure for there impact on annular diffuser performance. The data of Coladieiepro et al [1974] have included both low and high inlet turbulence intensity levels, and this may be explanation for the unusual measurements observed at different blockage. The second study is the work of Williams and Stevens [1969] and Stevens and Fry [1973], which showed that substantial improvements in radial momentum transport were achieved by turbulence producing grids and wall spoilers. Additional results by Hestermann et al [1995] and Klein [1995] also show that increasing the level of turbulence to 6 – 8.5 % is beneficial in increasing the pressure recovery and, in one case of removing the separation of stalled diffuser. Ubertini and Desideri [2000] determined the flow development in terms of the mean and fluctuating components of the velocity and turbulence dissipating eddy length scales in annular exhaust diffuser. The K-ε and other turbulent models are evaluated with respect to their applicability in swirling flows by Arora.B.B. et.al [2005]. In most of the past numerical simulations, swirling air is introduced around this, in most cases perpendicular to the axis. In this configuration, it is straightforward to specify the inlet velocity profiles Ogor Buntic et al, [2006] studied various Turbulence Model for Swirling Flow. Leschziner M.A.[2004] had done modelling turbulent separated flow in the context of aerodynamic applications. Bajcar Tom et al [2006] Heat transfer influenced by turbulent airflow inside an axially rotating diffuser. Tornblom

Olle[2006] give an Experimental and computational studies of turbulent separating internal flows The experimental investigation of the mean flow and turbulence properties revealed a flow with several interesting characteristics: strong and suddenly imposed shearing, non-equilibrium turbulence, separation, reattachment and turbulence relaxation. The conclusion of above study is that the effect of increasing inlet turbulence intensity is to increase pressure recovery.

2.2.4 Mach number Influence

Most annular diffuser research has been carried out at low inlet mach numbers. However, several studies have shown measurement at different Mach number. The study by Thayer [1971], Wood and Henry [1958] and Japikse and Pampreen [1979] illustrate virtual independence of recovery with Mach number up to some critical level of approximately 0.80 to 1.1. The actual level depends on method of measurement and the type of inlet. Wood and Henry [1971] show that a shock structure must be presented before the performance begins to deteriorate, but the reference Mach number may have little to do with the actual shock location and shock structure.

2.2.5 Reynolds Number Influence

Viscosity is an important parameter in any fluid dynamic process and normally appears in the form of a Reynolds number. Typically, diffusers are characterized by a Reynolds number based on an inlet hydraulic diameter. All studies reported that the Reynolds number is a comparatively weak parameter as long as the flow is in the fully turbulent regime. Crockrell and Markland [1963] state that a variation of the inlet Reynolds number has no significant effect on the diffuser performance if this variation is uncoupled from its effects on the inlet boundary layer parameters. For Reynolds number variation within the range of $2\times10^4 - 7\times10^5$, they also pointed out that the diffuser performance would be practically independent of Reynolds number provided the inlet boundary parameters remain constant. Sharan [1972] reported that for thick boundary layers, there is no change in pressure recovery as the Reynolds number increases.

2.2.6 Boundary Layer Parameter

The flow in diffuser is governed by the behaviour of the boundary layers at the diffuser walls. The deceleration of the flow through the diffuser produces a pressure rise in the stream wise direction. The wall shear layers are therefore subjected to a positive or adverse pressure gradient. As is well known, an adverse pressure gradients cause the wall boundary layers to thicken and possibly separate from the diffuser walls, forming areas of backflow in the diffuser. The net result of thinking of the wall boundary layers or the formation of regions of backflow is the blockage of flow area which reduces the effective area available to the flow. Reduction in effective flow area in turn results in a reduced pressure rise through the diffuser.

2.2.7 Boundary Layer Suction

The effect of suction consists in the removal of decelerated fluid particles from the boundary layer before they are given a chance to cause separation. Wilbur and Higginbotham [1957] investigated the suction phenomenon and found that a suction flow rate of 2.3% increased the static pressure rise by 25 – 60% and decreased the measured total pressure loss by 63%. In another study by Wilbur and Higginbotham [1955], it is shown that suction control is not efficient when applied in an extensive backflow region such as exists immediately downstream of an abruptly turned body. Experiments by Juhasz [1974], on short annular diffuser showed that the diffuser exit profiles could be shifted either towards the hub or towards the casing of annulus by bleeding off a small fraction of the flow through the inner and outer wall respectively. Boundary Layer Suction is also adopted by Ackert [1967], for both channel and conical diffuser with large divergence angle.

2.2.8 Blowing and Injection

Wilbur and Higginbotham [1955], found that at an injection rate of 3.4%, a 33% increases in the measured static pressure rise and a 50% decrease in the measured total pressure loss can be obtained. Juhasz [1974], have reported results of their investigations on the effect of injecting secondary fluid into wild angle conical diffusers through annular slot at inlet. Injection was found to result in considerable improvement in the uniformity of exit flow as well as in the magnitude of pressure recovery.

CFD ANALYSIS CHAPTER 3

FLUENT is a state-of-the-art computer program for modeling fluid flow and heat transfer in complex geometries. FLUENT provides complete mesh flexibility, solving your flow problems with unstructured meshes that can be generated about complex geometries with relative ease. Supported mesh types include 2D triangular/quadrilateral, 3D tetrahedral/hexahedral/pyramid/wedge, and mixed (hybrid) meshes. FLUENT also refine or coarsen grid based on the flow solution.

3.1 Program Capabilities

The FLUENT solver has the following modeling capabilities:

- 2D planar, 2D axisymmetric, 2D axisymmetric with swirl (rotationally symmetric), and 3D flows
- Quadrilateral, triangular, hexahedral (brick), tetrahedral, prism (wedge), pyramid, polyhedral, and mixed element meshes
- Steady-state or transient flows
- Incompressible or compressible flows, including all speed regimes (low subsonic, transonic, supersonic, and hypersonic flows)
- Inviscid, laminar, and turbulent flows
- Newtonian or non-Newtonian flows
- Heat transfer, including forced, natural, and mixed convection, conjugate (solid/fluid) heat transfer, and radiation
- Chemical species mixing and reaction, including homogeneous and heterogeneous combustion models and surface deposition/reaction models
- Free surface and multiphase models for gas-liquid, gas-solid, and liquid-solid flows
- Lagrangian trajectory calculation for dispersed phase (particles/droplets/bubbles), including coupling with continuous phase and spray modeling
- Cavitation model
- Phase change model for melting/solidification applications

- Porous media with non-isotropic permeability, inertial resistance, solid heat conduction, and porous-face pressure jump conditions
- Lumped parameter models for fans, pumps, radiators, and heat exchangers
- Acoustic models for predicting flow-induced noise
- Inertial (stationary) or non-inertial (rotating or accelerating) reference frames
- Multiple reference frame (MRF) and sliding mesh options for modeling multiple moving frames
- Mixing-plane model for modeling rotor-stator interactions, torque converters, and similar turbo-machinery applications with options for mass conservation and swirl conservation
- Volumetric sources of mass, momentum, heat, and chemical species

FLUENT is ideally suited for incompressible and compressible fluid-flow simulations in complex geometries.

3.2 Planning CFD Analysis

The following consideration should be taken while planning CFD analysis:

3.2.1 Definition of the Modeling Goals:

What specific results are required from the CFD model and how will they be used? What degree of accuracy is required from the model?

3.2.2 Grid Generation and its Independence:

What type of element will be used? What size of the mesh should be kept so as to optimize between accuracy and time and resources being cosumed?

3.2.3 Choice of the Computational Model:

How will you isolate a piece of the complete physical system to be modeled? Where will the computational domain begin and end? What boundary conditions will be used at the boundaries of the model? Can the problem be modeled in two dimensions or is a three-dimensional model required? What type of grid topology is best suited for this problem?

3.2.4 Choice of Physical Models:

Is the flow inviscid, laminar, or turbulent? Is the flow unsteady or steady? Is heat transfer important? Will you treat the fluid as incompressible or compressible? Are there other physical models that should be applied?

3.2.5 Determination of the Solution Procedure:

Can the problem be solved simply, using the default solver formulation and solution parameters? Can convergence be accelerated with a more judicious solution procedure? Will the problem fit within the memory constraints of your computer, including the use of multigrain? How long will the problem take to converge on your computer?

Careful consideration of these issues before beginning CFD analysis will contribute significantly to the success of modeling effort.

3.3 Discretization

The governing equations are converted into algebraic equations with the help of the finite volume technique that can be solved numerically. This control volume technique consists of integrating the governing equations about each control volume, yielding discrete equations that conserve each quantity on a control-volume basis.

Discretization of the governing equations can be illustrated most easily by considering the steady-state conservation equation for transport of a scalar quantity φ. This is demonstrated by the following equation written in integral form for an arbitrary control volume V as follows:

$$\oint \rho\phi \vec{v} . d\vec{A} = \oint \Gamma_\phi \nabla\phi . d\vec{A} + \int_V S_\phi dV$$

where

ρ = density

v = velocity vector A = surface area vector

Γ_φ = diffusion co-efficient for φ

φ = gradient of φ

S_φ = source of φ per unit volume

Above equation is applied to each control volume, or cell, in the computational domain. Discretization of Equation on a given cell yields

$$\sum_f^{N_{faces}} \rho_f \vec{v}_f \phi_f . \vec{A}_f = \sum_f^{N_{faces}} \Gamma_\phi (\nabla\phi)_n . \vec{A}_f + S_\phi V$$

Where

N_{faces} = number of faces enclosing cell

φf	=	value of φ convected through face f
$\rho_f v_f A_f$	=	mass flux through the face
A_f	=	area of face f, $\|A$
$(\varphi)_n$	=	magnitude of φ normal to face f
V	=	cell volume

The equations take the same general form as the one given above and apply readily to multi-dimensional, unstructured meshes composed of arbitrary polyhedral, the discrete values of the scalar φ at the cell centers. However, face values φ_f is required for the convection terms in Equation and must be interpolated from the cell center values. This is accomplished using an upwind scheme.

Up winding means that the face value φf is derived from quantities in the cell upstream, or "upwind," relative to the direction of the normal velocity v_n

3.4 Convergence Criteria

Finally, one needs to set the convergence criteria for the iterative method. Usually, there are two levels of iterations, within which the linear equations are solved and outer iteration that deal with the non-linearity and coupling of the equations. Deciding when to stop the iterative process on each level is important, from both the efficiency and accuracy point of view. A numerical is said to be convergent if the solution of the discretized equations tend to exact the solution of the differential as the grid spacing tends to be zero. For convergence criteria around 10^{-6} for X velocity variable, the results are stable in the present problem.

3.5 Implementation of boundary conditions

Each CV provides one algebric equation. Volume integrals are calculated for every control volume, but flux through Cv faces coinciding with the domain boundary requires special treatment. These boundary fluxes must be known, or be expressed as a combination of interior values and boundary data. Two types of boundary conditions need to be specified.

3.5.1 Inlet boundary condition

The present analysis involves the velocity with and without swirl. The incorporation of velocity without swirl can be specified by any one of the velocity specification

methods described in FLUENT. Turbulence intensity is specified as

$I = 0.16(Re_{DH})^{-1/8}$ x100

The inlet based on the Reynolds number with respect to equivalent flow diameter.

Where, Re_{DH} is the Reynolds number based on the hydraulic diameter.

For specifying the velocity in case of flow with swirl, tangential component of velocity will also have to be defined along with axial component. Inlet velocity of 60 m/s with flat profile is considered for both the cases.

3.5.2 Outlet boundary condition

Atmospheric pressure condition is applied at the outlet boundary condition and set a "back flow" conditions is also specified if the flow reverses direction at the pressure outlet boundary during the solution process. In the "back flow" condition turbulence intensity is specified based on the equivalent flow diameter.

3.5.3 Wall boundary condition

Wall boundary conditions are used to bind fluid and solid regions. In viscous flows the no slip boundary condition is enforced at the walls. Wall roughness affects the drag (resistance) and heat and mass transfer on the walls. Hence roughness effects were considered for the present analysis and a specified roughness based on law of wall modified for roughness is considered. Two inputs to be specified are the physical roughness height and the roughness constant. And the default roughness constant (0.5) is assigned which indicates the uniform sand grain roughness.

3.6 Simulation Procedure

(STEP 1) Modeling (In Gambit):

- Diffuser geometry is created
- Stabilizing length equal to D was attached at inlet.
- Boundary layer was attached to both the hub and casing wall with growth factor 1.1 and 10 rows.
- The model has been meshed with quadratic-mesh. Fine meshing with spacing 0.07 was done and mesh elements range from 12000 – 75000 elements.

- Boundary conditions taken were for velocity at inlet, pressure at outlet and wall type for both the hub and casing.
- Fluid was specified as air for the continuum type and the mesh was exported to Fluent for post processing.

(STEP 2) Post Processing (In Fluent):

- Grid was checked and scaled.
- 2D axisymmetric solver and segregated solution method was chosen.
- Air was chosen as the fluid for flow, and its properties were selected.
- K-ε RNG models is selected.
- At air inlet section, the inlet velocity of 60 m/s with different swirl intensity was specified.
- Turbulence intensity of 3% based on inlet flow diameter was specified. At the exit section, the pressure was specified being equal to atmospheric pressure.
- Second order upwind scheme was selected to solve continuity and momentum equations.
- Convergence criteria of 10^{-6} were taken.
- Solution was initialized at inlet and made to iterate until it converges.

Once solution is converged, various data for pressure and velocity were obtained and graphs were plotted.

MATHEMATICAL MODELLING CHAPTER 4

The present study involves various models and basic laws of fluid mechanics to attain the results. FLUENT provides comprehensive modeling capabilities for a wide range of incompressible laminar and turbulent fluid problems. In FLUENT, a broad range of mathematical models for transport phenomena (like heat transfer swirl and chemical reactions) is combined with the ability to model complex geometries. The range of problems that can be addressed is very wide. The turbulence models provided have broad range of applicability without the need for fine tuning to a specific application.

FLUENT uses four equations to simulate a 2-D flow problem in addition to the turbulence modelling equations. These four equations are:

- Conservation Principle
  - Momentum equation
  - Continuity equation
- Velocity Equations
  - X- velocity equation
  - Y- velocity equation

4.1 Conservation principals

Conservation laws can be derived considering a given quantity of matter or control mass and its extensive properties, such as mass, momentum and energy. This approach is used to study the dynamics of solid bodies. In fluid flows, however it is difficult to follow a parcel of matter. It is more convenient to deal with the flow within a certain spatial region we call a control volume, rather than a parcel of matter, which quickly passes through the region of interest. For all fluid flows the two extensive properties mass and momentum are solved. Flows involving heat and mass transfer or compressibility, an additional equation of energy conservation are solved. Additional flow transport equations are solved when the flow is turbulent.

4.1.1 Mass Conservation Equation (Continuity Equation)

The equation for conservation of mass, or continuity equation, can be written as follows:

$$\frac{\partial p}{\partial t} + \nabla.(\rho \overset{r}{v}) = S_m$$

Equation is the general form of the mass conservation equation and is valid for incompressible as well as compressible flows. The source S_m is the mass added to the continuous phase from the dispersed second phase (e.g., due to vaporization of liquid droplets) and any user-defined sources.

For 2D ax symmetric geometries, the continuity equation is given by

$$\frac{\partial p}{\partial t} + \frac{\partial}{\partial x}(\rho v_x) + \frac{\partial}{\partial r}(\rho v_r) = S_m$$

Where x is the axial coordinate, r is the radial coordinate, v_x is the axial velocity, and v_r is the radial velocity.

4.1.2 Momentum Conservation Equations

Conservation of momentum in an inertial (non-accelerating) reference frame

$$\frac{\partial}{\partial t}(\rho \overset{r}{v}) + \nabla.(\rho \overset{r}{v}\overset{r}{v}) = -\nabla p + \nabla.(\overline{\overline{\tau}}) + \rho \overset{r}{g} + \overset{r}{F}$$

where p is the static pressure, τ is the stress tensor (described below), and ρg and F are the gravitational body force and external body forces (e.g., that arise from interaction with the dispersed phase), respectively. F also contains other model-dependent source terms such as porous-media and user-defined sources.

The stress tensor τ is given by

$$\overline{\overline{\tau}} = \mu\left[\left(\nabla \vec{v} + \nabla \vec{v}^{T}\right) - \frac{2}{3}\nabla \cdot \vec{v} I\right]$$

Where μ is the molecular viscosity, I is the unit tensor, and the second term on the right hand side is the effect of volume dilation.

For 2D axisymmetric geometries, the axial and radial momentum conservation equations are given by

$$\frac{\partial}{\partial t}(\rho v_x) + \frac{1}{r}\frac{\partial}{\partial x}(r\rho v_x v_x) + \frac{1}{r}\frac{\partial}{\partial r}(r\rho v_r v_x) = -\frac{\partial p}{\partial x} + \frac{1}{r}\frac{\partial}{\partial x}\left[r\mu\left(2\frac{\partial v_x}{\partial x} - \frac{2}{3}(\nabla \cdot \overset{r}{v})\right)\right] + \frac{1}{r}\frac{\partial}{\partial r}\left[r\mu\left(\frac{\partial v_x}{\partial r} + \frac{\partial v_r}{\partial x}\right)\right] + F_x$$

and

$$\frac{\partial}{\partial t}(\rho v_r)+\frac{1}{r}\frac{\partial}{\partial x}(r\rho v_x v_r)+\frac{1}{r}\frac{\partial}{\partial r}(r\rho v_r v_r) = -\frac{\partial p}{\partial r}+\frac{1}{r}\frac{\partial}{\partial x}\left[r\mu\left(\frac{\partial v_r}{\partial x}+\frac{\partial v_x}{\partial r}\right)\right] + \frac{1}{r}\frac{\partial}{\partial r}\left[r\mu\left(2\frac{\partial v_r}{\partial r}-\frac{2}{3}(\nabla\cdot\vec{v})\right)\right]-2\mu\frac{v_r}{r^2}+\frac{2}{3}\frac{\mu}{r}(\nabla\cdot\vec{v})+\rho\frac{v_z^2}{r}+F_r$$

where

$$\nabla\cdot\vec{v}=\frac{\partial v_x}{\partial x}+\frac{\partial v_r}{\partial r}+\frac{v_z}{r}$$

and v_z is the swirl velocity

The tangential momentum equation for 2D swirling flows may be written as

$$\frac{\partial}{\partial t}(\rho v_z)+\frac{1}{r}\frac{\partial}{\partial x}(r\rho v_x v_z)+\frac{1}{r}\frac{\partial}{\partial r}(r\rho v_r v_z)=\frac{1}{r}\frac{\partial}{\partial x}\left[r\mu\frac{\partial v_z}{\partial x}\right]-\rho\frac{v_r v_z}{r} + \frac{1}{r^2}\frac{\partial}{\partial r}\left[r^3\mu\frac{\partial}{\partial r}\left(\frac{v_z}{r}\right)\right]$$

4.2 TURBULENCE MODELLING

Turbulent flows are characterized by fluctuating velocity fields. These fluctuations mix with transported quantities such as momentum, energy, and species concentration, and cause the transported quantities to fluctuate as well. Since these fluctuations can be of small scale and high frequency, they are too computationally expensive to simulate directly in practical engineering calculations. Instead, the instantaneous (exact) governing equations can be time-averaged, ensemble-averaged, or otherwise manipulated to remove the small scales, resulting in a modified set of equations that are computationally less expensive to solve. However, the modified equations contain additional unknown variables, and turbulence models are needed to determine these variables in terms of known quantities.

4.2.1 Choosing a Turbulence Model

It is an unfortunate fact that no single turbulence model is universally accepted as being superior for all classes of problems. The choice of turbulence model will depend on considerations such as the physics encompassed in the flow, the

established practice for a specific class of problem, the level of accuracy required, the available computational resources, and the amount of time available for the simulation. To make the most appropriate choice of model for your application, one needs to understand the capabilities and limitations of the various options. The purpose of this section is to give an overview of issues related to the turbulence models provided in FLUENT. The computational effort and cost in terms of CPU time and memory of the individual models is discussed. While it is impossible to state categorically which model is best for a specific application, general guidelines are presented to help you choose the appropriate turbulence model for the flow you want to model.

FLUENT provides the following choices of turbulence models:

- Spalart-Allmaras model
- k- ε models
  - Standard k- ε model
  - Renormalization-group (RNG) k- ε model
  - Realizable k- ε model
- k- ω models
  - Standard k- ω model
  - Shear-stress transport (SST) k- ω model
- Reynolds stress model (RSM)
- Large eddy simulation (LES) model

4.3 The Standard, RNG, and Realizable k- ε Models

All three models have similar forms, with transport equations for k and ε. The major differences in the models are as follows:

- the method of calculating turbulent viscosity
- the turbulent Prandtl numbers governing the turbulent diffusion of k and ε
- the generation and destruction terms in the ε equation

The transport equations, methods of calculating turbulent viscosity, and model constants are presented separately for each model.

4.3.1 The Standard k-ε Model

The simplest “complete models" of turbulence are two-equation models in which the solution of two separate transport equations allows the turbulent velocity and length scales to be independently determined. The standard k- ε model in FLUENT falls within this class of turbulence model and has become the workhorse of practical engineering flow calculations in the time since it was proposed by Launder and Spalding. Robustness, economy, and reasonable accuracy for a wide range of turbulent flows explain its popularity in industrial flow and heat transfer simulations. It is a semi-empirical model, and the derivation of the model equations relies on phenomenological considerations and empiricism.

The standard k- ε model is a semi-empirical model based on model transport equations for the turbulence kinetic energy (k) and its dissipation rate (ε). The model transport equation for k is derived from the exact equation, while the model transport equation for ε was obtained using physical reasoning and bears little resemblance to its mathematically exact counterpart.

For k- ε model, it was assumed that the flow is fully turbulent, and the effects of molecular viscosity are negligible, therefore valid only for fully turbulent flows.

4.3.2 Transport Equations for the Standard k-ε Model

The turbulence kinetic energy, k, and its rate of dissipation, ε, are obtained from the following transport equations:

$$\frac{\partial}{\partial t}(\rho k)+\frac{\partial}{\partial x_i}(\rho k u_i)=\frac{\partial}{\partial x_j}\left[\left(\mu+\frac{\mu_t}{\sigma_k}\right)\frac{\partial k}{\partial x_j}\right]+G_k+G_b-\rho\varepsilon-Y_M+S_k$$

and

$$\frac{\partial}{\partial t}(\rho\varepsilon)+\frac{\partial}{\partial x_i}(\rho\varepsilon u_i)=\frac{\partial}{\partial x_j}\left[\left(\mu+\frac{\mu_t}{\sigma_\varepsilon}\right)\frac{\partial \varepsilon}{\partial x_j}\right]+C_{1\varepsilon}\frac{\varepsilon}{k}(G_k+C_{3\varepsilon}G_b)-C_{2\varepsilon}\rho\frac{\varepsilon^2}{k}+S_\varepsilon$$

In these equations, G_k represents the generation of turbulence kinetic energy due to the mean velocity gradients. G_b is the generation of turbulence kinetic energy due to buoyancy. Y_M represents the contribution of the fluctuating dilatation in compressible turbulence to the overall dissipation rate. $C_{1\varepsilon}$, $C_{2\varepsilon}$, and $C_{3\varepsilon}$ are constants. σ_k and σ_ε are the turbulent Prandtl numbers for k and ε , respectively.

4.3.3 Modeling the Turbulent Viscosity

The turbulent (or eddy) viscosity, μ_t, is computed by combining k and ε as follows:

$$\mu_t = \rho C_\mu \frac{k^2}{\varepsilon}$$

where C_μ is a constant.

4.3.4 The model constants

$C_{1\varepsilon}$, $C_{2\varepsilon}$, C_μ, σ_k, and σ_v have the following default values:

$C_{1\varepsilon} = 1.44$, $C_{2\varepsilon} = 1.92$, $C_\mu = 0.09$, $\sigma_k = 1.0$, $\sigma_\varepsilon = 1.3$

These default values have been determined from experiments with air and water for fundamental turbulent shear flows including homogeneous shear flows and decaying isotropic grid turbulence. They have been found to work fairly well for a wide range of wall-bounded and free shear flows.

4.3.5 The RNG k-ε Model

The RNG-based k-ε turbulence model is derived from the instantaneous Navier-Stokes equations, using a mathematical technique called "renormalization group" (RNG) methods. It is similar in form to the standard k-ε model, but includes the following refinements:

- The RNG model has an additional term in its ε equation that significantly improves the accuracy for rapidly strained flows.
- The effect of swirl on turbulence is included in the RNG model, enhancing accuracy for swirling flows.
- The RNG theory provides an analytical formula for turbulent Prandtl numbers, while the standard k-ε model uses user-specified, constant values.
- While the standard k-ε model is a high-Reynolds-number model, the RNG theory provides an analytically-derived differential formula for effective viscosity that accounts for low-Reynolds-number effects. Effective use of this feature does, however, depend on an appropriate treatment of the near-wall region.

These features make the RNG k-ε model more accurate and reliable for a wider class of flows than the standard k-ε model.

4.3.6 Transport Equations for the RNG k-ε Model

The RNG k- ε model has a similar form to the standard k-ε model:

$$\frac{\partial}{\partial t}(\rho k)+\frac{\partial}{\partial x_i}(\rho k u_i)=\frac{\partial}{\partial x_j}\left[\alpha_k \mu_{eff}\frac{\partial k}{\partial x_j}\right]+G_k+G_b-\rho\varepsilon-Y_M+S_k$$

and

$$\frac{\partial}{\partial t}(\rho\varepsilon)+\frac{\partial}{\partial x_i}(\rho\varepsilon u_i)=\frac{\partial}{\partial x_j}\left[\alpha_k \mu_{eff}\frac{\partial \varepsilon}{\partial x_j}\right]+C_{1\varepsilon}\frac{\varepsilon}{k}(G_k+C_{3\varepsilon}G_b)$$
$$-C_{2\varepsilon}\rho\frac{\varepsilon^2}{k}-R_\varepsilon+S_\varepsilon$$

In these equations, G_k represents the generation of turbulence kinetic energy due to the mean velocity gradients. G_b is the generation of turbulence kinetic energy due to buoyancy. Y_M represents the contribution of the fluctuating dilatation in compressible turbulence to the overall dissipation rate,. The quantities α_k and α_ε are the inverse effective Prandtl numbers for k and ε, respectively. S_k and S_ε are user-defined source terms.

4.3.7 Modeling the Effective Viscosity

The scale elimination procedure in RNG theory results in a differential equation for turbulent viscosity:

$$d\left(\frac{\rho^2 k}{\sqrt{\varepsilon\mu}}\right)=1.72\frac{\tilde{\nu}}{\sqrt{\tilde{\nu}^3-1+C_\nu}}$$

where

$$\tilde{\nu}=\mu_{eff}/\mu \qquad C_\nu \approx 100$$

Equation is integrated to obtain an accurate description of how the effective turbulent transport varies with the effective Reynolds number (or eddy scale), allowing the model to better handle low-Reynolds-number and near-wall flows.

In the high-Reynolds-number limit, Equation gives

$$\mu_t = \rho C_\mu \frac{k^2}{\varepsilon}$$

with C_μ =0.0845, derived using RNG theory. It is interesting to note that this value of Cμ is very close to the empirically-determined value of 0.09 used in the standard k- ε model.

4.3.8 The Realizable k-ε Model

The realizable k-ε model is a relatively recent development and differs from the standard k-ε model in two important ways:

- The realizable k-ε model contains a new formulation for the turbulent viscosity.
- A new transport equation for the dissipation rate, ε, has been derived from an exact equation for the transport of the mean-square vorticity fluctuation.

The term “realizable" means that the model satisfies certain mathematical constraints on the Reynolds stresses, consistent with the physics of turbulent flows. Neither the standard k-ε model nor the RNG k- ε model is realizable. An immediate benefit of the realizable k-ε model is that it more accurately predicts the spreading rate of both planar and round jets. It is also likely to provide superior performance for flows involving rotation, boundary layers under strong adverse pressure gradients, separation, and recirculation. Since the model is still relatively new, it is not clear in exactly which instances the realizable k-ε model consistently outperforms the RNG model. One limitation of the realizable k-ε model is that it produces non-physical turbulent viscosities in situations when the computational domain contains both rotating and stationary fluid zones (e.g., multiple reference frames, rotating sliding meshes). This is due to the fact that the realizable k- ε model includes the effects of mean rotation in the definition of the turbulent viscosity**.** This extra rotation effect has been tested on single rotating reference frame systems and showed superior behavior over the standard k-ε model.

4.3.9 Transport Equations for the Realizable k-ε Model

The modeled transport equations for k and ε in the realizable k-ε model are

$$\frac{\partial}{\partial t}(\rho k)+\frac{\partial}{\partial x_i}(\rho k u_i)=\frac{\partial}{\partial x_j}\left[\left(\mu+\frac{\mu_t}{\sigma_k}\right)\frac{\partial k}{\partial x_j}\right]+G_k+G_b-\rho\varepsilon-Y_M+S_k$$

and

$$\frac{\partial}{\partial t}(\rho\varepsilon)+\frac{\partial}{\partial x_i}(\rho\varepsilon u_i)=\frac{\partial}{\partial x_j}\left[\left(\mu+\frac{\mu_t}{\sigma_\varepsilon}\right)\frac{\partial \varepsilon}{\partial x_j}\right]+\rho C_1 S_\varepsilon+C_{1\varepsilon}\frac{\varepsilon}{k}(C_{3\varepsilon}G_b)$$
$$-C_2\rho\frac{\varepsilon^2}{k+\sqrt{\nu\varepsilon}}+S_\varepsilon$$

where

$$C_1=\max\left[0.43,\frac{\eta}{\eta+5}\right] \qquad \eta=S\frac{k}{\varepsilon}$$

4.3.10 Modeling the Turbulent Viscosity

As in other k-ε models, the eddy viscosity is computed from

$$\mu_t=\rho C_\mu\frac{k^2}{\varepsilon}$$

The difference between the realizable k-ε model and the standard and RNG k-ε models is that C_μ is no longer constant. It is computed from

$$C_\mu=\frac{1}{A_0+A_s\frac{kU^*}{\varepsilon}}$$

where

$$U^*=\sqrt{S_{ij}S_{ij}+\tilde{\Omega}_{ij}\tilde{\Omega}_{ij}}$$

and

$$\tilde{\Omega}_{ij}=\Omega_{ij}-2\varepsilon_{ijk}\omega_k$$
$$\tilde{\Omega}_{ij}=\bar{\Omega}_{ij}-\varepsilon_{ijk}\omega_k$$

4.3.11 Model Constants

The model constants C_2, σ_k, and σ_ε have been established to ensure that the model performs well for certain canonical flows. The model constants are

$C_{1\varepsilon}$ = 1:44; C2 = 1:9; σ_k = 1:0; σ_ε = 1:2

4.4 Turbulence Modeling in Swirling Flows

If you are modeling turbulent flow with a signiflcant amount of swirl (e.g., cyclone flows, swirling jets), you should consider using one of FLUENT's advanced turbulence models: the RNG k-ε model, realizable k- ε model, or Reynolds stress model. The appropriate choice depends on the strength of the swirl, which can be gauged by the swirl number. The swirl number is deflned as the ratio of the axial flux of angular momentum to the axial flux of axial momentum:

$$S = \frac{\int r\omega\upsilon . dA}{R\int u\upsilon . dA}$$

where R is the hydraulic radius.

For swirling flows encountered in devices such as cyclone separators and swirl combustors, near-wall turbulence modeling is quite often a secondary issue at most. The fldelity of the predictions in these cases is mainly determined by the accuracy of the turbulence model in the core region. However, in cases where walls actively participate in the generation of swirl (i.e., where the secondary flows and vortical flows are generated by pressure gradients), non-equilibrium wall functions can often improve the predictions since they use a law of the wall for mean velocity sensitized to pressure gradients.

VALIDATION CHAPTER 5

5.1 Grid Independence

For grid independence an experimental inlet profile was taken with casing and hub diverging at same angle of 10° without any swirl. At a velocity profile of 60m/s. The grid independence is studied for the k-ε RNG model employing four sizes of grids to examine the sensitivity of grid. As we decrease the mesh size we get a more fine mesh and better results, but due to more numbers of nodes the computation time increases. So we have to optimize the grid size with the accuracy required. We took the following mesh sizes:

	Element Type	Mesh Size	No. of Cells	No. of Face	No. of Nodes	Computation Time (hrs)
Coarse mesh	**Quad.**	**0.09**	**37076**	**74812**	**37737**	**3.5**
Fine mesh	**Quad.**	**0.08**	**45024**	**90787**	**45764**	**6.1**
Finer mesh	**Quad.**	**0.07**	**56064**	**112969**	**56906**	**12.2**
Finer mesh	**Quad.**	**0.06**	**73554**	**148087**	**74534**	**19.9**

5.1.1 Validation with experimental results [5]:-

Velocity Graph:

- Figure 00 shows with k-ε RNG model the results of mesh size of 0.08 and 0.09 cm shows deviation in there values, thus need to go for more finer mesh.
- The results of mesh size 0.06 and 0.07 remain almost same, thus mesh size of 0.07 cm is considered optimum for the CFD modeling of diffuser.

Pressure coefficient Graph:

Figure 00 shows that k-ε RNG model has least variation from experimental results[5].

- At casing:
- At hub:

All mesh gave same results, which shows that pressure coefficient was grid independent much before the mesh size of 0.09 cm, but there is variation in velocity values.

5.2 Turbulence Model Validation:

FLUENT provide many models to model the turbulence in the flow. But the following turbulence models and were test against experimental results [5]:

- k- ε models
  - Standard k- ε model
  - Renormalization-group (RNG) k- ε model
  - Realizable k- ε model
- Reynolds stress model (RSM)

These models were tested against an experimental profile with casing and hub diverging at same angle of 10° with swirl of 0° and 12° separately. At a velocity profile of 60m/s.

5.2.1 Validation with experimental results [5]:-

Velocity Graph with velocity of 60m/s and no swirl (0°):

Figure 00 shows that k-ε RNG model most nearer to the experimental results[5].

- At x= 0.3L: RNG and Realizable are very near to the experimental results.
- At x= 0.5L: RNG and Realizable are very near to the experimental results, but Realizable start deviating from experimental results
- At x= 0.7L: Only RNG model is in accordance to the experimental results
- At x= 0.9L: Only RNG model has least variation from experimental results

Pressure coefficient Graph:

Figure 00 shows that k-ε RNG model has least variation from experimental results[5].

- At casing: RNG model results are marginally higher than the experimental results, but are closer to the experimental results.
- At hub: RNG model results are marginally higher than the experimental results, but are closer to the experimental results than any other model.

Velocity Graph with velocity of 60m/s and swirl of 12°:

Figure 00 shows that k-ε RNG model most nearer to the experimental results [5].

- Ø At x= 0.3L: Almost every model varies from experimental results.
- Ø At x= 0.5L: RNG and Reynolds Stress model are near to the experimental results.
- Ø At x= 0.7L: Only RNG model is in accordance to the experimental results.
- Ø At x= 0.9L: Only RNG model results are nearer to the experimental results

Pressure coefficient Graph:

Figure 00 shows that k-ε RNG model has least variation from experimental results[5].

- Ø At casing: RNG model results are marginally higher than the experimental results, but are closer to the experimental results.
- Ø At hub: RNG model results are marginally higher than the experimental results, but are closer to the experimental results than any other model.

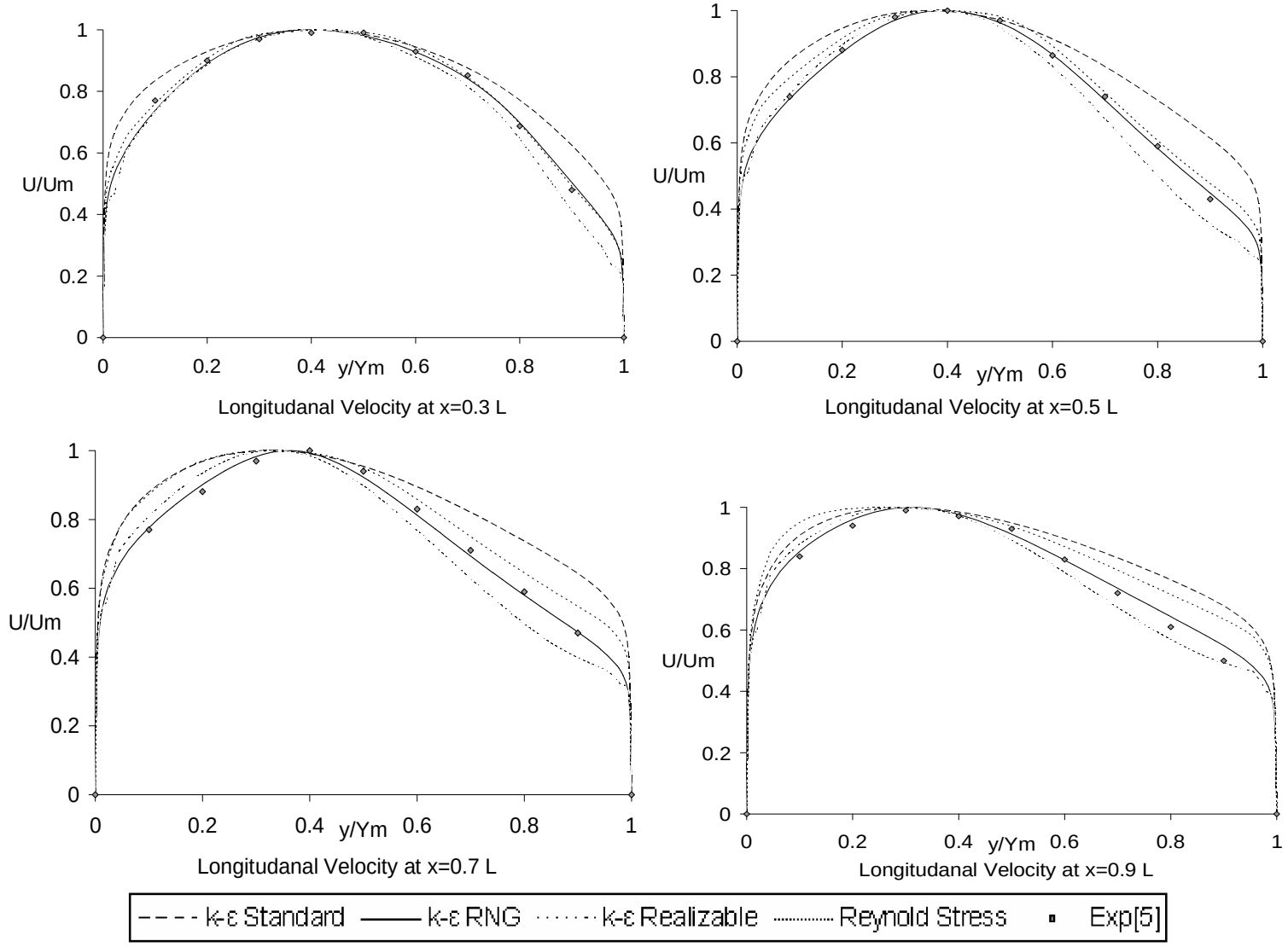

Figure 5.1: Longitudinal Velocity (0°) Exp10/10, AR 2

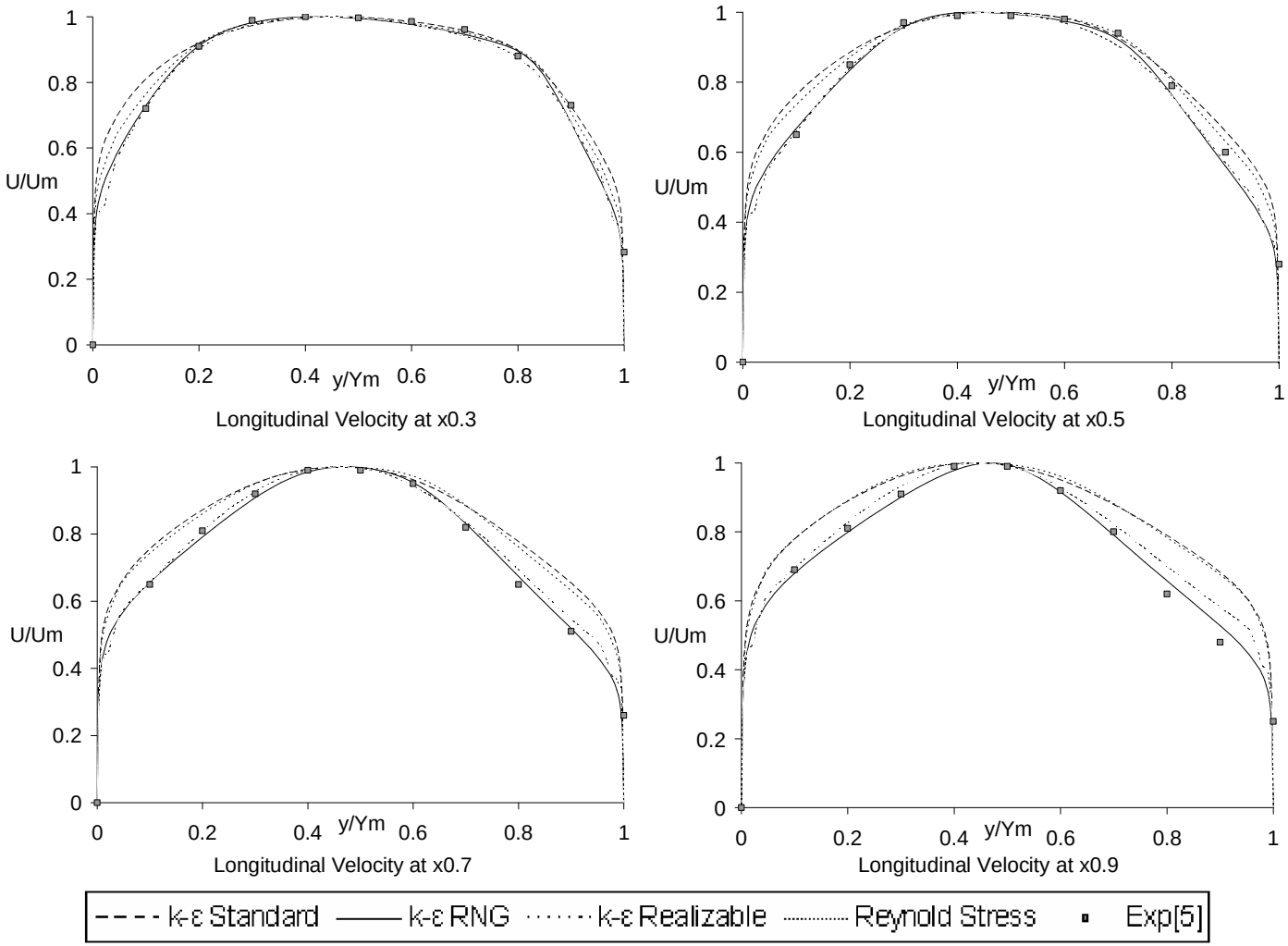

Figure 5.2: Longitudinal Velocity (12°), Exp10/10, AR 2

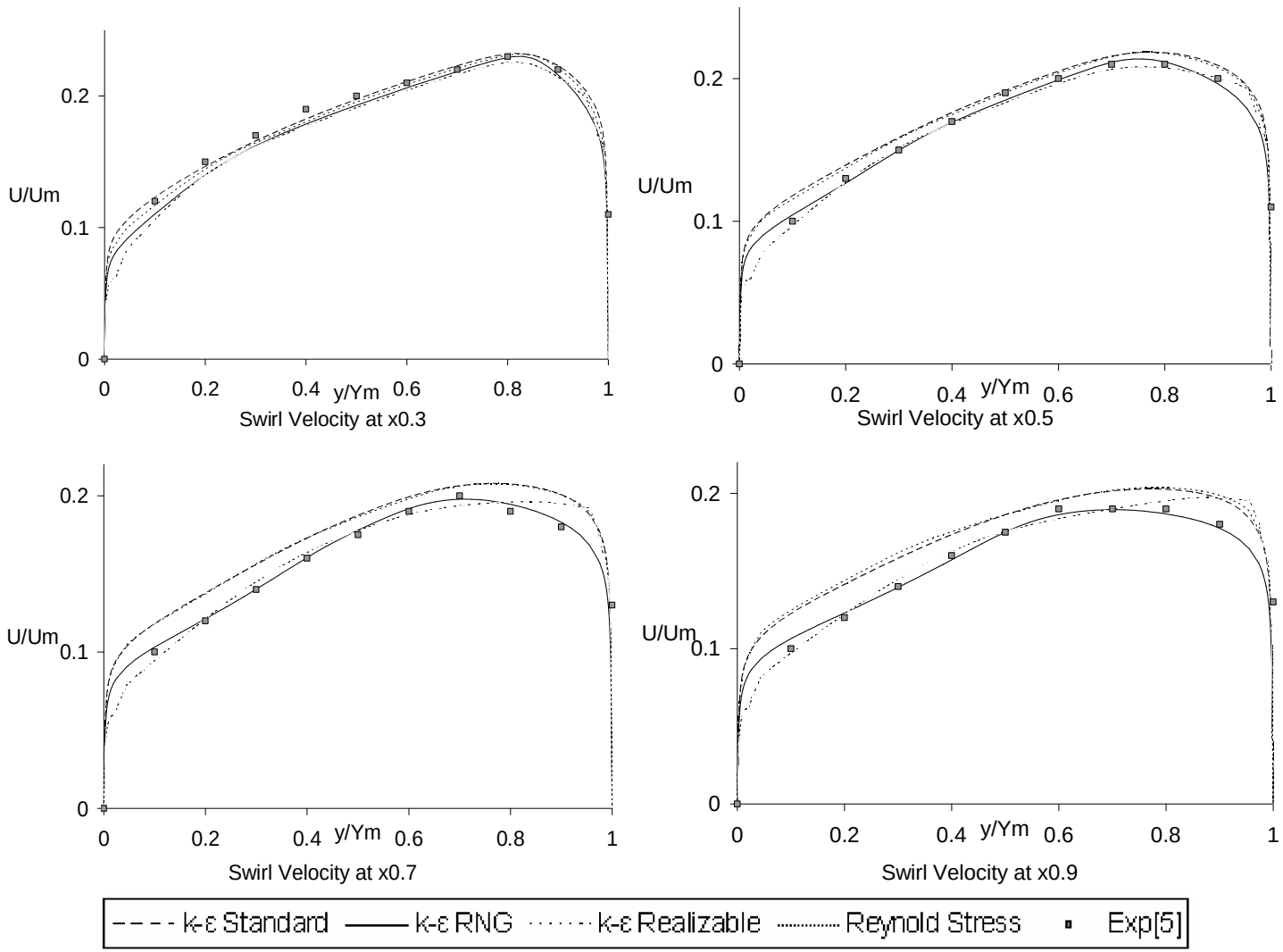

Figure 5.3: Swirl Velocity (12°), Exp10/10, AR 2

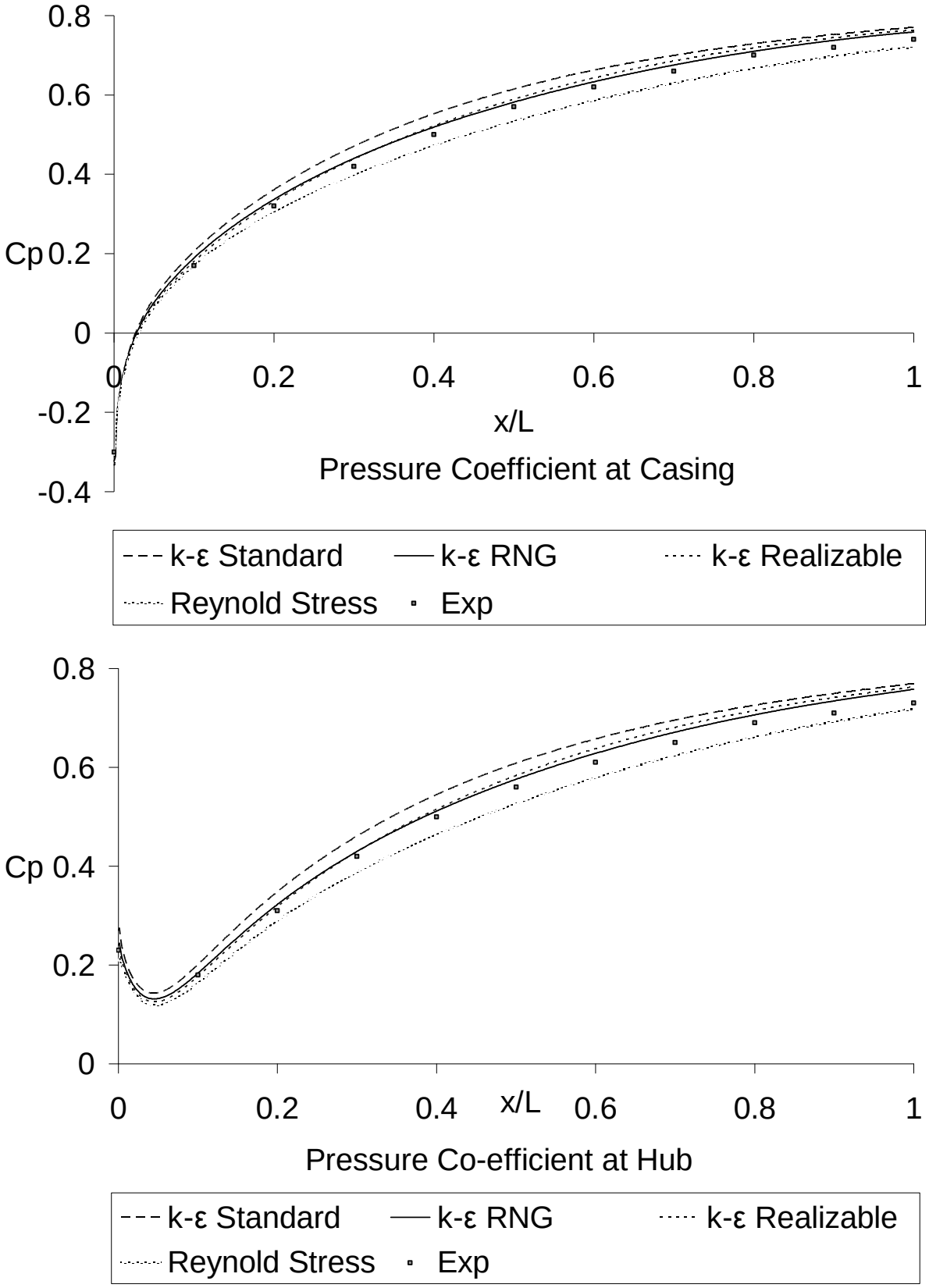

Figure 5.4: Pressure Coefficient (0°), Exp10/10, AR 2

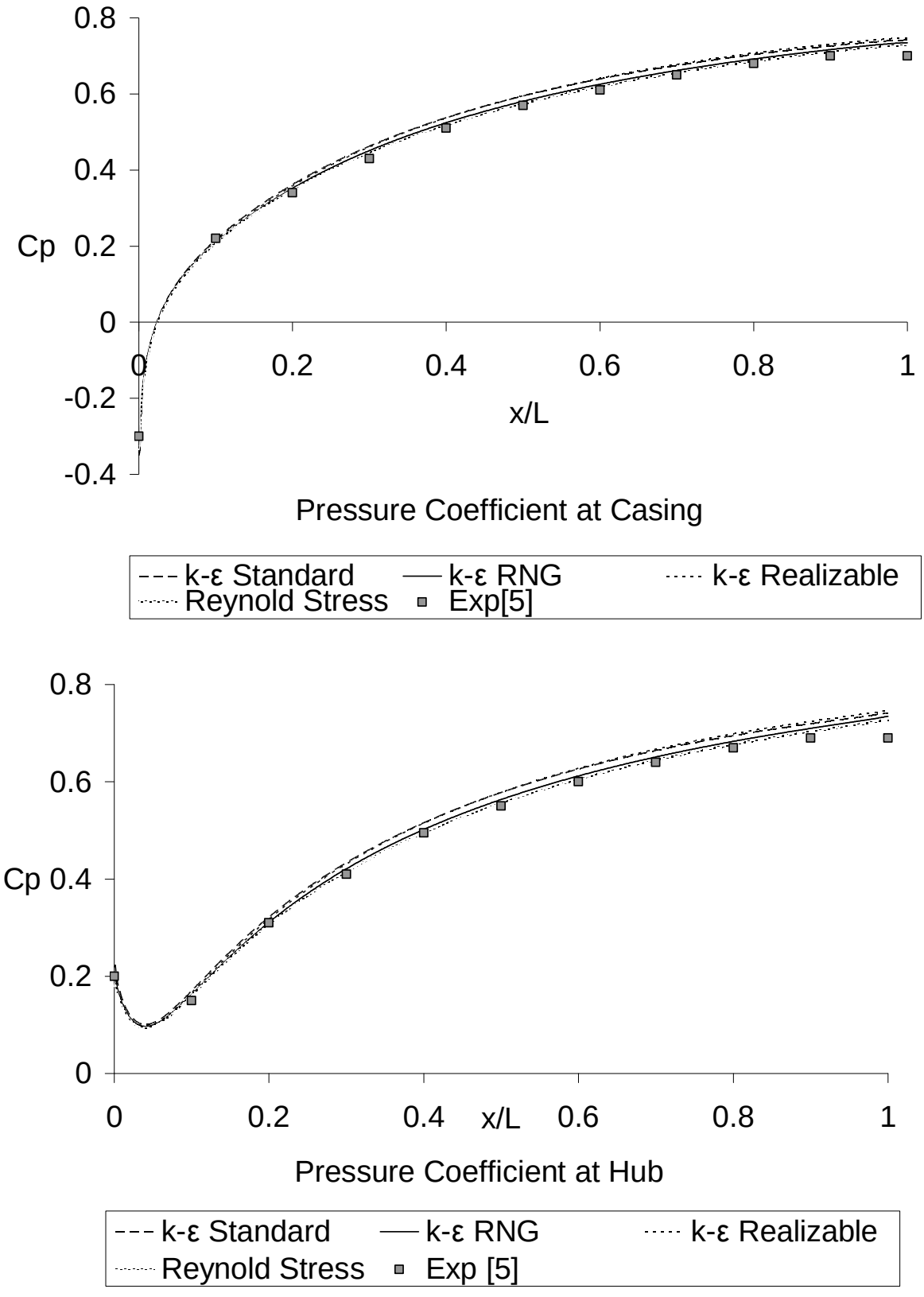

Figure 5.5: Pressure Coefficient (12°), Exp10/10, AR 2

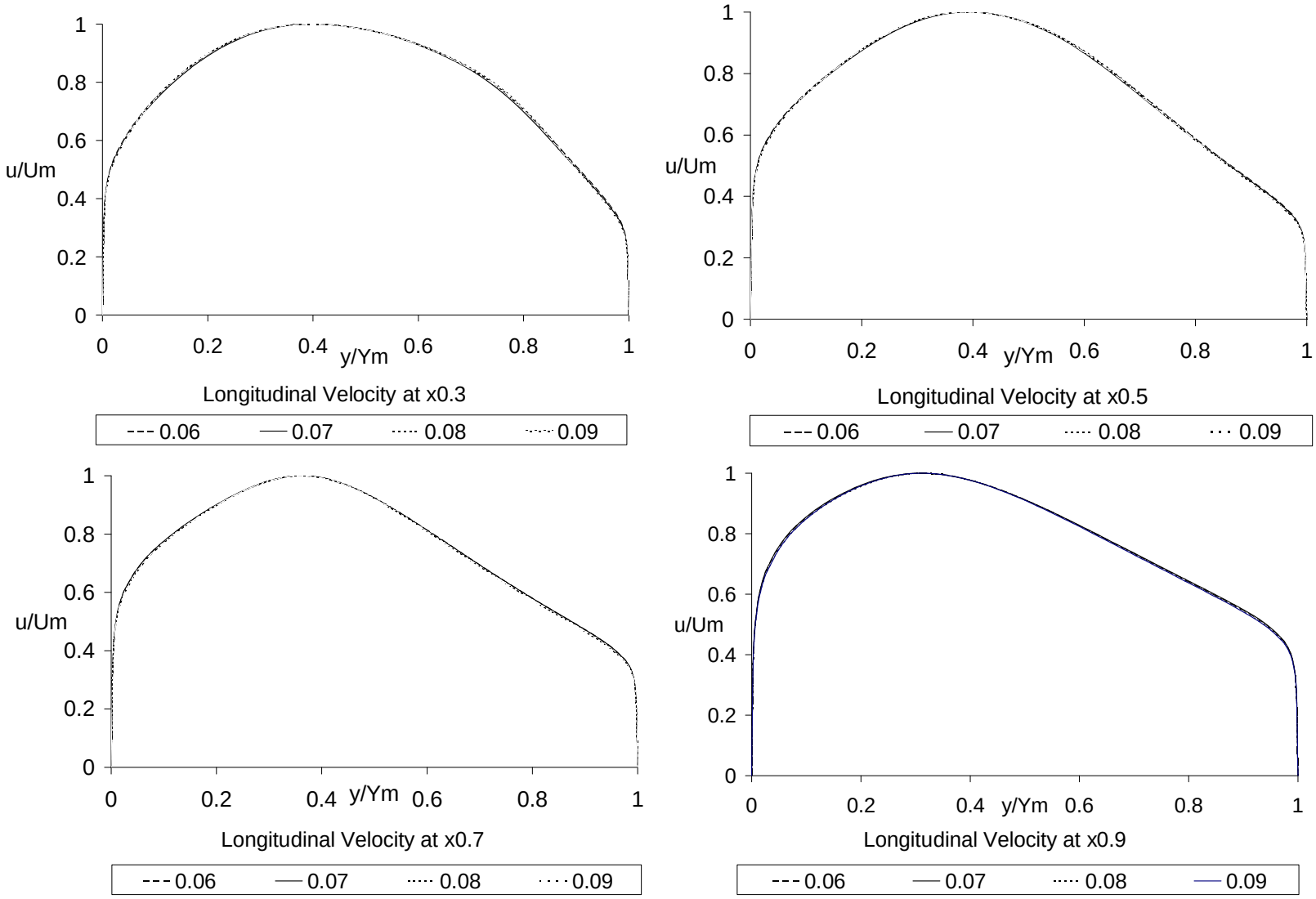

Figure 5.6: Longitudinal Velocity (0°), Exp10/10, AR 2

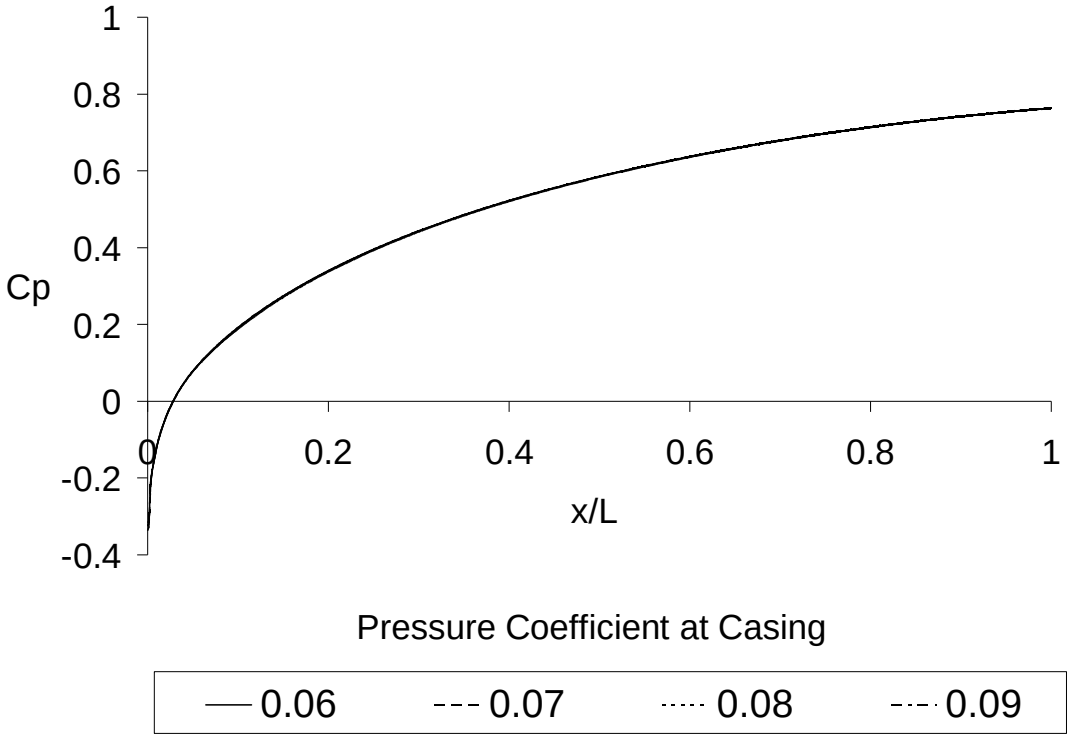

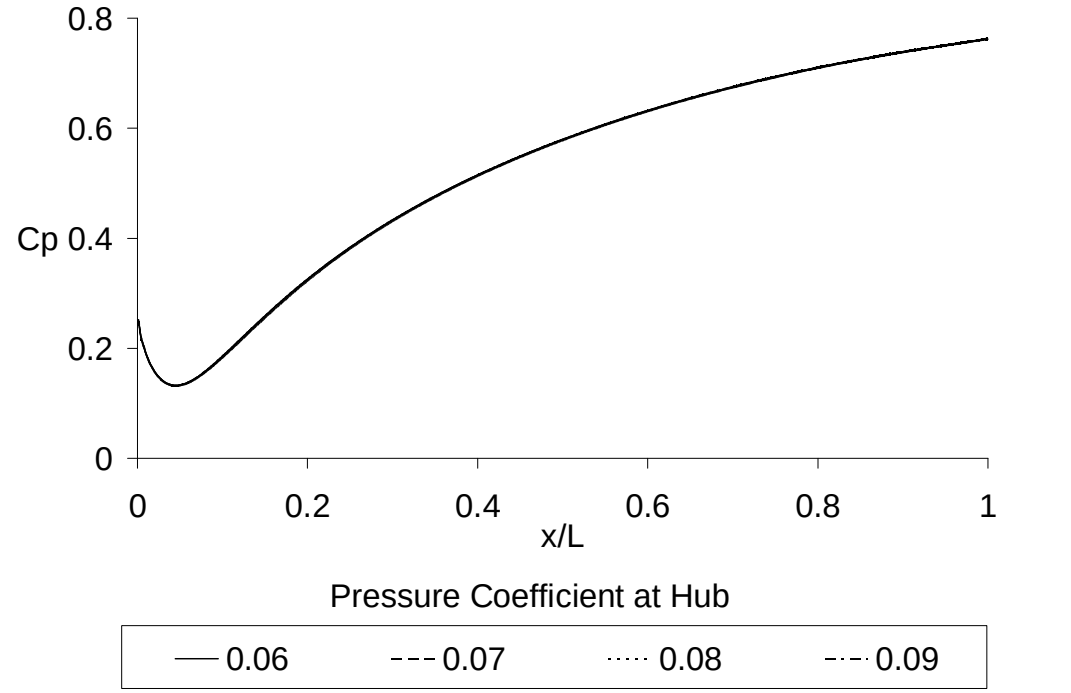

Figure 5.7: Pressure Coefficient (12°), Exp10/10, AR 2

CHAPTER 6

RESULTS AND DISCUSSION

Investigation of annular diffuser has been carried out with help of FLUENT, a CFD tool to simulate the effect of swirl on the pressure recovery. The annular diffuser considered is both hub and casing diverging type with constant area ratio. The velocity profile was of 60m/s with different swirling intensity as 0°, 12°, 17° and 25°. The flow is subsonic turbulent. It is assumed that the flow is exhausted to atmosphere, so pressure at exit of diffuser is assumed to be atmospheric.

Analysis gives the effect of inlet swirl on pressure recovery coefficient, boundary layer effect, reverse flow in diverging part of diffuser and pressure on hub and casing wall.

The following conclusions can be drawn from the results

1. Fig 1-12 shows the result generated by FLUENT. In these figures the fluid characteristics like velocity and pressure coefficient are shown by different colors. A particular color does not give single value of these characteristics, but shows the range of these values. If the value of a characteristic at a particular point falls in this range, there will be color of that range.
2. Fig 1 &28 shows that Up to casing wall angle of 15° there is no separation at the casing wall for no swirl condition.
3. From 6 , 9 ,31 & 34, it is explicit that for casing wall angle of 20° & 25°, separation occurs at the casing wall for no swirl condition and it increases with any further enhancement of casing wall angle. Hence, it can be concluded that for no swirl condition optimum casing wall exists between 15° and 20°.
4. Fig 38 shows that for casing wall angle of 15°, no separation is observed up to swirl of 12° and for swirl of 17° separation is observed on the hub. And as the swirl increase beyond this value separation expands over the more length of diffuser.
5. For casing wall angle of 20° and no swirl condition, separation is observed at the casing and it increases with increment in swirl value. Up to swirl of 12° separation occurs on casing side. With further increase in swirl separation shifts

from casing to hub. For swirl of 17° separation is observed on the hub and it increases with an increment in swirl value. Hence, it can be concluded that to suppress the separation some swirl is necessary and its value lies between 12° to 17°. Similar trend is observed for casing wall angle of 25°. Fig.38 & 39 can be referred.

6. For no swirl condition, no separation is observed for 15° casing wall angle. There is a separation for casing wall angle of 20° and 25°. Hence for zero swirl conditions to avoid separation case wall angle lies between 20° to 25°. Fig 40 can be referred.
7. Up to swirl of 12°, there is no separation for casing wall angle of 15°. Separation is observed on casing for casing wall angle of 20° and 25°. Hence for swirl of 12° condition optimum case wall angle lies between 20° to 25°. Fig 41 can be referred
8. For swirl of 17°, separation is observed on hub side of diffuser for all casing wall angle of 15°, 20°& 25°. Hence for swirl of 17° to avoid separation casing wall should be less than 15°. Fig 42 can be referred.
9. For casing wall angle of 15°, pressure coefficient increases with increase in swirl. Maximum pressure recovery is obtained for swirl of 12°.With further increase in swirl results in fall of pressure coefficient. Similar trend is followed for casing wall angle of 20° & 25°. Maximum value of pressure recovery coefficient for casing wall angle is 0.74 and minimum value is 0.43. These values decrease continuously with increase in casing wall angle. Hence maximum pressure recovery is obtained for casing wall angle of 15°. Fig 25, 26 & 27 can be referred.
10. Fig 13-16 show that the difference in pressure coefficient values for hub and casing wall increases with increase in swirl angle.
11. Over a short span of diffuser length the rate of pressure at casing wall increases with increase in swirl. Beyond the length of 70 percent of span, rate of pressure rise decrease with an increase in swirl beyond 17°. With increase in casing wall angle this span reduces and rate pressure rise increase only up to swirl of 12°. Fig 25- 27 can be referred.
12. Fig 28 - 35 shows the distribution of velocity at various section of diffuser during the flow for various casing wall angles. It can be seen from figures that at a

particular section longitudinal velocity increases rapidly and attains its maximum value then reduces to zero at casing. As the flow proceeds towards the outlet magnitude of maximum longitudinal velocity decreases. With increase in casing wall angle the point of maximum velocity shifts towards the hub because of separation at casing wall.

13. With an increase in swirl angle for constant casing wall angle the point of maximum velocity shifts towards the casing wall. Swirl causes the flow to divert towards the casing wall and reduces the zone of separation. For higher than 12° swirl the flow start separating near the hub wall as can be seen from fig 37.
14. Fig 44-46 shows the distribution of swirl velocity at various sections for various casing wall angle. it is observed that at inlet swirl velocity increases steeply than rate of increase decreases. The maximum swirl is observed near the casing at all sections. As the flow proceeds from inlet to outlet, the maximum swirl velocity position shifts away from the casing.
15. Casing wall angle has negligible effect on the maximum non dimensional swirl velocity. But with increase in Casing wall angle position of maximum swirl shifts towards the core.
16. Turbulence is affected by the swirl in the mean flow; hence in order to account for the effects of swirl the turbulent viscosity in k-ε model must be modified for swirling flows. The effect of swirl on the flow is well predicted by considering the advanced turbulence model (RNG k-ε) available in FLUENT code which yields an appreciable improvement in flow characteristics over the standard k-ε model.

RECOMMENDATIONS FOR FUTURE WORK CHAPTER7

- The present work was done for sub-sonic flow uncompressible flow only. The scope can be extended to compressible and sonic flows.

- Annular diffuser in considered in the present study. Future work can be done on conical, rectangular, radial type diffusers.

- The present analysis is done for a diverging type diffuser. As the geometry is an important parameter, which indicates the overall diffusion and hence varying the geometry type can extend further studies.

- The effect of hub-generated swirl can be considered for future study.

- The effect of Mach number can be studied.

- The present analysis is done for stationary hub and casing. Further studies can be done on rotating hub and casing diffuser.

- Modeling of the geometry can be modified by attaching a tailpipe at the exit to recover some of the excess kinetic energy of a non-uniform diffuser exit profile in to pressure energy.

- The analysis is basically performed with an advanced k-ε RNG model for swirling flows. Using higher order discretization schemes and better turbulence models can be used for better results in case of swirling flows.

REFRENCES

1. Ackert, J. 1967. “Aspect of Internal Flow. Fluid Mechanics of Internal Flow” Ed. Sovaran G., Elsvier Amsterdum, ppl.
2. Adkins R.C ,Jacobsen OH , Chevealier P, 1983, “A Premilary Study of Annular Diffuser With Constant Diameter Outer Wall” ASIVIE paper no. 83-GT-218
3. Adkins R.C., 1983. “A simple Method for Design Optimum Annular Diffusers” ASTVE Paper No. 83-GT-42.
4. Awai T., Nakagawa T., Sakai T., 1986. “Study of Axially Curved Mixed Flow Vane-less Diffuser”. Bull JSME 29, 1759-1764.
5. Arora, B.B., 2007, “Aerodynamic Analysis of Diffuser”, PhD Thesis, 2007, DU, Delhi.
6. Arora, B.B.,Pathak, B.D.,2005 “Flow characteristics of parallel hub diverging casing axial annular diffusers”. ISME publication pp 794-798.
7. Cockrell, D.J., Markland, E., 1963. “A Review of Incompressible Diffuser Flow” Aircraft Engg. Volume 35, pp 286.
8. Coladipietro, R., Schneider, J.M., Sridhar, K.1974. “Effects of Inlet Flow Conditions on the Performance of Equiangular Annular Diffusers,” Trans. CSME 3 (2): pp. 75-82.
9. Dovzhik, S.A., Kartavenko, V.M., 1975. “Measurement of the Effect of Flow Swirl on the Efficiency of Annular Ducts and exhaust Nozzles of Axial Turbo-machines,” Fluid Mechanics/Soviet Research 4(4): 156-172.
10. Goebel J. H., Japikse D., 1981. “The Performance of an Annular Diffuser Subject to Various Inlet Blockage and Rotor Discharge Effects “. Consortium Final Report, Creare TN-325.
11. Hesterman R., Kim S., Ban Khalid A., Witting S., 1995. “Flow Field and Performances Characteristics of Combustor Diffusers”. ASME Journal Engineering for Gas Turbine and Power 117, pp 686-694.
12. Hoadley D., 1970. “Three Dimensional Turbulent Boundary Layers in an Annular Diffuser “. Ph.D. Thesis University of Cambridge.
13. Hoadley D., Hughes D .W, 1969. “Swirling Flow in an Annular Diffuser”. University of Cambridge, Department of Engineering, Report CUED/ATurbo/TR5.

14. Howard J. H. G., Thornton, Trump A. B., Henseler H. J., 1967. “Performance and Flow Regime for Annular Diffusers “. ASME Paper No. 67-WA/FE-2 1.
15. Ishkawa K,Nakamura I, 1989. “An Experimental Study on The Performance of Mixed Flow Type Conical Wall Annular Diffuser”, ASIVIE FED-69.
16. Japikse, D., 1986. “A New Diffuser Mapping Technique — Studies in Component Performance: Part 1,” ASIVIE Paper No. 84-GT-237, Amsterdam, June 1984; also, Journal of Fluids Engineering, Vol. 108, No. 2. pp. 148-156.
17. Japikse, D., and Pampreen, R., “Annular Diffuser Performance for an Automotive Gas Turbine,” ASIVIE Publication 78-GT-147. 1978.
18. Japikse, D., 1980. “The Influence of Inlet Turbulence on Diffuser Performance,” Concepts ETI, Inc., Design Data Sheet No. 1,
19. Japikse, D., 2000. “Performance of Annular Diffusers Subject to Inlet Flow Field Variations and Exit Distortion,” Presented at the ISROMAC conference in Honolulu, Hawaii, March 26-30,.
20. Johanston I.H., 1959. “Effect of Inlet Conditions on the Flow in Annular Diffusers.” National Gas Turbine Establishment Memo No. 167,Cp No.178
21. Johnston J. P., 1959. “Summary of Results of Test on Short Conical Diffuser with Flow Control Inserts”: as of June 1, 1959.Ingersoll —Rand TN No. 71.
22. Juhasz,A.J. 1974. “Performance Of An Asymmetric Annular Diffuser With Non Diverging Inner Wall Using Suction”, NASA TN -7575.
23. Kamonicek V., Hibs M., 1974. “Results of Experimental and Theoretical Investigation ofAnnular Dffuiser.” CSIRO, Division of Mechanical Egg.
24. Klein, A., 1995. “Characteristics of Combustor Diffusers.” Program Aerospace Science 31: 171-271
25. Mahalakshmi N.V., Krithiga G., Sandhya S., Vikraman J., Ganesan V., 2007, “Experimental investigations of flow through conical diffusers with and without wake type velocity distortions at inlet” Experimental Thermal and Fluid Science (2007), doi: 10.1016/j.expthermflusci. 2007.
26. Moller E.S, 1965. “Radial Diffuser Using Incompressible Flow between Disks.” ASIVIE paper no. 65-FE-12.
27. Moller ES., 1965. “Radial Flow without Swirl between Parallel Disks Having both Supersonic and Subsonic Regions.” ASME Paper No. 65-FE-li.

28. Shaalan, M.R.A., Shabaka, I.M.M., 1975. “An Experimental Investigation of the Swirling Flow Performance of an Annular Diffuser at Low Speed,” ASIVIE Paper No. 75-WA/FE-17.
29. Sharan V K, 1972.Diffuser Performance Co-Relations. JASI, Volume 24, pp 4l5.
30. Sovran, G., Klomp, E.D., 1967. “Experimentally Determined Optimum Geometries for Rectilinear Diffusers with Rectangular, Conical or Annular Cross- Section,” Fluid Dynamics of Internal Flow, Elsevier Publishing Company.
31. Srinath T, 1968, “An Investigation of the Effects of Swirl on The Flow Regimes and Performance of Annular Diffuser With Equal Inner and Outer Cone Angles. “ M.A. Science Thesis , University of Waterloo Canada
32. Stafford W. Wilbur, James T.H. 1957. “Investigation of Short Annular Diffuser Configuration Utilizing Suction as a Means of Boundary Layer Control”, NACA TN-3996
33. Stafford W.Willbur, James T.H. 1957. “Investigation Of Short Annular Diffuser Configuration Utilizing Suction As A Means Of Boundary Layer Control.” NACA TN-3996
34. Stafford, W. Wilbur, James T. Higginbotham, 1955. “Investigation of Two Short Annular Diffuser Configurations Utilizing Suction and Injection as Means of Boundary Layer Control”. NACA RI\4 L54K18.
35. Stevan S. J., Williams G.J., 1980. “The Influence of Inlet Conditions on The Performance of Annular Diffuser.” Trans. ASIVIE Journal Fluids Engg. 2002, 357-363.
36. Stevens S. J., Fry P., 1973. “Measurements of the Boundary Layer Growth in Annular Diffusers”. Journal Aircraft Feb., pp 73-89.
37. Stevens S. J., Williams G. J., 1969. “Performance of Annular Diffusers” Gas Turbine Collaboration Committee Report No. 299.
38. Stevens S. J., Williams G. J., 1980. “The Influence of Inlet Conditions on the Performance of Annular Diffuser”. Trans. ASME Journal Fluids Egg. 102, 357-363.
39. Stevens S.J., Fry P., 1973. “Measurements of the Boundary Layer Growth in Annular Diffusers.” Journal Aircraft Feb., pp 73-89.

40. Takehira A., et. al., 1977. “An Experimental Study of the Annular Diffusers in Axial-Flow Compressors and Turbines” Japan Society of Mechanical Engineers, Paper No.39, 1977.
41. Takehira, A., et al., 1977, “An Experimental Study of the Annular Diffusers in Axial- Flow Compressors and Turbines,” Japan Society of Mechanical Engineers, Paper No.39, 1977.
42. Thayer E B, 1971 “Evaluation of Curved Wall Annular Diffuser” ASIVIE paper no .71 -WA/FE-3 5
43. Thayer E. B., 1971. “Evaluation of Curved Wall Annular Diffuser” ASME Paper No.71 -WA/FE-3 5
44. Wood C.C., Henry J. R., 1958. “Effects of Shock Boundary Layer Interaction on the Long and Short Subsonic Annular Diffuser” .NACA RI\4 L5 8A3 1.
45. Wood, C .C. Henary, JR., 1958. “Effects of Shock Boundary Layer Interaction on the Long and Short Subsonic Annular Diffuser”, NACA RIVI L58A3 1.

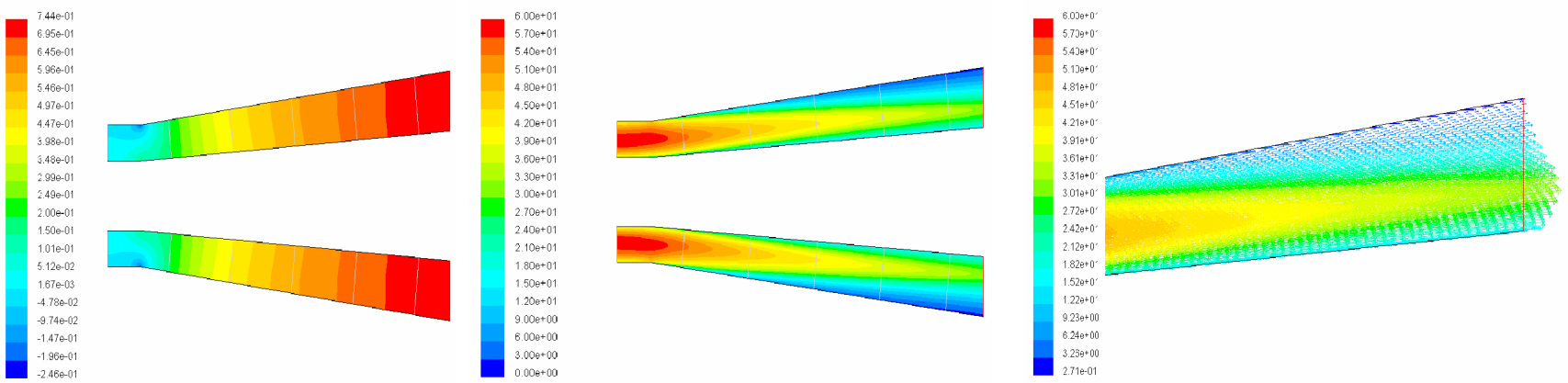

Pressure Coefficient Contours **Contours of Velocity Magnitude (m/s)** **Velocity Vectors**

Fig 1 AR3, Casing Wall Angle=15, Swirl Angle=0°, Velocity=60 m/s

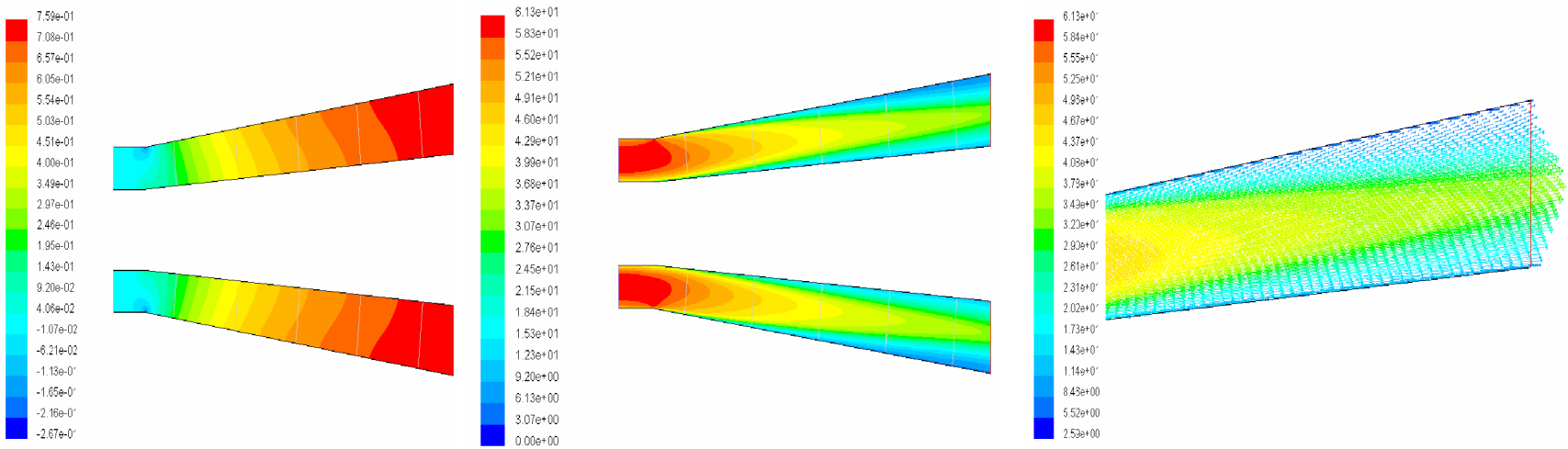

Pressure Coefficient Contours **Contours of Velocity Magnitude (m/s)** **Velocity Vectors**

Fig 2 AR3, Casing Wall Angle=15, Swirl Angle=12°, Velocity=60 m/s

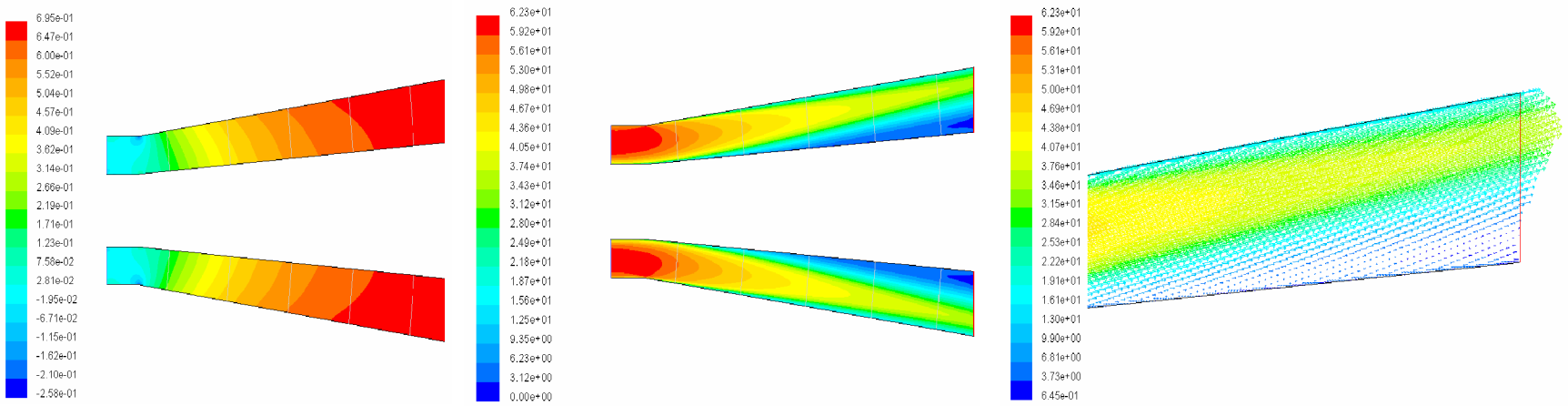

Pressure Coefficient Contours **Contours of Velocity Magnitude (m/s)** **Velocity Vectors**

Fig 3 AR3, Casing Wall Angle=15, Swirl Angle=17° , Velocity=60 m/s

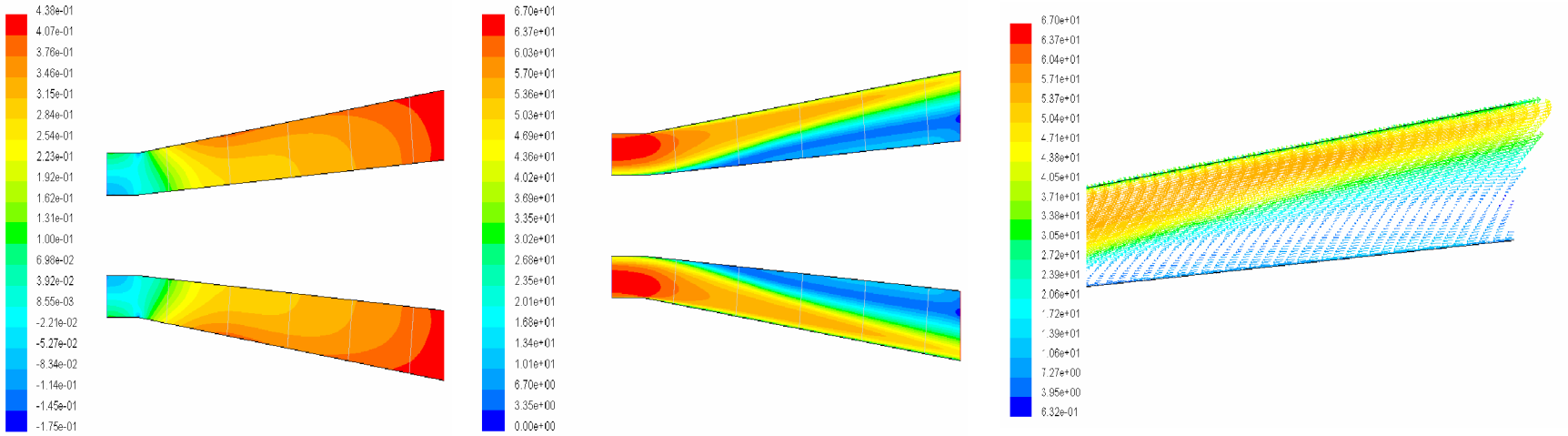

Pressure Coefficient Contours **Contours of Velocity Magnitude (m/s)** **Velocity Vectors**

Fig 4 AR3, Casing Wall Angle=15, Swirl Angle=25°, Velocity=60 m/s

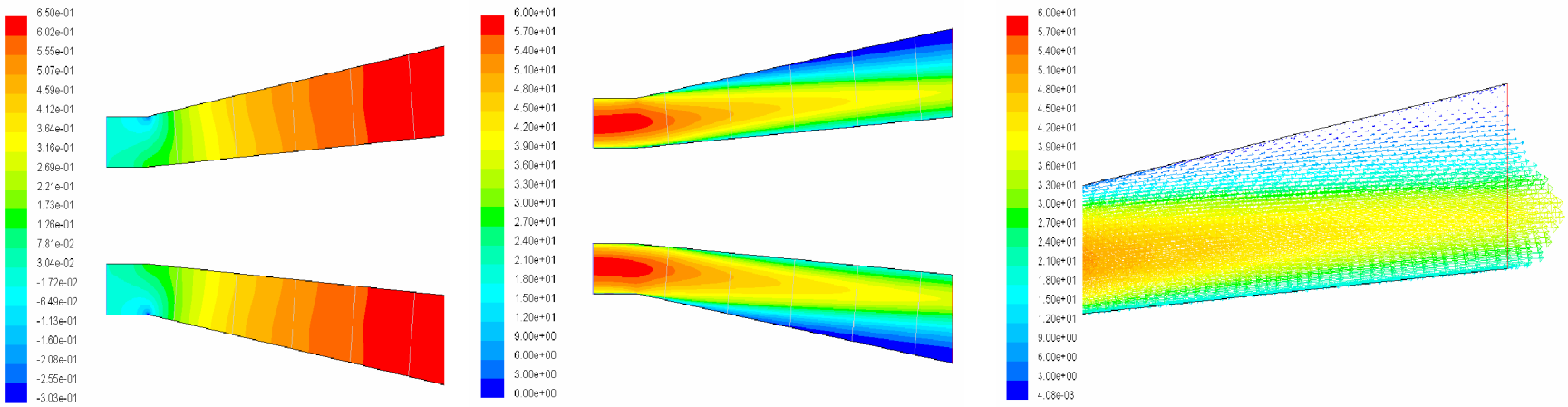

Pressure Coefficient Contours **Contours of Velocity Magnitude (m/s)** **Velocity Vectors**

Fig 5 AR3, Casing Wall Angle=20°, Swirl Angle=0°, Velocity=60 m/s

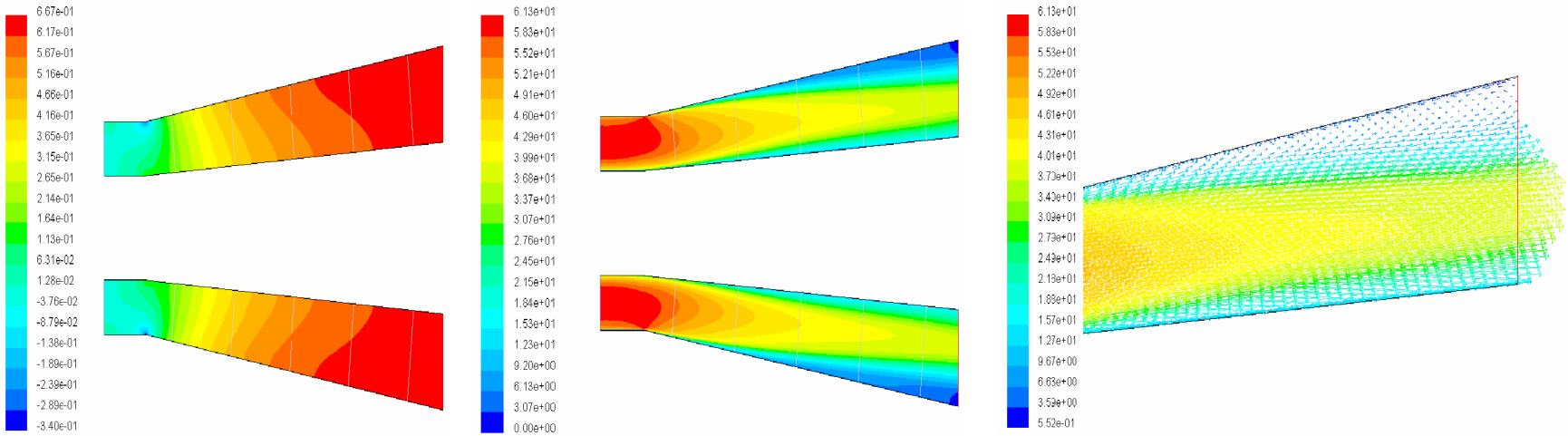

Pressure Coefficient Contours **Contours of Velocity Magnitude (m/s)** **Velocity Vectors**

Fig 6 AR3, Casing Wall Angle=20°, Swirl Angle=12°, Velocity=60 m/s

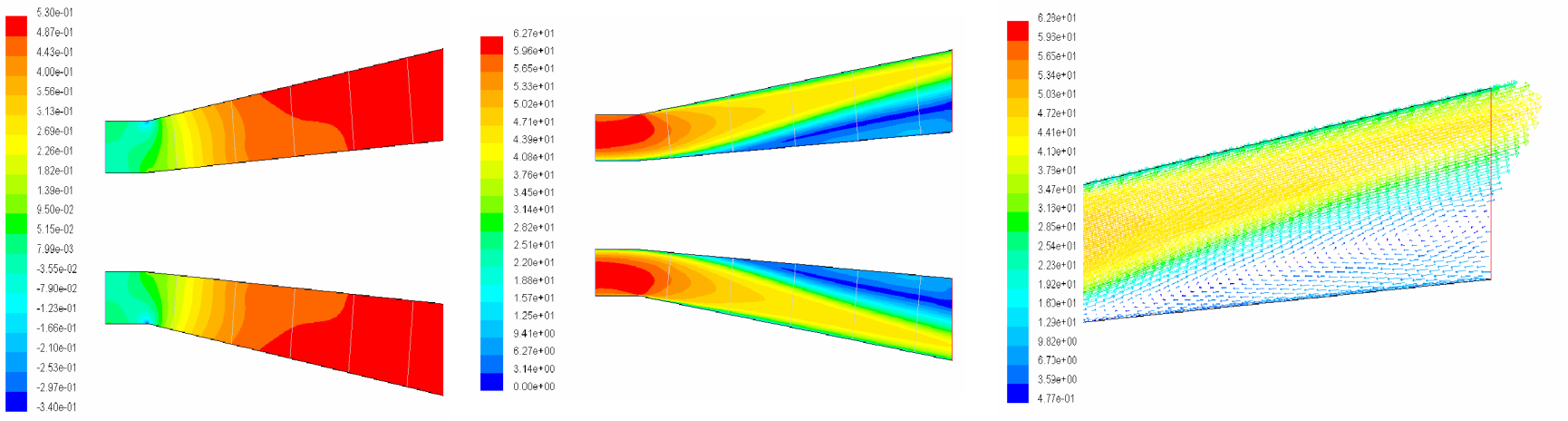

Pressure Coefficient Contours **Contours of Velocity Magnitude (m/s)** **Velocity Vectors**

Fig 7 AR3, Casing Wall Angle=20°, Swirl Angle=17°, Velocity=60 m/

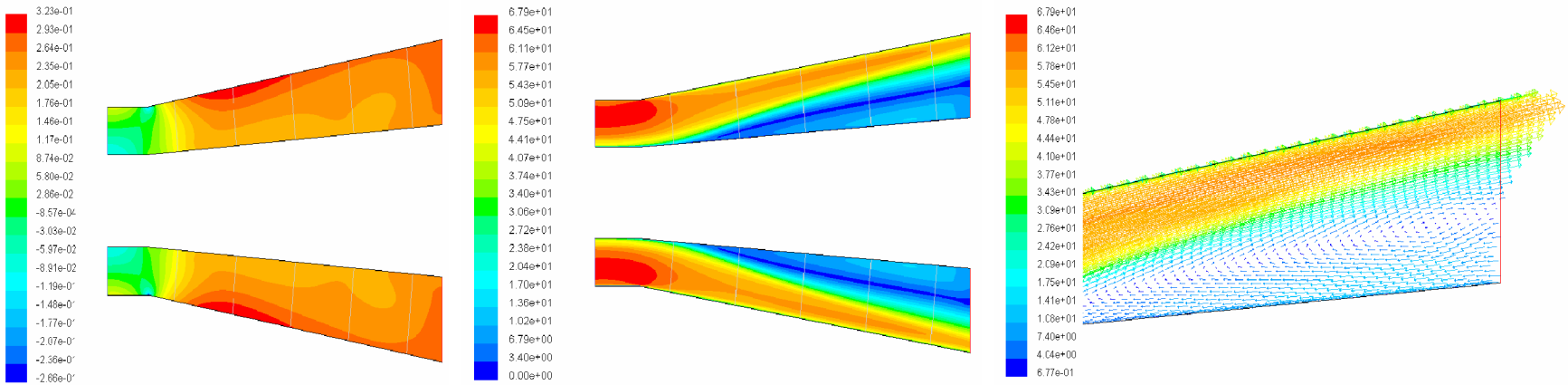

Pressure Coefficient Contours **Contours of Velocity Magnitude (m/s)** **Velocity Vectors**

Fig 8 AR3, Equivalent Casing Wall Angle=20°, Swirl Angle=25°, Velocity=60 m/s

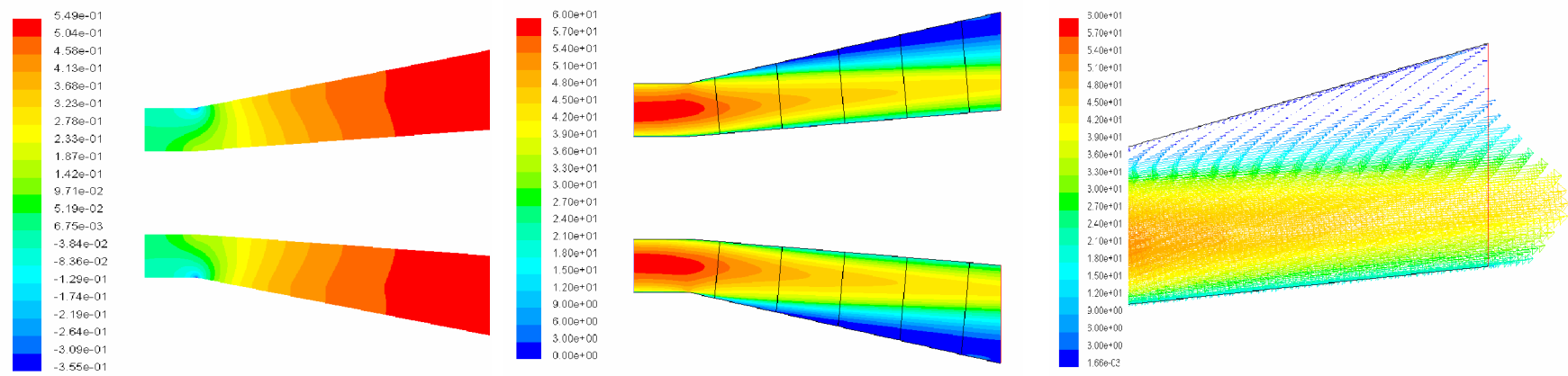

Pressure Coefficient Contours **Contours of Velocity Magnitude (m/s)** **Velocity Vectors**

Fig 9 AR3, Equivalent Casing Wall Angle=25°, Swirl Angle=0°, Velocity=60 m/s

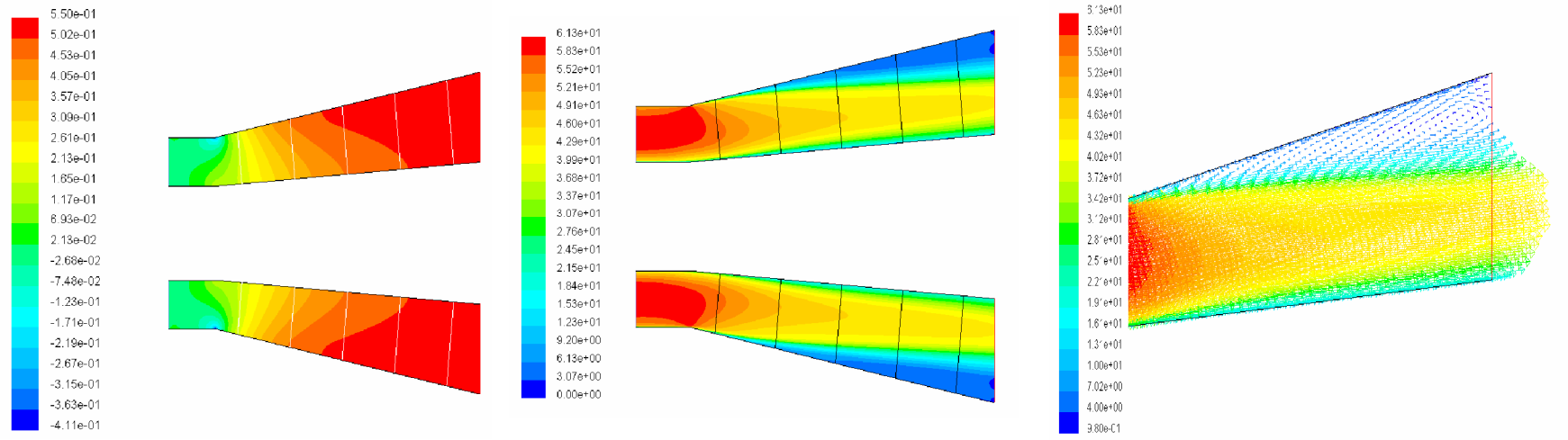

Pressure Coefficient Contours **Contours of Velocity Magnitude (m/s)** **Velocity Vectors**

Fig 10 AR3, Equivalent Casing Wall Angle=25°, Swirl Angle=12°, Velocity=60 m/s

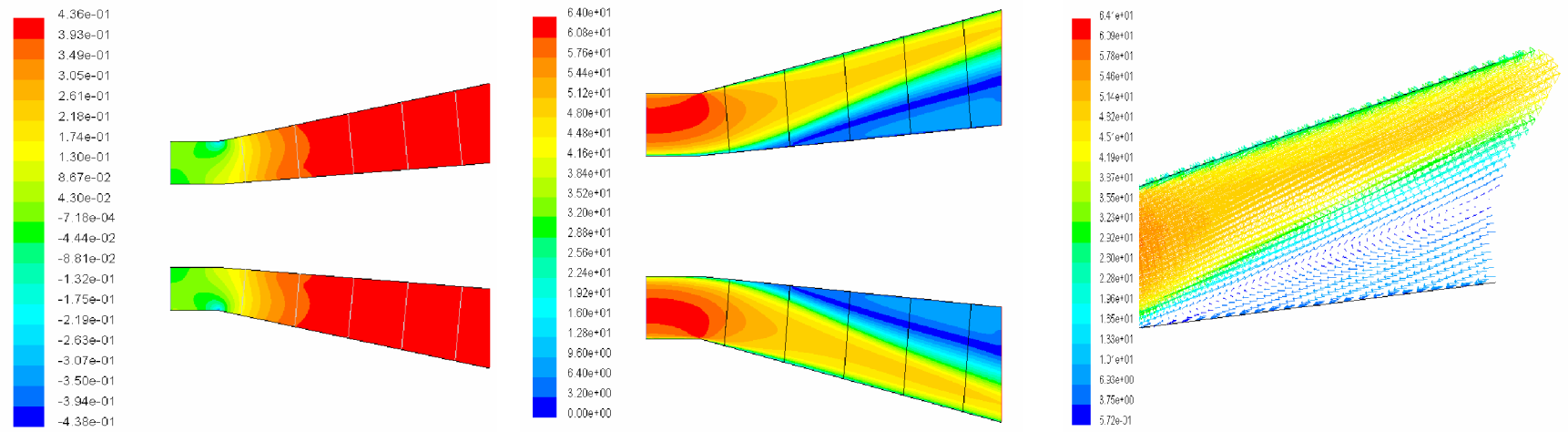

Pressure Coefficient Contours **Contours of Velocity Magnitude (m/s)** **Velocity Vectors**

Fig 11 AR3, Equivalent Casing Wall Angle=25°, Swirl Angle=17° , Velocity=60 m/s

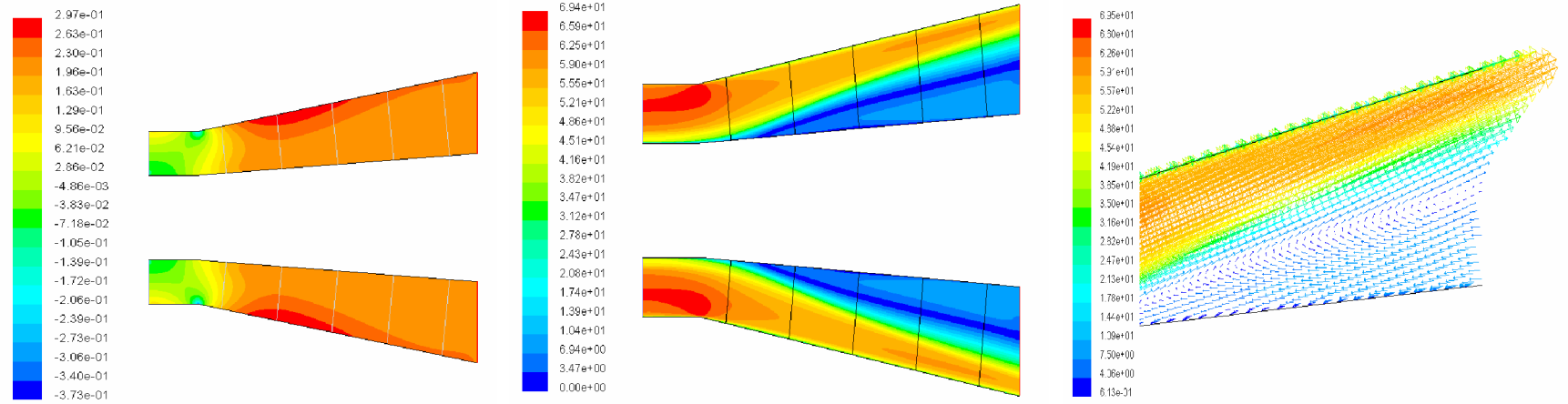

Pressure Coefficient Contours **Contours of Velocity Magnitude (m/s)** **Velocity Vectors**

Fig 12 AR3, Equivalent Casing Wall Angle=25°, Swirl Angle=25°, Velocity=60 m/s

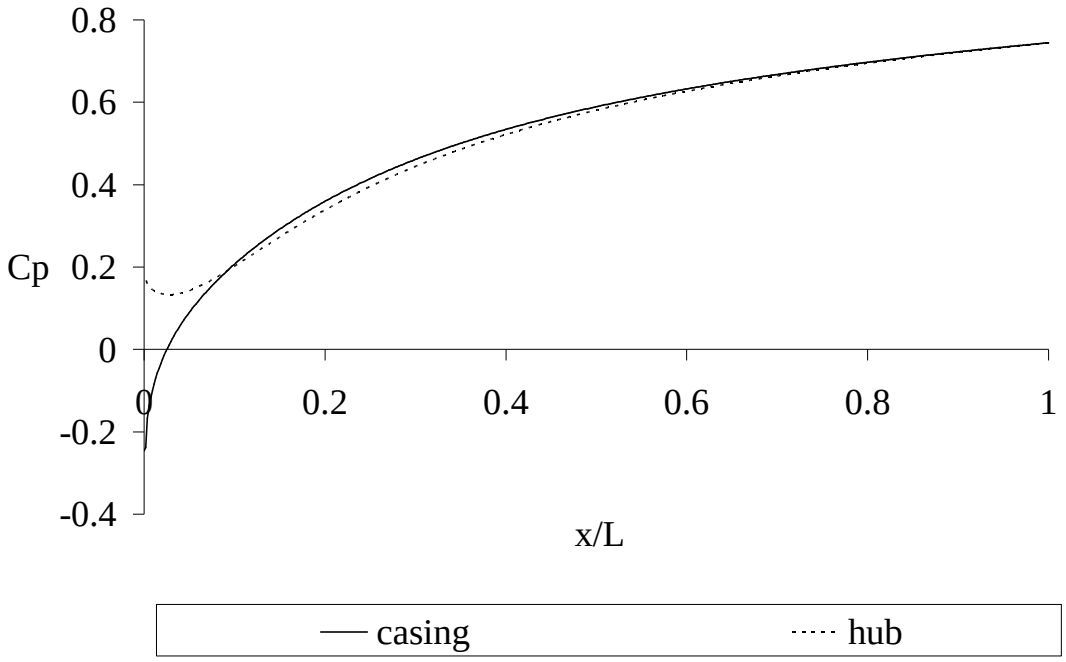

Pressure Coefficient (0°), 15C, AR3

Fig 13 AR=3, Casing Wall Angle=15°, Swirl =0°, Re = 3×10^5

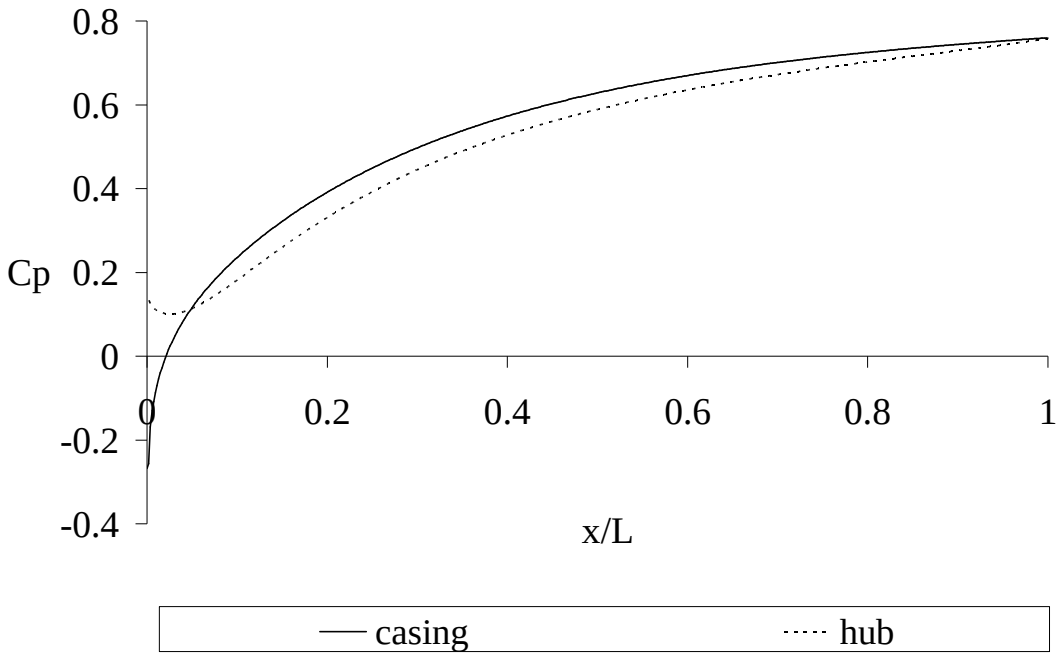

Pressure Coefficient (12°), 15C, AR3

Fig 14 AR=3, Casing Wall Angle=15°, Swirl =12°, Re = 3×10^5

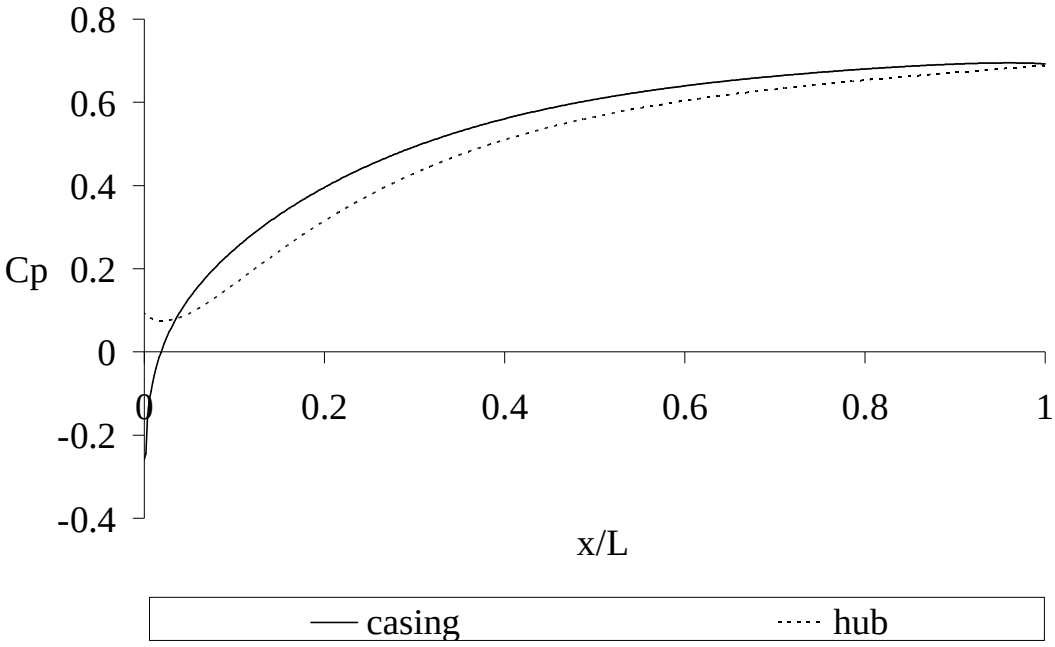

Pressure Coefficient (17°), 15C, AR3

Fig 15 AR=3, Casing Wall Angle=15°, Swirl =17°, Re = 3×10^5

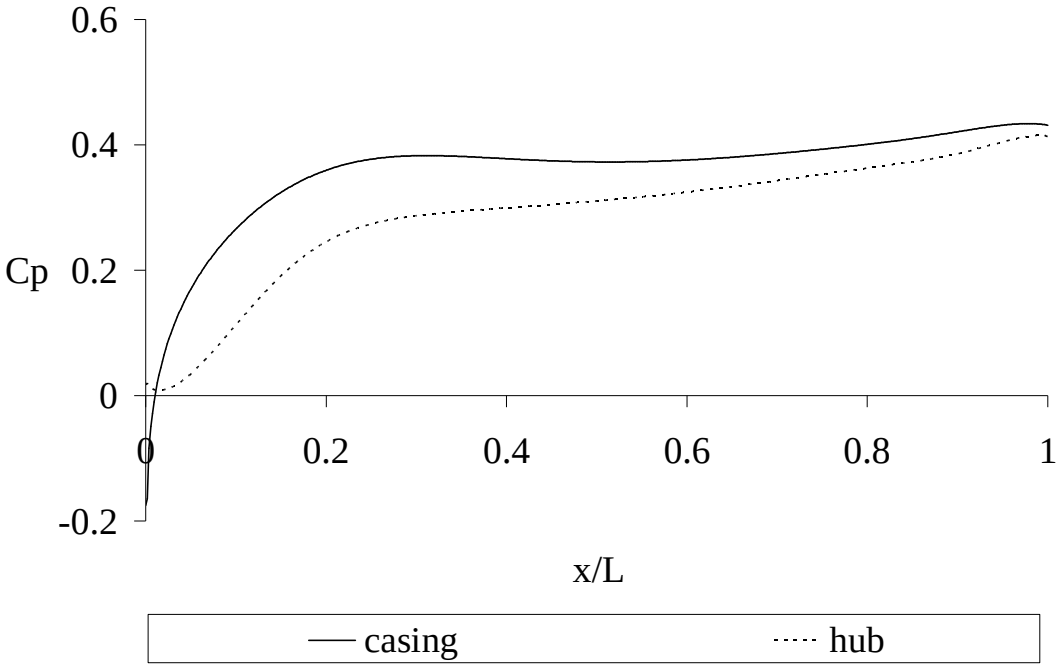

Pressure Coefficient (25°), 15C, AR3

Fig 16 AR=3, Casing Wall Angle=15°, Swirl =25°, Re = 3×10^5

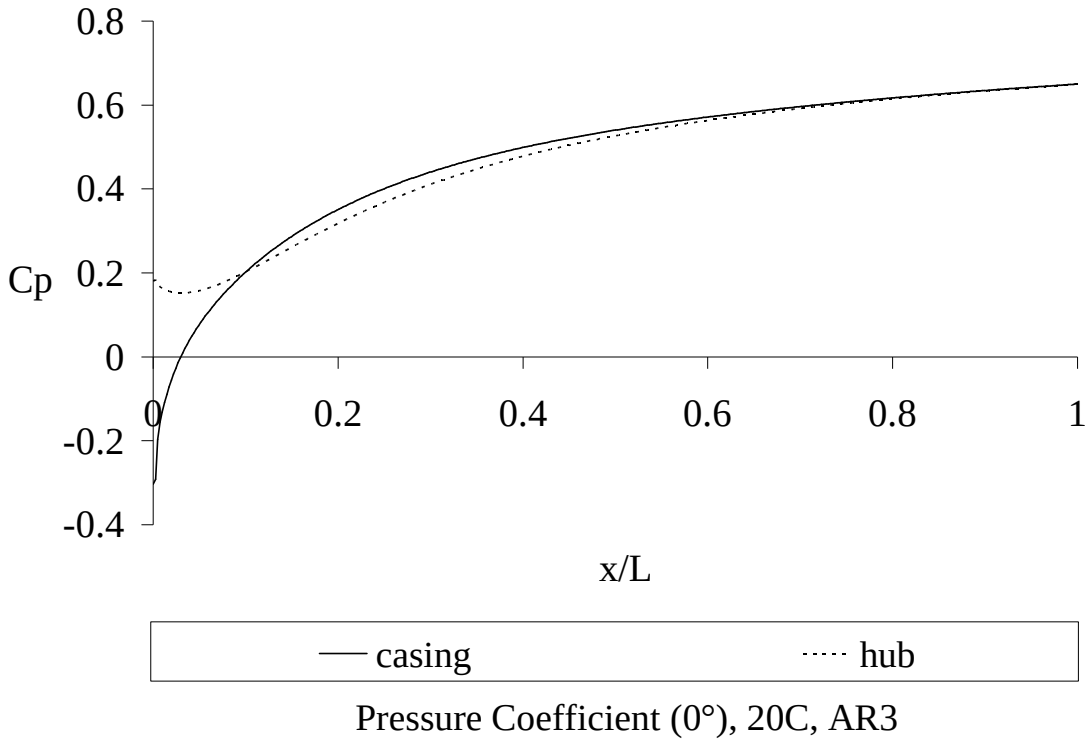

Fig 17 AR=3, Casing Wall Angle=20°, Swirl =0, Re = 3×10^5

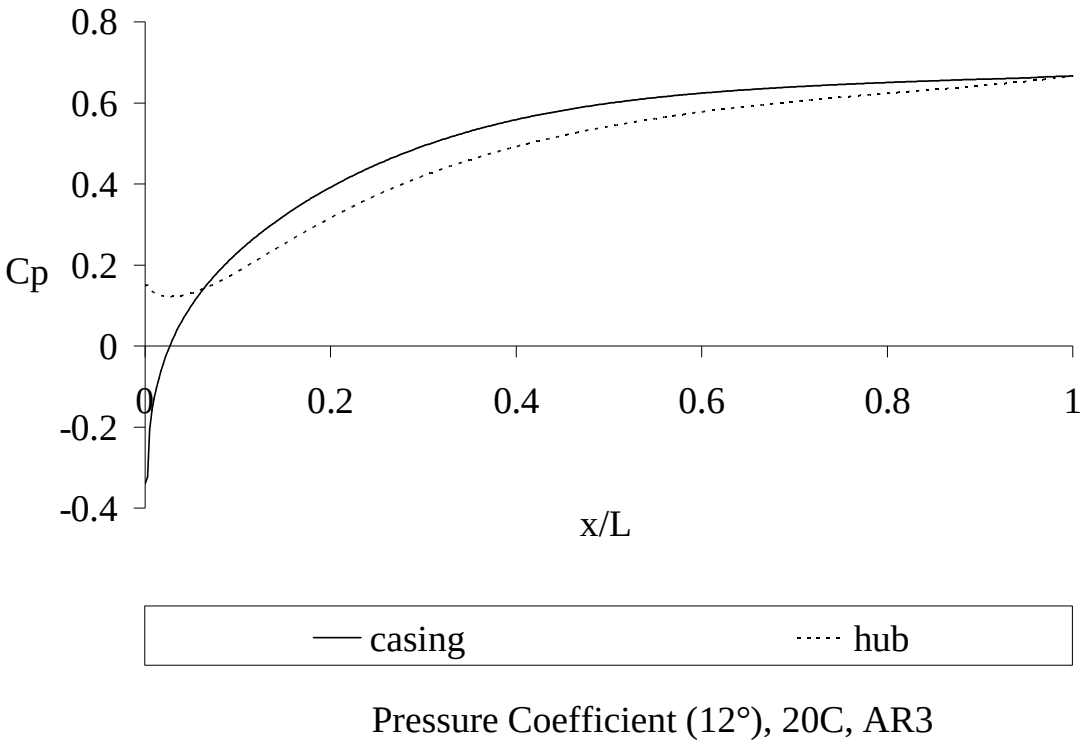

Fig 18 AR=3, Casing Wall Angle=20°, Swirl =12°, Re = 3×10^5

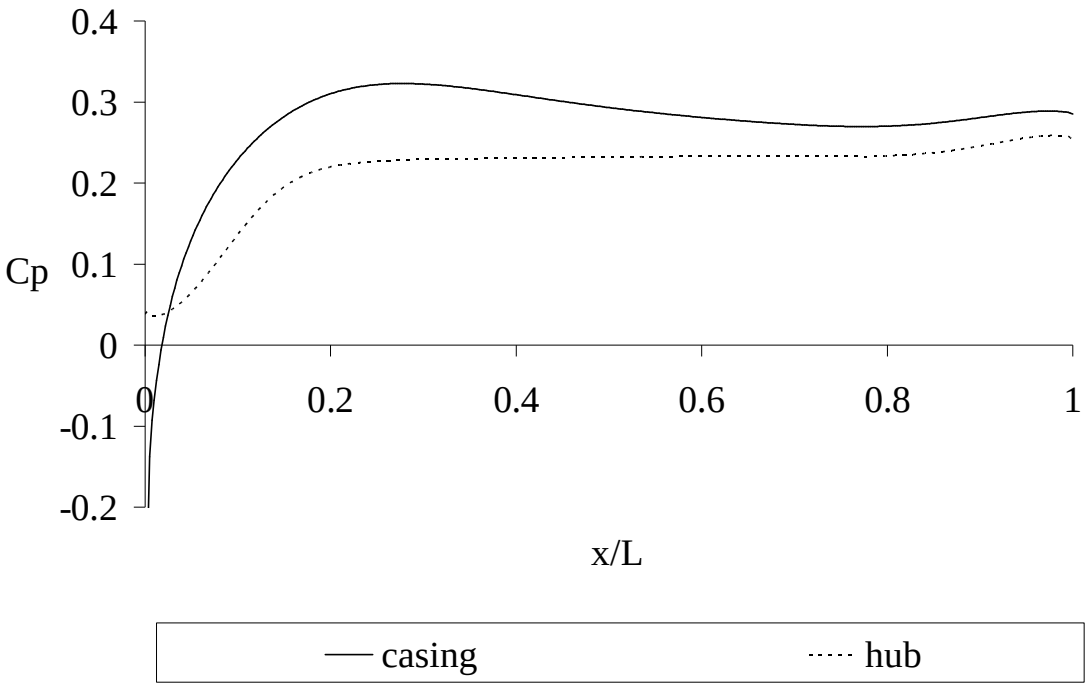

Pressure Coefficient (17°), 20C, AR3

Fig 19 AR=3, Casing Wall Angle=20°, Swirl =17°, Re = 3×10^5

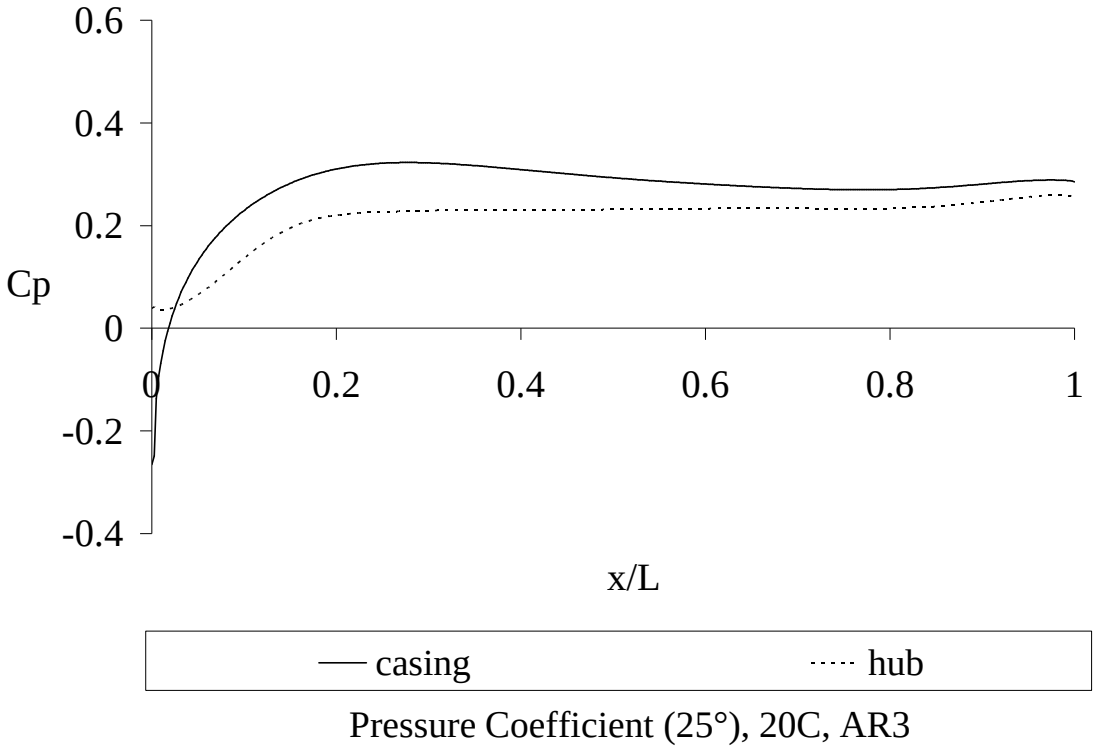

Fig 20 AR=3, Casing Wall Angle=20°, Swirl =25°, Re = 3×10^5

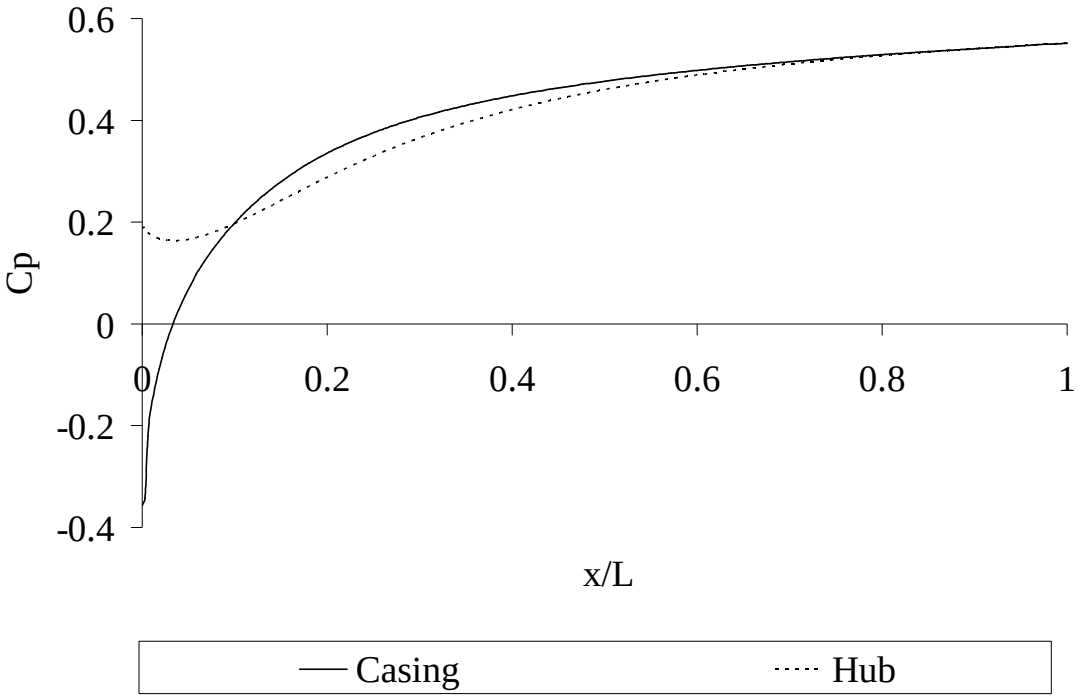

Pressure Coefficient (0º), 25C, AR3

Fig 21 AR=3, Casing Wall Angle=25°, Swirl =0°, Re = 3×10^5

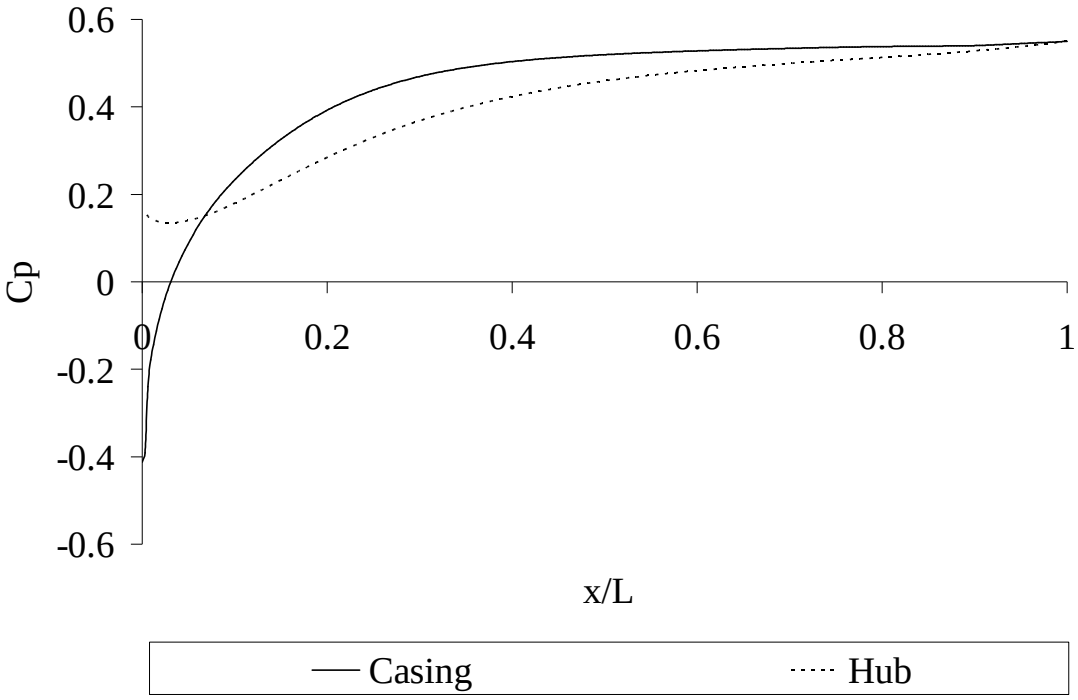

Fig 22 AR=3, Casing Wall Angle=25°, Swirl =12°, Re = 3 × 10^5

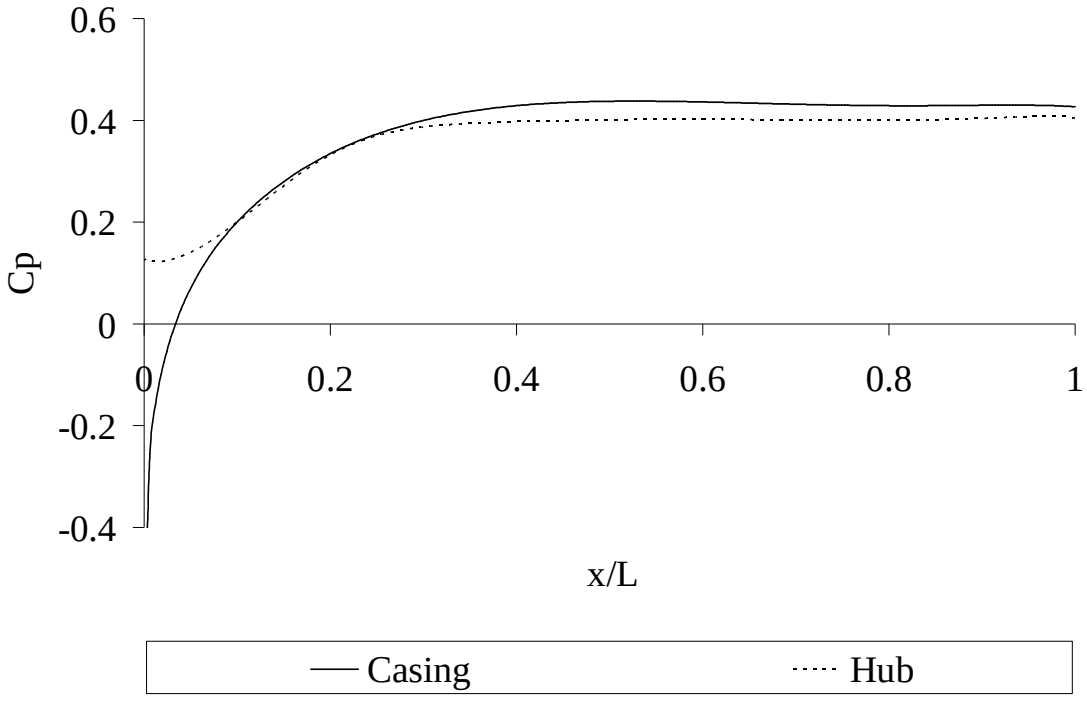

Fig 23 AR=3, Casing Wall Angle=25°, Swirl =17°, Re = 3×10^5

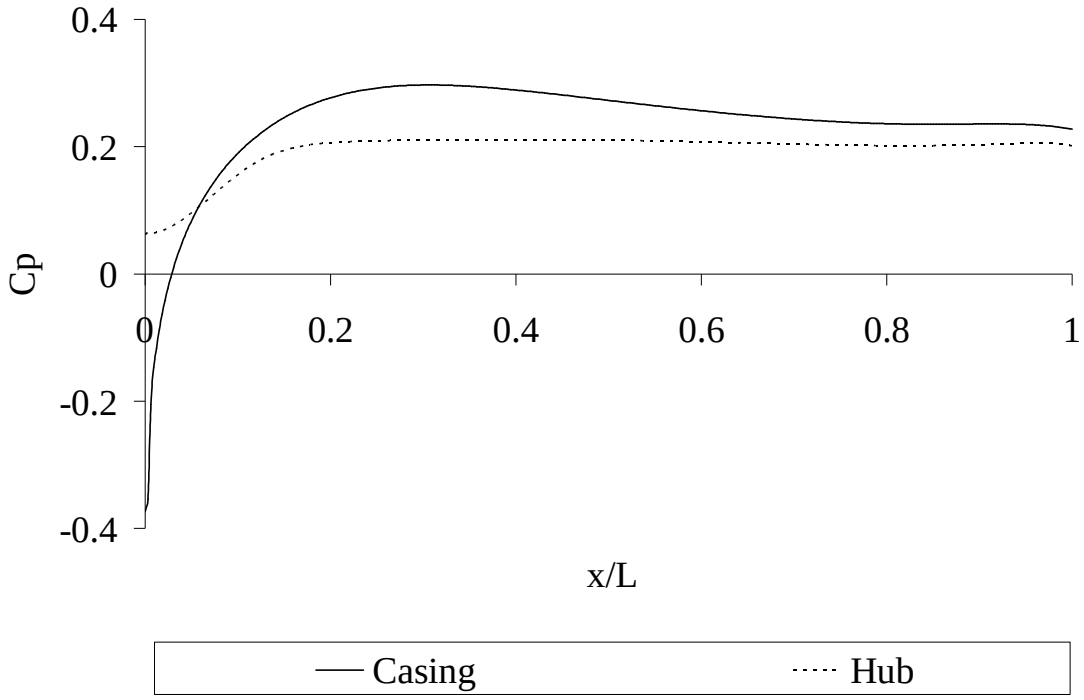

Pressure Coefficient (25º), 25C, AR3

Fig 24 AR=3, Casing Wall Angle=25°, Swirl =25°, Re = 3×10^5

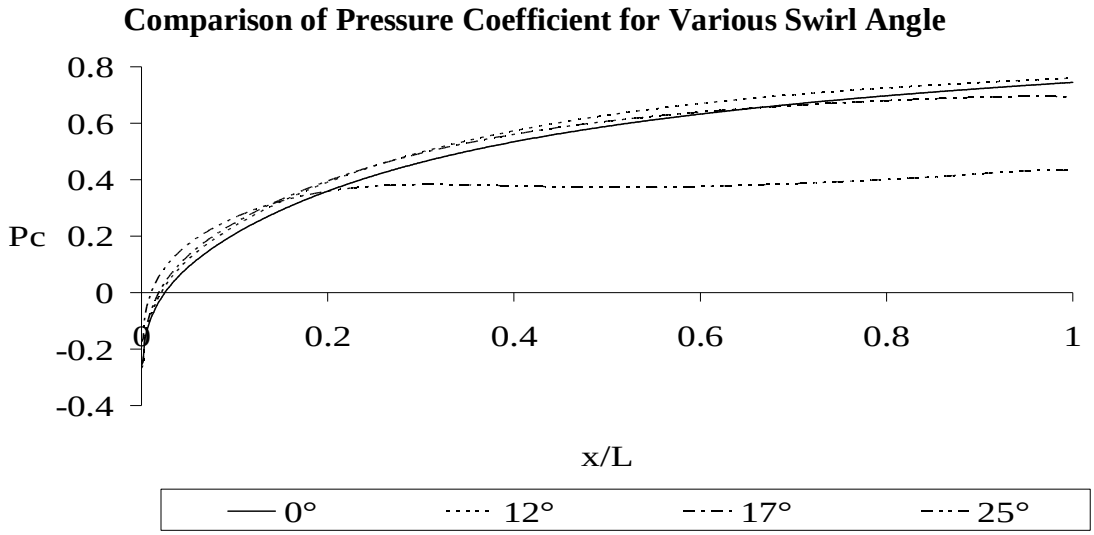

Pressure Coefficient at Casing, 15C, AR3

Fig 25 AR=3, Casing Wall Angle=15°

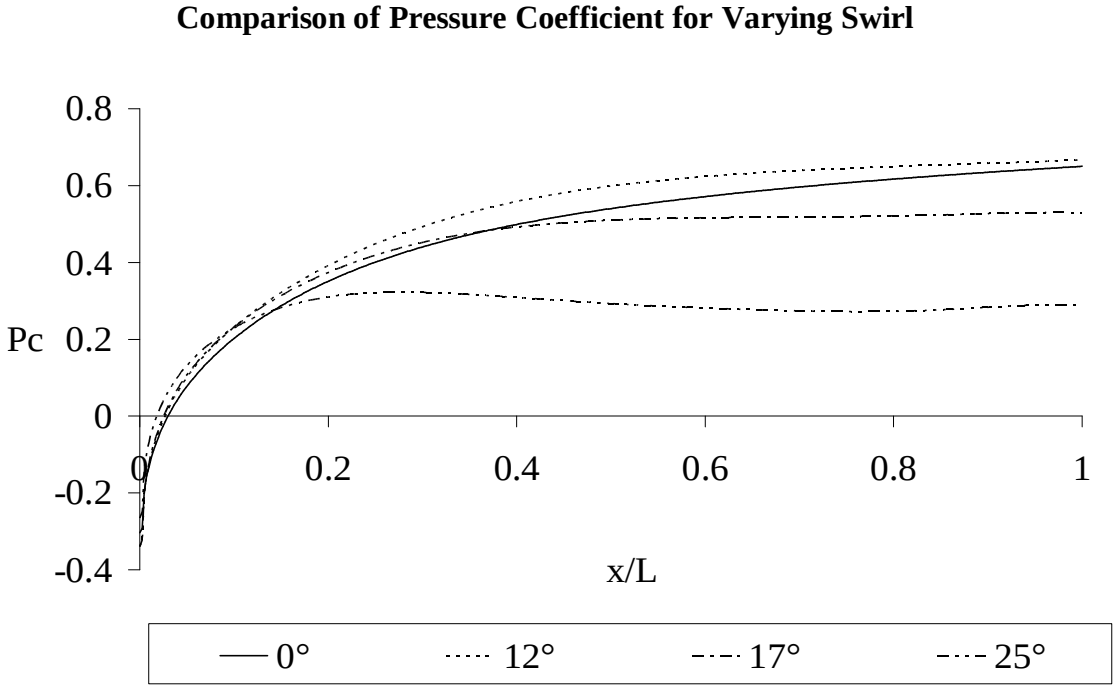

Pressure Coefficient at Casing, 20C, AR3

Fig 26 AR=3, Casing Wall Angle=20°

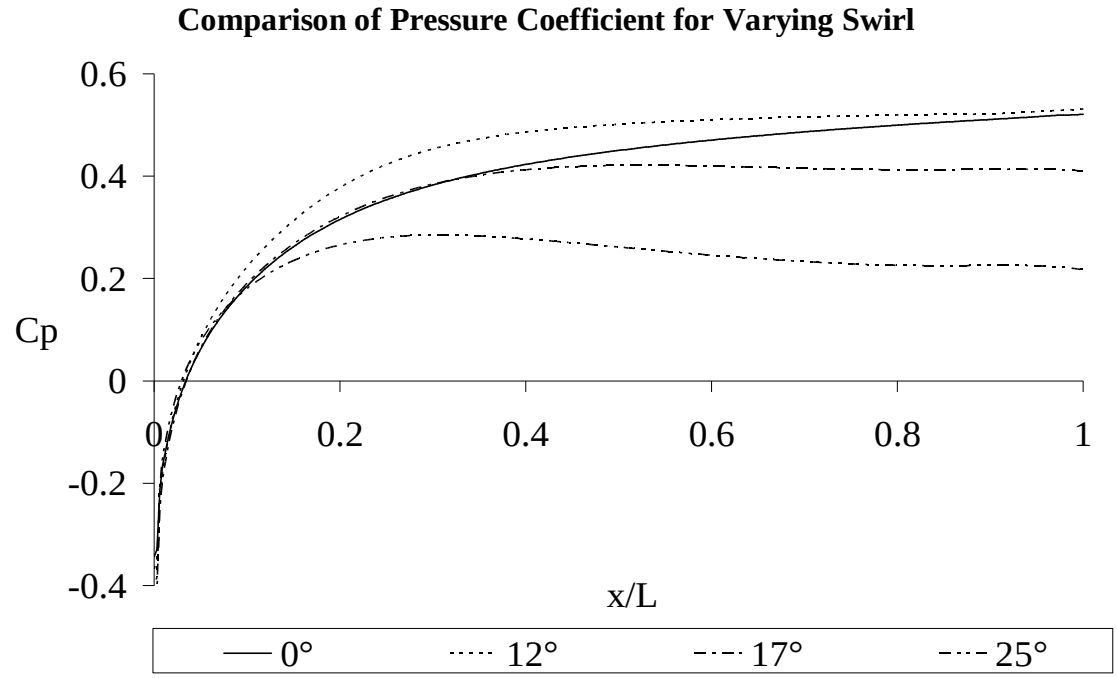

Fig 27 AR=3, Casing Wall Angle=25°

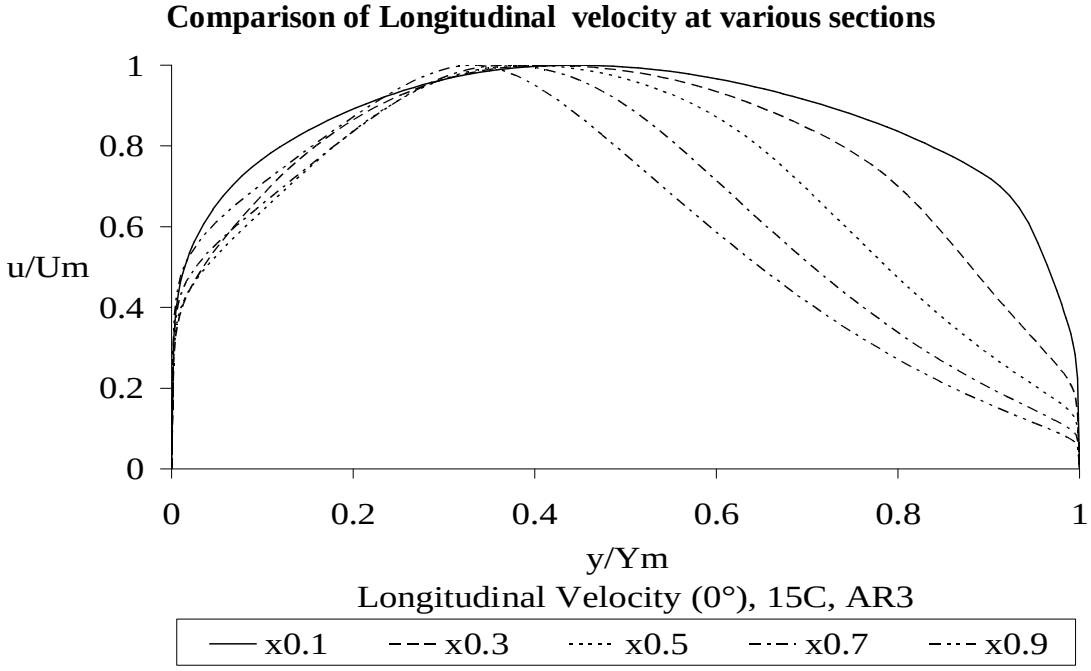

Fig 28 AR=3, Casing Wall Angle=15°

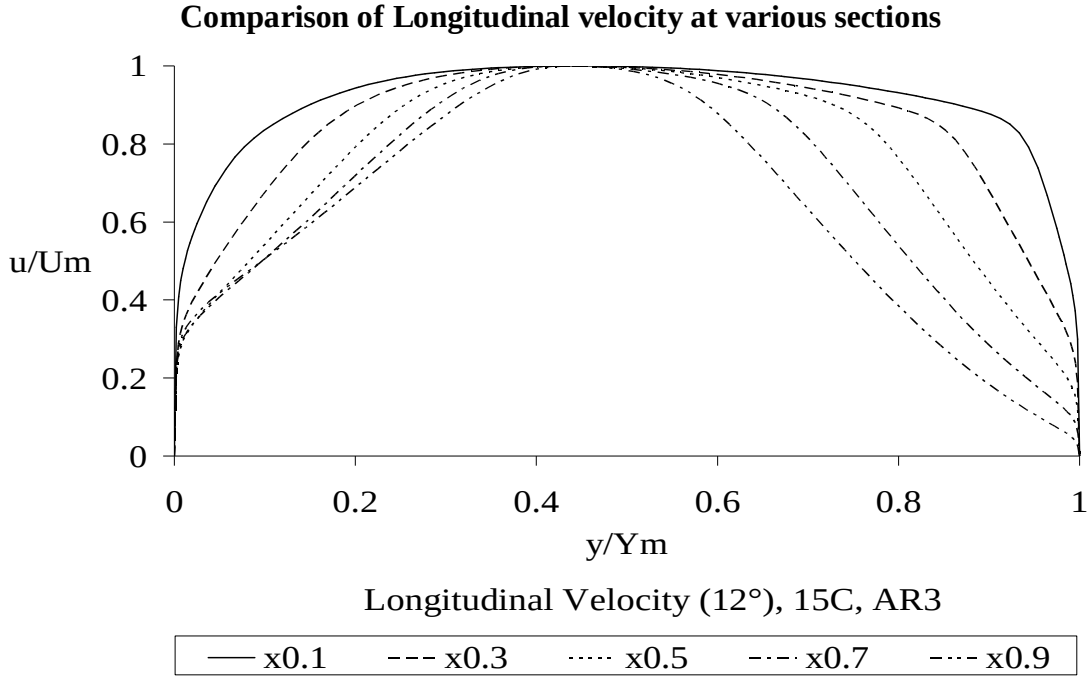

Fig 29 AR=3, Casing Wall Angle=15°

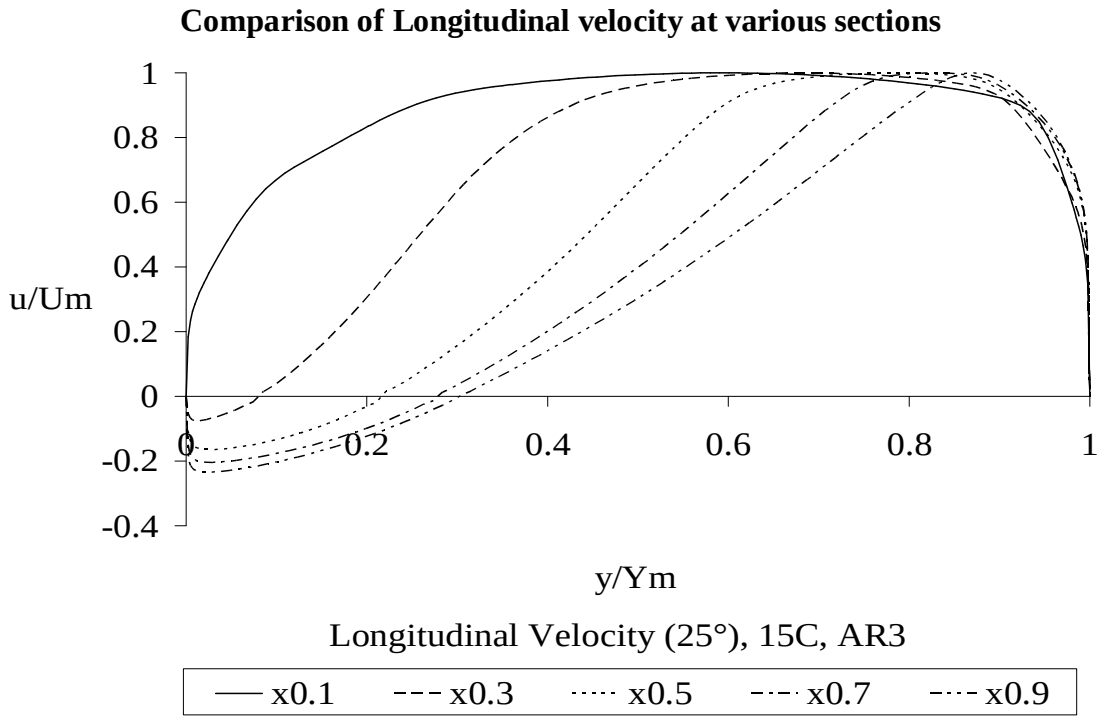

Fig 30 AR=3, Casing Wall Angle=15°

Comparison of Longitudinal velocity at various sections

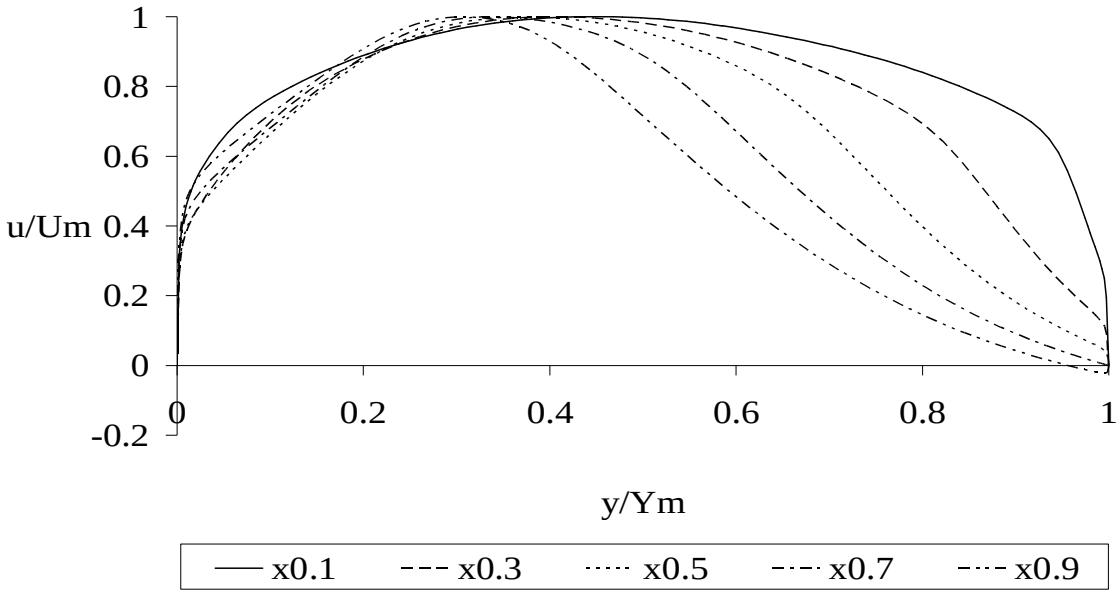

Longitudinal Velocity (0°), 20C, AR3

Fig 31 AR=3, Casing Wall Angle=20°

Comparison of Longitudinal velocity at various sections

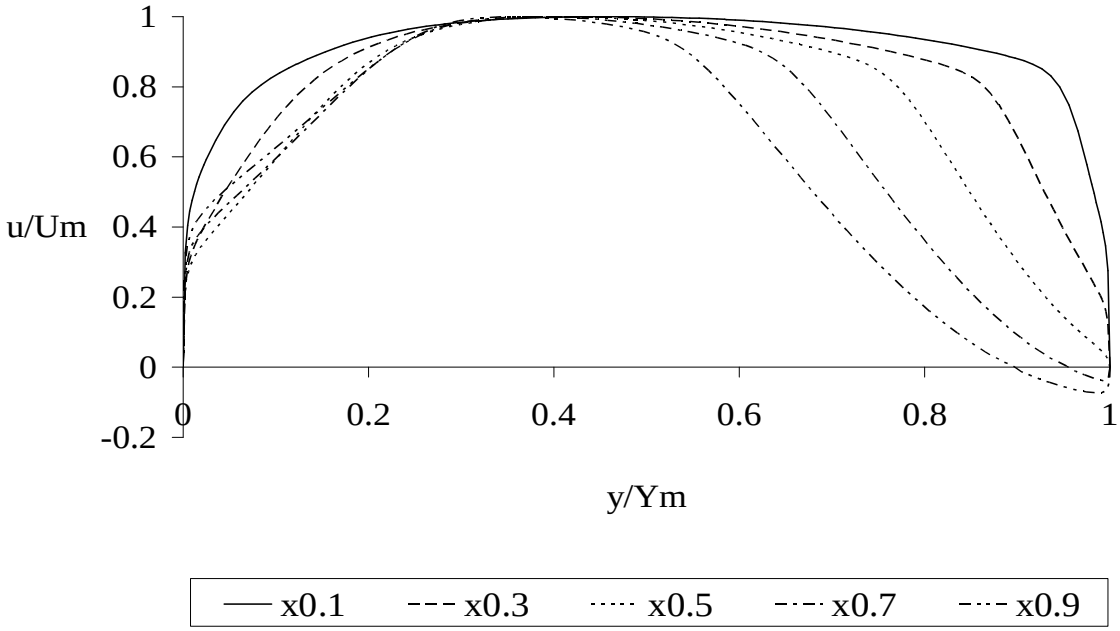

Longitudinal Velocity (12°), 20C, AR3

Fig 32 AR=3, Casing Wall Angle=20°

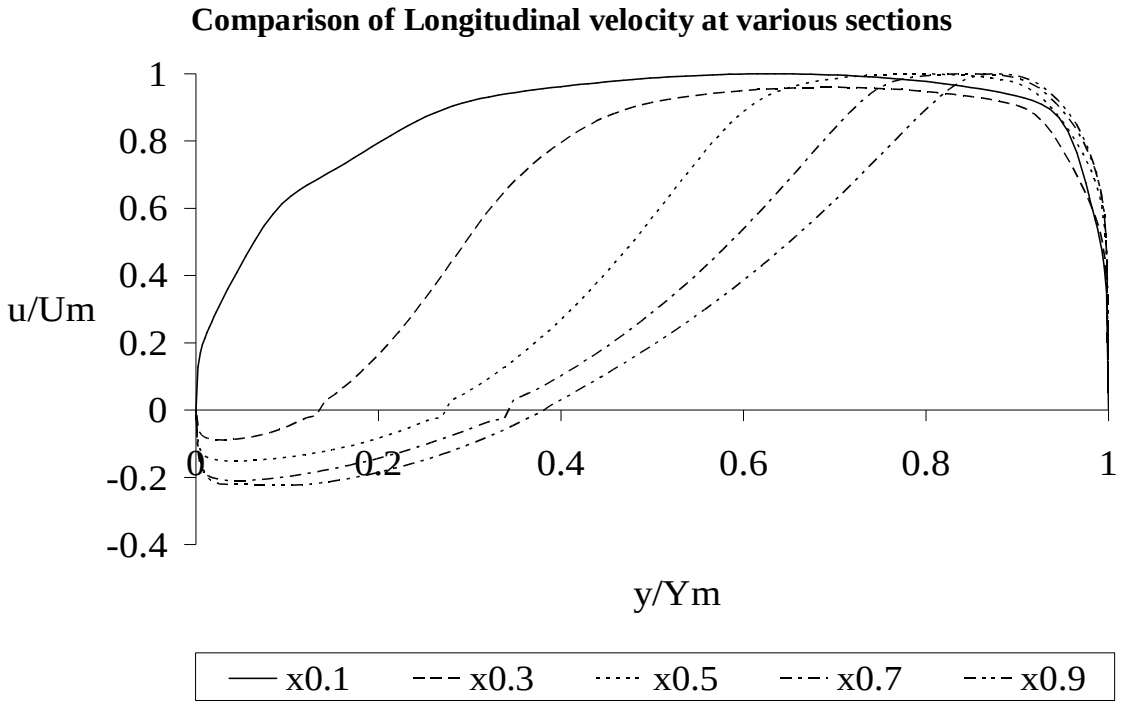

Fig 33 AR=3, Casing Wall Angle=20°

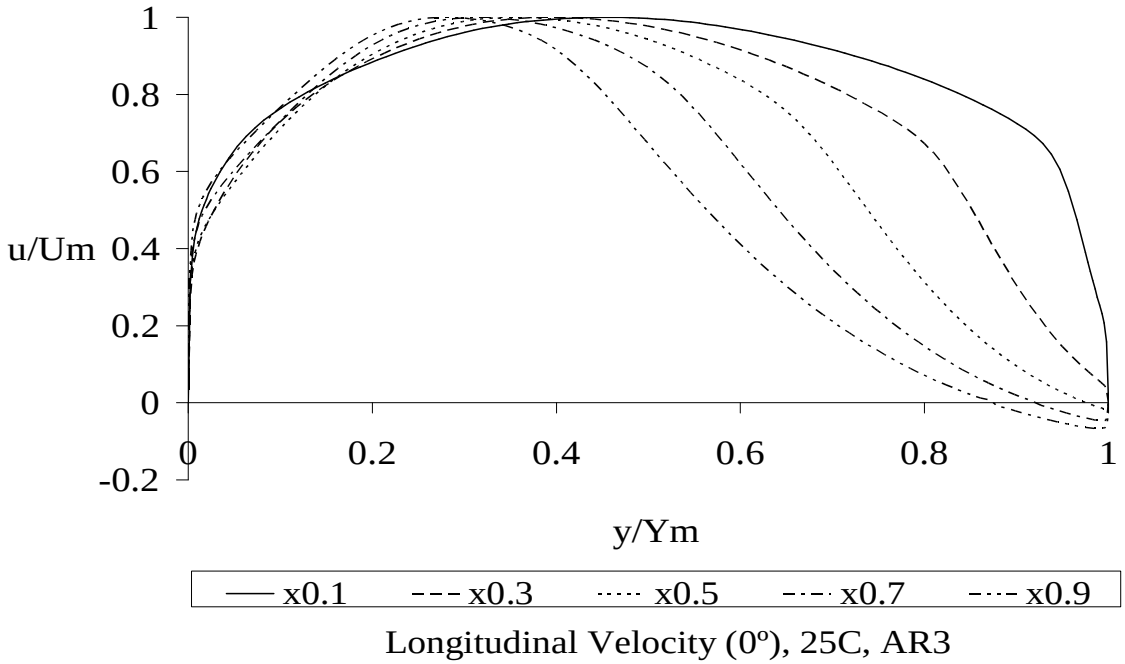

Fig 34 AR=3, Casing Wall Angle=25°

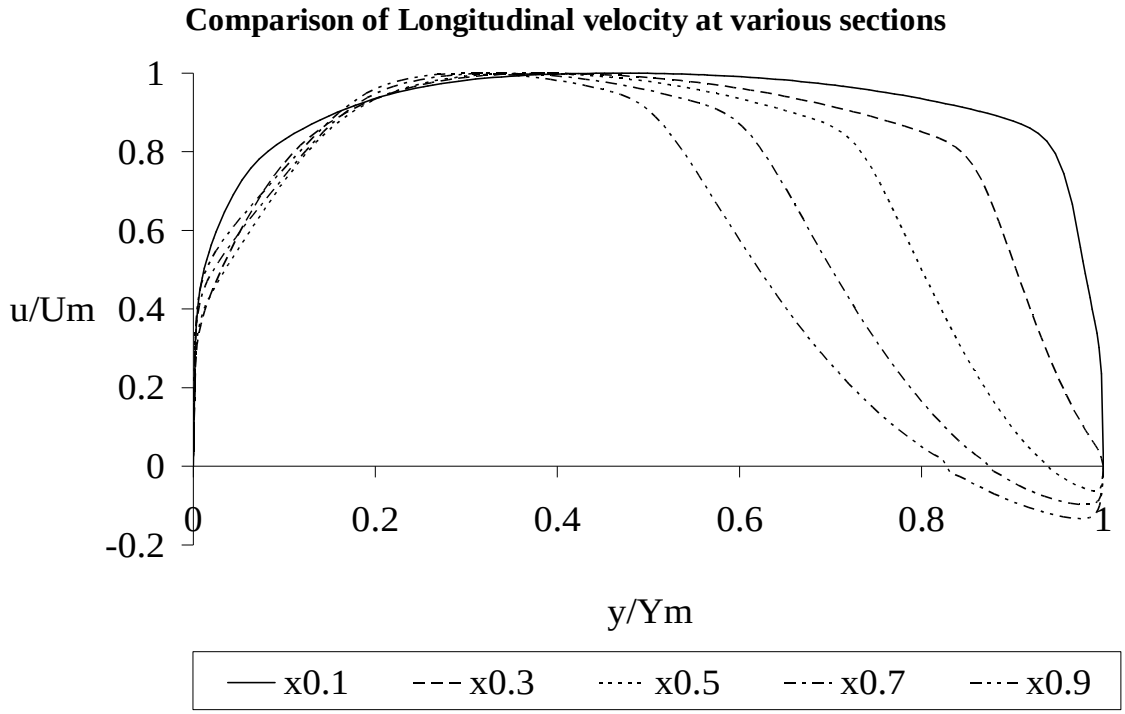

Longitudinal Velocity (12º), 25C, AR3

Fig 35 AR=3, Casing Wall Angle=25°

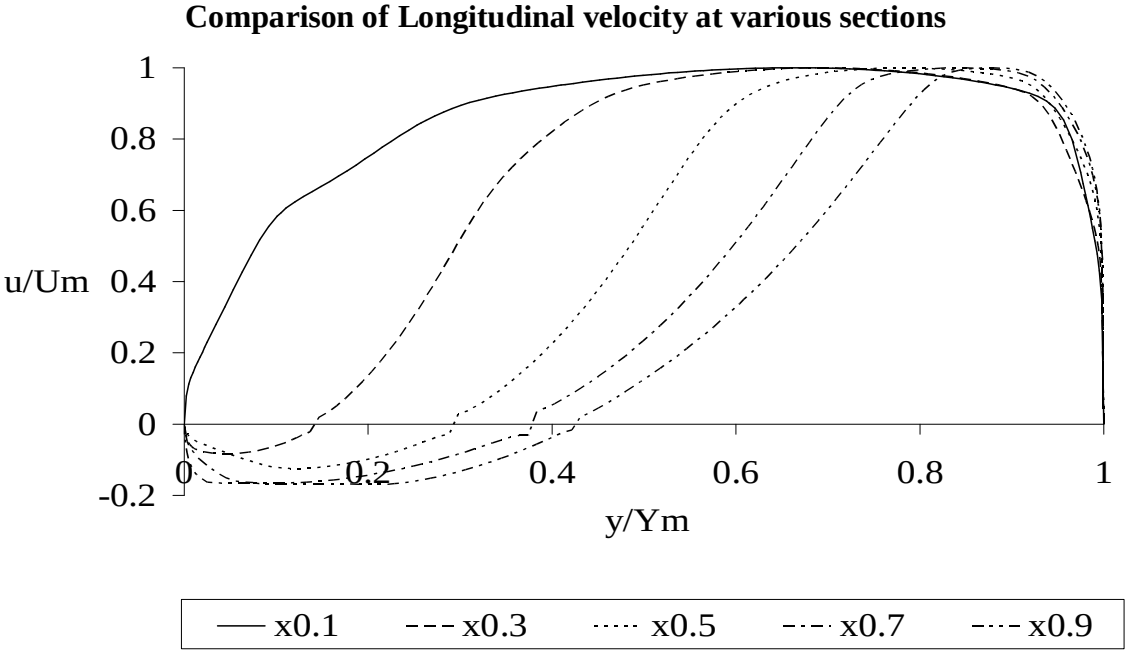

Longitudinal Velocity (25º), 25C, AR3

Fig 36 AR=3, Casing Wall Angle=25°

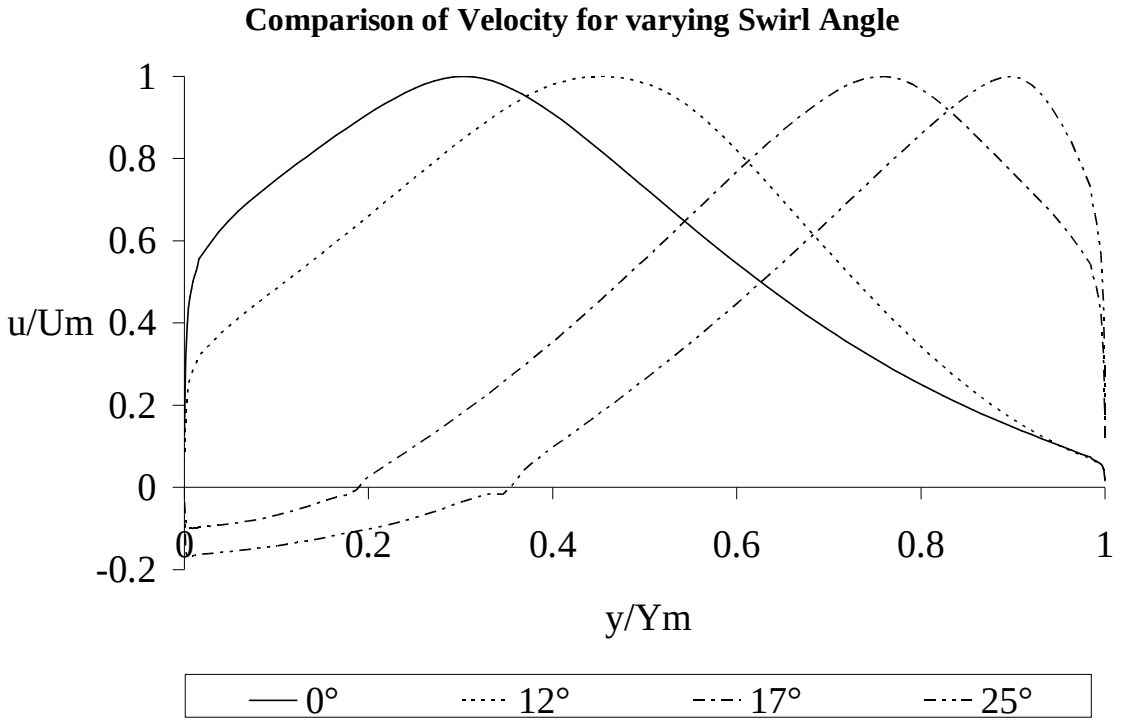

Longitudinal Velocity (15°), Case C, AR3

Fig 37 AR=3, Casing Wall Angle=15°

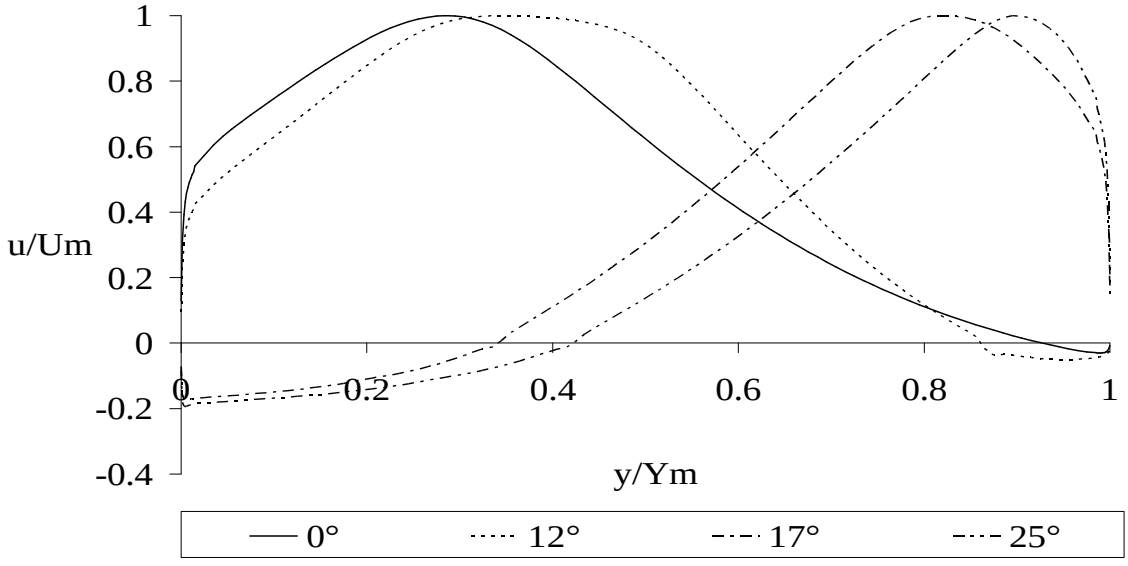

Longitudinal Velocity (20°), Case C, AR3

Fig 38 AR=3, Casing Wall Angle=20°

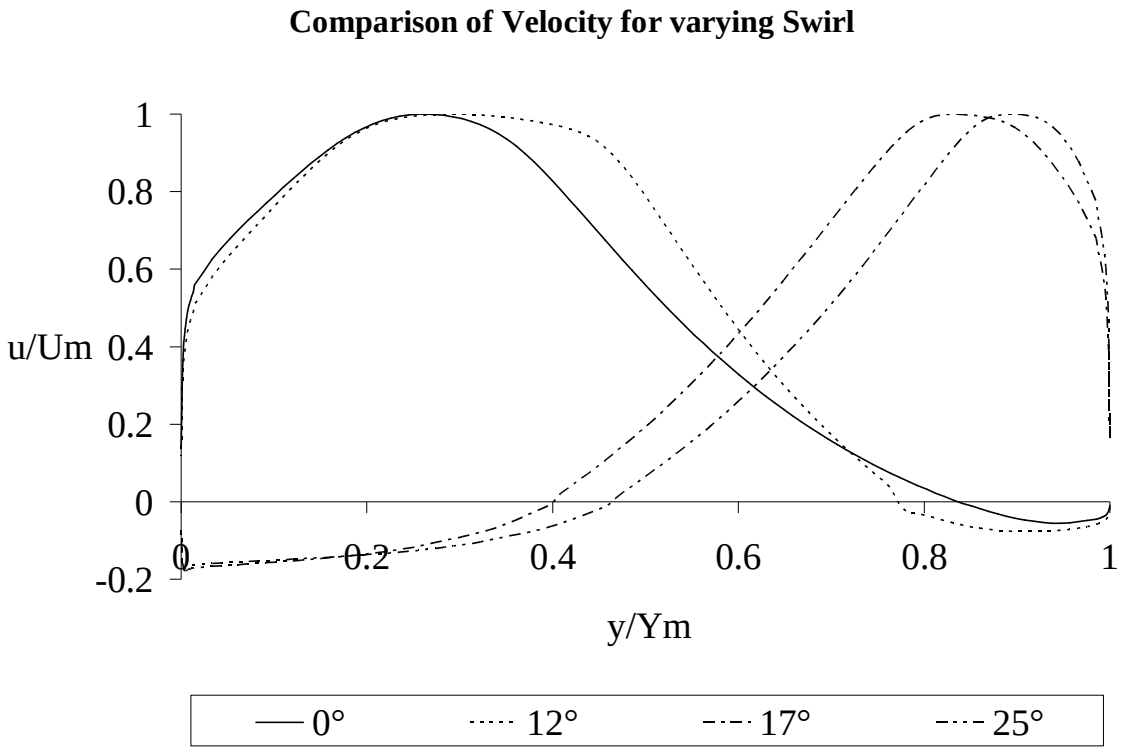

Longitudanal Velocity (25°), Case C, AR3

Fig 39 AR=3, Casing Wall Angle=25°

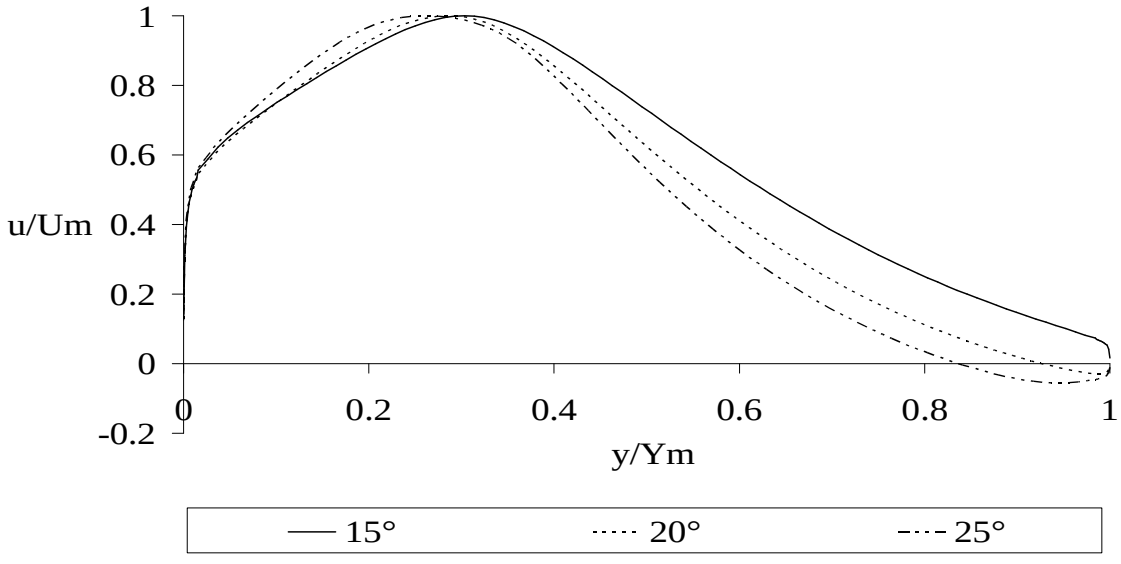

Longitudinal Velocity (0°), Case C, AR 3

Fig 40 AR=3, Swirl Angle=0°

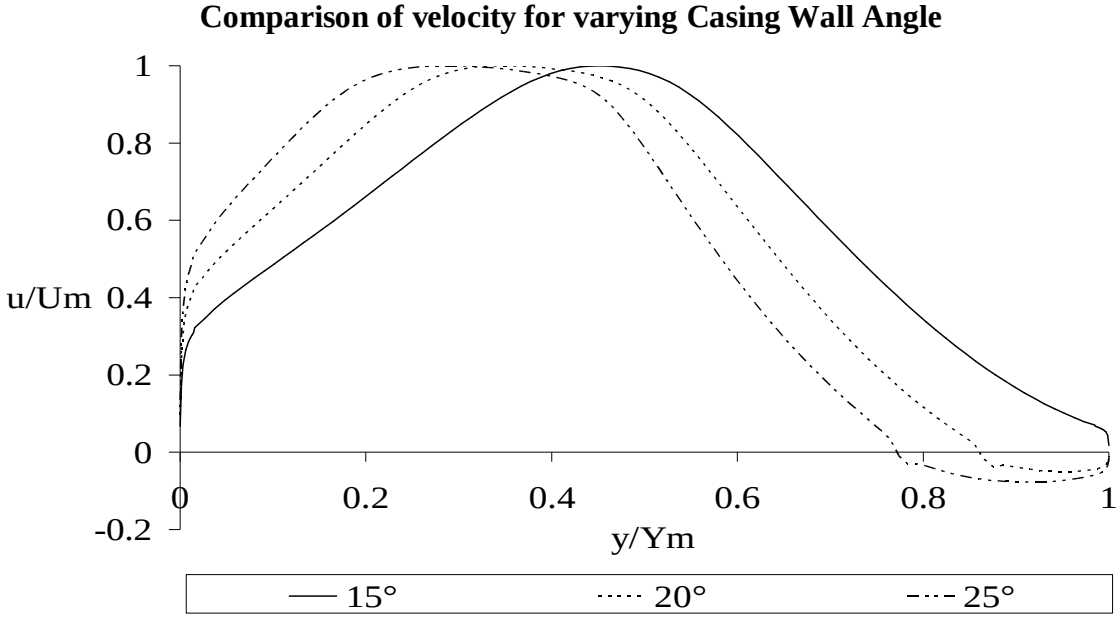

Longitudinal Velocity (12°), Case C, AR3

Fig 41 **AR=3, Swirl Angle=12°**

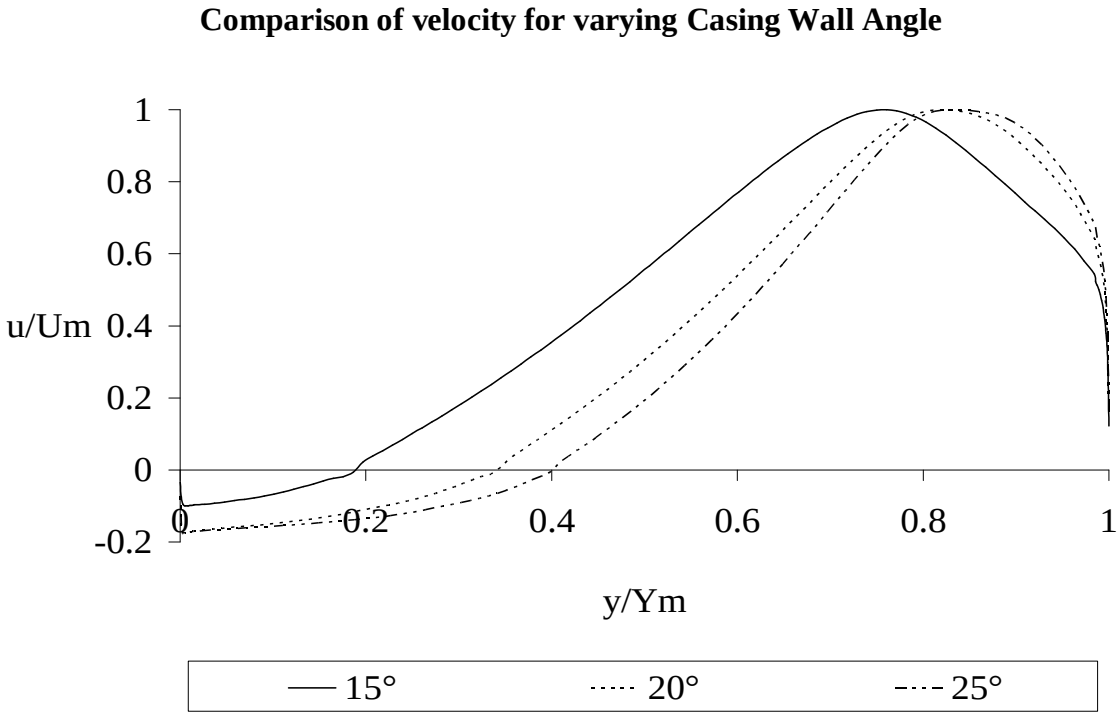

Longitudinal Velocity (17°), Case C, AR3

Fig 42 **AR=3, Swirl Angle=17°**

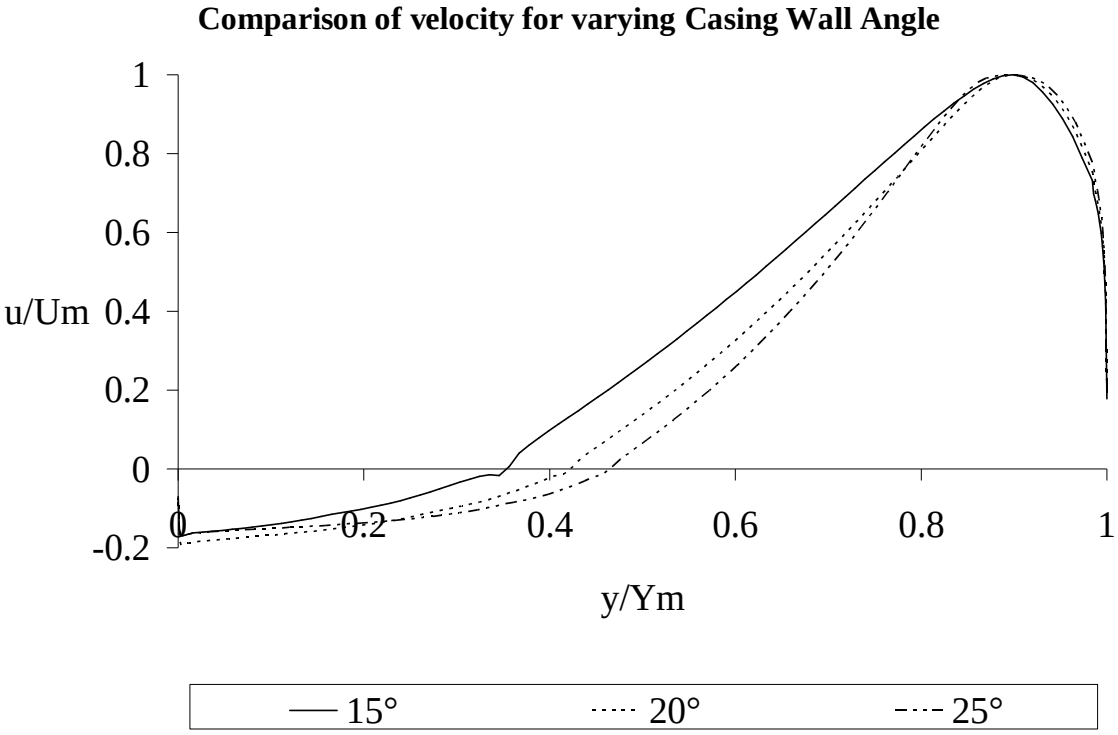

Longitudinal Velocity (25°), Case C, AR3

Fig 43 AR=3, Swirl Angle=25°

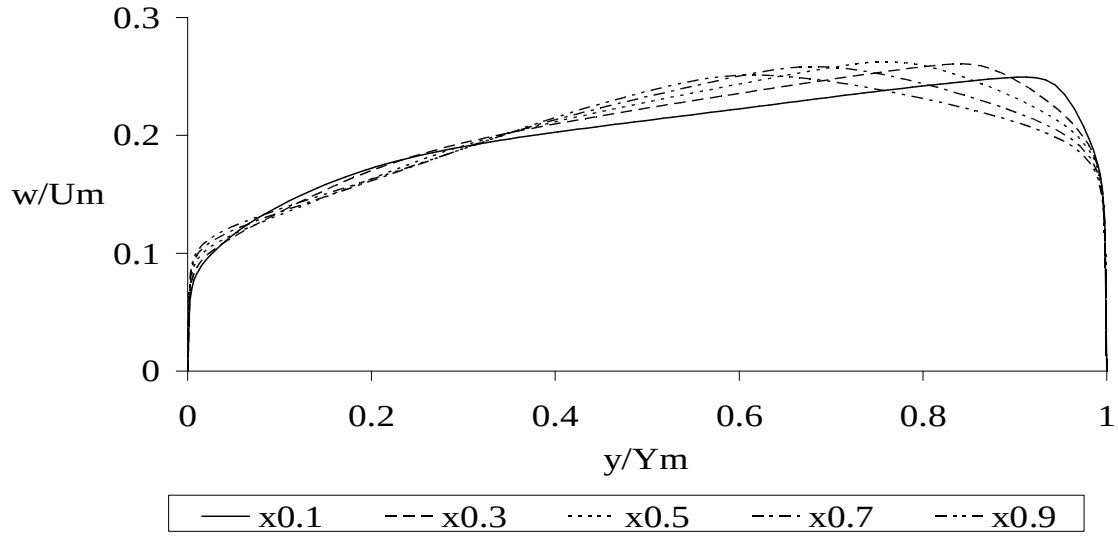

Swirl Velocity (12°), 15C, AR3

Fig 44 AR=3, Casing Wall Angle=15°

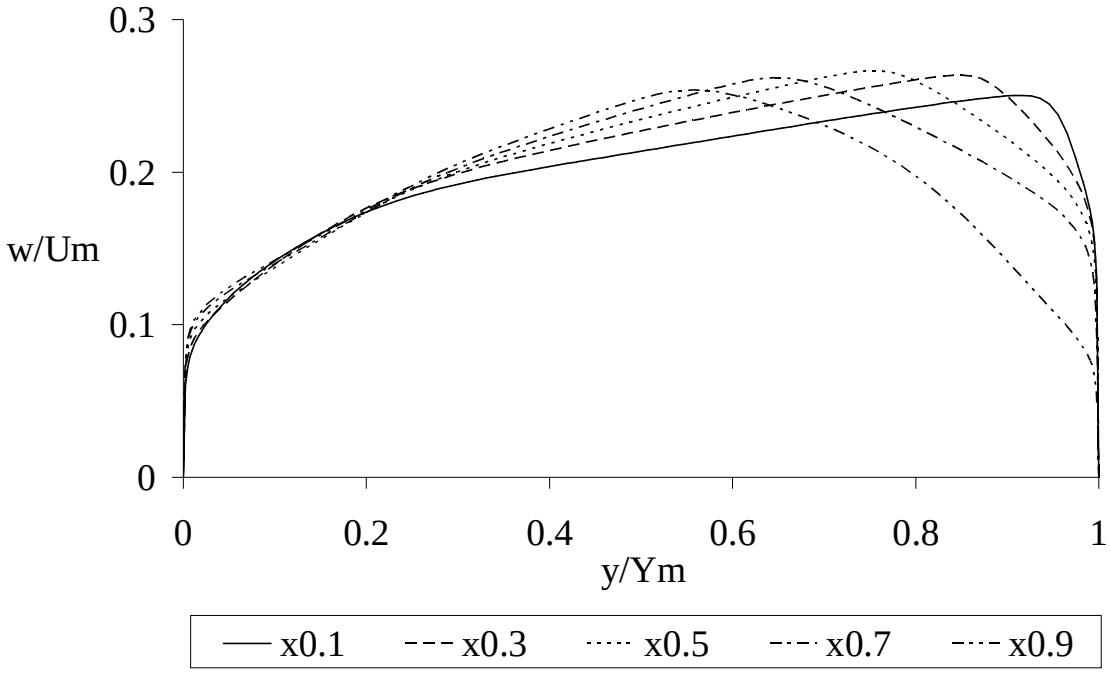

Swirl Velocity (12°), 20C, AR3

Fig 45 AR=3, Casing Wall Angle=20°

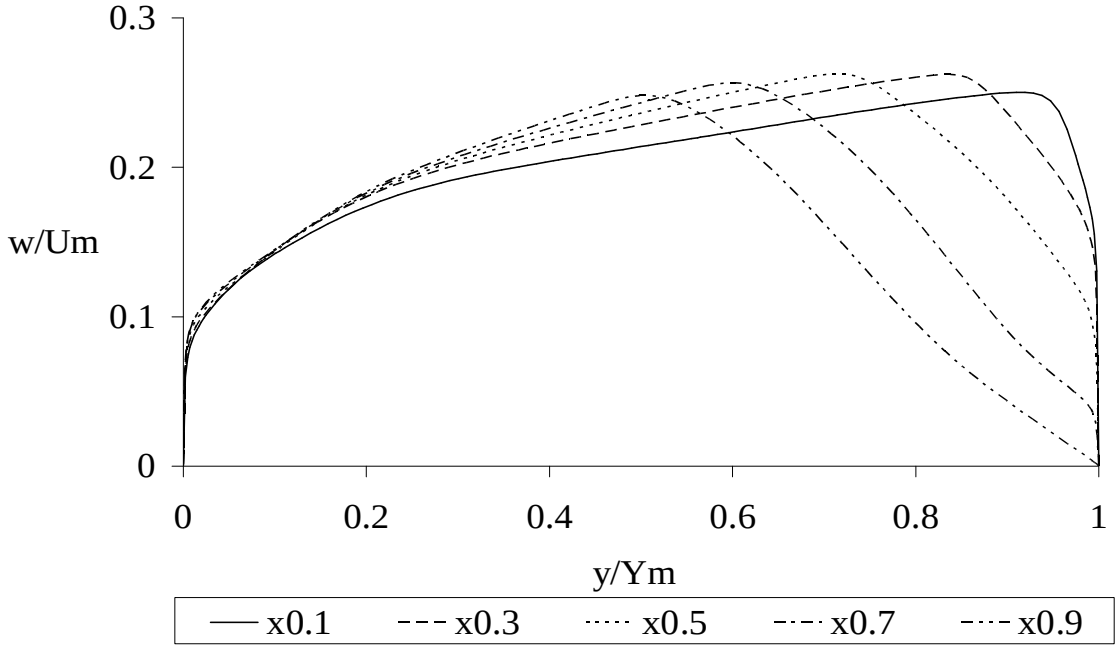

Swirl Velocity (12º), 25C, AR3

Fig 46 AR=3, Casing Wall Angle=25°

APPENDIX

Flow-Chart for CFD Modeling and Simulation